Network Reduction for Power System Planning

by

Yingying QI

A Thesis Presented in Partial Fulfillment

of the Requirements for the Degree

Master of Science

Approved November 2013 by the
Graduate Supervisory Committee:

Daniel Tylavsky, Chair
Kory Hedman
Lalitha Sankar

ARIZONA STATE UNIVERSITY

December 2013

ABSTRACT

Due to great challenges from aggressive environmental regulations, increased demand due to new technologies and the integration of renewable energy sources, the energy industry may radically change the way the power system is operated and designed. With the motivation of studying and planning the future power system under these new challenges, the development of the new tools is required. A network equivalent that can be used in such planning tools needs to be generated based on an accurate power flow model and an equivalencing procedure that preserves the key characteristics of the original system. Considering the pervasive use of the dc power flow models, their accuracy is of great concern. The industry seems to be sanguine about the performance of dc power flow models, but recent research has shown that the performance of different formulations is highly variable.

In this thesis, several dc power-flow models are analyzed theoretically and evaluated numerically in IEEE 118-bus system and Eastern Interconnection 62,000-bus system. As shown in the numerical example, the alpha-matching dc power flow model performs best in matching the original ac power flow solution. Also, the possibility of applying these dc models in the various applications has been explored and demonstrated. Furthermore, a novel hot-start optimal dc power-flow model based on ac power transfer distribution factors (PTDFs) is proposed, implemented and tested. This optimal-reactance-only dc model not only matches the original ac PF solution well, but also preserves the congestion pattern obtain from the OPF results of the original ac model. Three improved strategies were proposed for applying the bus-aggregation technique to the large-scale systems, like EI and ERCOT, to improve the execution time, and memory requirements when building a reduced equivalent model. Speed improvements of up to a factor of 200 were observed.

ACKNOWLEDGEMENTS

I would like to express my deepest appreciation and thanks to my advisors, Dr. Tylavsky, for his guidance, encouragement and invaluable support. I am also grateful to Dr. Hedman and Dr. Sankar for lending their practical insights for this research and being members of my supervisory committee. Gratefully acknowledged is the support for this research provided by the Consortium for Energy Reliability Technology Solutions (CERTS) and the Power Systems Engineering Research Center (PSERC).

TABLE OF CONTENTS

LIST OF TABLES

Table Page

LIST OF FIGURES

NOMENCLATURE

ac	Alternating current
b_{ij}	Susceptance of the line *i-j*
$\boldsymbol{B}_{bus}$	Bus susceptance matrix with the dimension of N by N
$\boldsymbol{B}_{branch}$	Branch susceptance matrix with the dimension of L by N
$\boldsymbol{C}$	Node-branch incidence matrix of the full system with dimension of L by N
$\boldsymbol{C}_R$	Node-branch incidence matrix of the reduced system with the dimension of L_R-by-N_R.
dc	Direct current
diag(x)	Diagonal matrix with the diagonal elements of x
EI	Eastern Interconnection
ERCOT	Electric Reliability Council of Texas
g_{ij}	Conductance of the line *i-j*
$\boldsymbol{G}_{bus}$	Bus conductance matrix with the dimension of N by N
GHG	Greenhouse gas
LMP	Locational marginal price
L	Number of branches in the full network
L_R	Number of branches in the reduced network
MMWG	Multi-regional Modeling Working Group
N	Number of non-slack buses in the full network
N_R	Number of non-slack buses in the reduced network
OPF	Optimal power flow
P_i	Real power injected into bus i
PF	Power flow
$\boldsymbol{P}_{inj}$	Bus net injection vector of full system with the dimension of N by 1
$(P_{inj})_R$	Bus net injection vector of reduced system with the dimension of N_R by 1
$\boldsymbol{P}_{flow}$	Branch power flow vector with the dimension of L by 1
$P_{flow}^{inter-zonal}$	Inter-zonal power flows with the dimension of L_R by 1
$(\mathbf{P}_{flow}^{\text{inter}-\text{zonal}})_R$	Bus net injection vector of the reduced system with the dimension of N_R-by-1
PTDF	Power transfer distribution factor
Q_i	Reactive power injected into bus i
$r_{ij:}$	Resistance of the line *i-j*
t_i	Tap ratio magnitude
TL	Transmission line
x_{ij}	Resistance of the line *i-j*
$\boldsymbol{x}$	Branch reactance vector of the full system with the dimension of L-by-1
$\boldsymbol{x}_R$	Branch reactance vector of the reduced system with the dimension of L_R-by-1
v_i	Magnitudes of bus voltage at bus i
δ_i	Bus voltage angles at bus i
τ_i	Phase shift angle
λ	The single multiplier for loss compensation in dc power flow modeling

$\boldsymbol{\Theta}$	Bus voltage angle vector with the dimension of N by 1
$\boldsymbol{\Phi}$	PTDF matrix with dimension of L by N
$\boldsymbol{\Phi}'$	ac PTDF matrix with dimension of L by N
$\boldsymbol{\Phi}_R$	PTDF matrix of the reduced system with the dimension of L_R-by-N_R
Ψ	matrix representing each zone's contribution to the inter-zonal power flows with the dimension of L_R-by-N_R
$\prod_{flow}$	Matrix used to sum up the line flows with the dimension of L_R by L
$\prod_g$	Sum the bus injections with the dimension of N_R-by-N matrix
Λ	matrix whose null space includes x_R with the dimension of $L_R N_R$-by-L_R
$\|\|\cdot\|\|$	Euclidean norm of a vector
$(\cdot)^T$	Transpose of a matrix

CHAPTER 1 . INTRODUCTION

1.1 Background

With growing concerns over climate change, a number of environmental policies and regulations regarding the energy industry have been enacted and proposed by both the federal and state governments. Climate change, driven by the rising greenhouse gas (GHG) levels, plays an important role in economics and politics [1]. As the primary GHG, CO_2 contributes up to 77% of the greenhouse gas effect [2]-[5]. As indicated by [3], electricity is responsible for 40% of annual CO_2 emissions, which is the largest single source of CO_2 in US. Because of this, the energy industry is facing new challenges due to more aggressive environmental regulations [1]–[7]. Because of these regulations and because renewables have become more and more cost-effective, the electric power system is gradually shifting toward cleaner and more efficient energy sources [8]. That is to say, bulk connection of renewable energy resources imposes new challenges on the electric-power industry. Furthermore, increased demand from new technologies like electrical vehicles is likely to have a great effect on the electric-power industry. These factors taken together have the potential to radically change the way the power system is operated and designed. With the motivation of studying and planning the future power system under these new challenges, the development of the new tools is required.

Generally, the most accurate way for power-market analysis and system-planning studies to be conducted is to use the full system ac power-flow model [9]. However, the on-line network optimization, and market calculations based on the full ac power-flow model for large systems leads to a serious computational burden [10] and an optimal power flow (OPF) algorithm whose convergence is unreliable. In order to efficiently approach these analyses, two compromises are

usually made. First, a small network equivalent reduces the execution time of power flow and OPF algorithms.

Second, approximate power-flow models have been introduced due to the convergence difficulties and time-consuming iteration process of the full ac OPF. These approximate methods are especially helpful when it comes to analyzing the effect of a large number of contingencies. The biggest use of dc-type models is in linear SCOPF (security-constrained optimal power flow).

1.2 Literature Review

Generally, network equivalencing techniques designed to maintain the key power-system characteristics. The reduced model represents an "equivalent" snapshot of the system and is used for market-based system planning, and power-system operations [12].

Presently, there are several types of network reduction methods. Among these, the Ward-type equivalents, radial equivalent independent type (REI), and variations of these two basic methods are the most commonly used [12]-[13].

The Ward equivalent [14] was first introduced in the 1940's by J. B. Ward and further discussed throughout the literature, for example [15]-[18]. The Ward reduction divides the original network into an internal subsystem, boundary subsystem and external subsystem. By eliminating the external subsystem through Gaussian elimination, the internal subsystem is kept intact.

The classical Ward reduction has two versions [17], usually referring to as the Ward injection method and Ward admittance method. Their difference lies in the modeling of bus injections at each bus. The Ward injection method converts all the power injections at each bus into constant current injections before the reduction process and converts them back to power injections after the reduction process. Alternatively, the Ward admittance method models power injections as

shunt admittances before the reduction process. Given the possibility of yielding unrealistic admittances in the reduced equivalent, this method is less preferred. However, since the classical Ward method is unable to model the reactive power response from the external subsystem during contingency analysis, several modified versions of the classical Ward method were proposed in [16]-[20]. The extended Ward equivalent [20] attaches a fictitious PV bus to each boundary bus in the reduced model to provide adjustable reactive power. The reactive power provided varies with the deviation from the base operating point. F.F. Wu et al. [16] dealt with the problem by retaining all the external PV buses during the reduction process. Given its computational inefficiency and increased size of external subsystem, a reduced equivalent is proposed in [21] which aggregate the external PV buses into several groups. After the bus aggregation, each group is replaced by an equivalent PV bus. This reduced equivalent not only increases the computational efficiency of the reduced equivalent but also maintains the dynamic characteristics by using the Zhukov method [22].

For the purpose of market analysis and system planning, the Ward-type equivalent was further improved and a combined equivalent method was proposed [23] and [24]. During the process of generating such a combined equivalent, instead of modeling fractions of generators located at many buses, it retains all the generators in their entirety at the buses and move them to the nearest (means the bus directly connected by the smallest impedance branch) bus in the reduced model. The reduced model proposed in [23] is constructed based on the ac power-flow model and it aggregates all the generators from the external system to be a equivalent generator at the buses. By using the historical information based on the bus locations, the generator bid function for this equivalent generator is updated. On the other hand, the reduced model described in [24] is constructed based on the dc power-flow model and retains all the generators

individually at the buses, which preserves all the original generator bid functions of these generators in the reduced equivalent. Both of resulting equivalents based on [23] and [24] are used in system planning studies and market-based studies.

Another commonly used external equivalent is the REI-type equivalent. The REI equivalent was first proposed by P. Dimo [25] and expanded by W. Tinney [26]. The REI equivalent aggregates one or more sets of external loads and generators at a few fictitious REI PQ and PV buses. The criteria for defining the sets of buses can be selected based on load and generation conformity, geographic location, electrical distance, ownership groupings, etc.

However, there are many limitations in the REI equivalent and its variants. The major concern about the REI equivalent is the voltage magnitude of fictitious REI buses. To overcome this problem, many improved REI equivalents were proposed and promising results were observed by comparing it against other type of equivalents [27]-[29]. Also, since the REI equivalent is constructed to match the tie-line flow based on the base-case operating point, the accuracy will worsen as the operating condition deviates further from the base case. Also, since in the REI equivalencing method the external system is represented by one or more fictitious REI buses, the number of equivalent REI buses and different bus-aggregation criteria for replacing the external system have great influence in the accuracy of the REI equivalent. Furthermore, because of its operating-point dependency, the REI equivalents may yield significant errors when contingency analysis is conducted toward the internal power system. Reference [30] proposed a solution to this problem based on the sensitivity analysis for the power flows on the branches of the internal power system due to the changes of the bus power injections of external power system. Furthermore, due to the extra introduction of the REI nodes and their interconnection

with the boundary buses, the REI network seems less computational efficient by comparison to the Ward equivalent.

Recently, several new network reduction techniques were proposed for system planning and market analysis [30]-[34]. The methods discussed in [31]-[33] were based on the classical dc power-flow model and bus aggregation using a similarity metric based on power transfer distribution factor (PTDF). The basic idea of these reduction methods was to generate approximate equivalent dc-network PTDF matrices while preserving, as closely as possible, the same line flows as in the full (original) system. However, simulation results have shown that inter-zonal power flows obtained from the reduced equivalents generated by these three methods are different from the original system, even for the base case. Furthermore, with these approaches, there is no present way of determining flow limits on the inter-zonal equivalent lines generated. Since congestion is a key factor in OPF and system planning studies and since congestion may only be identified for lines that have limits, without appropriate line-flow limits for the aggregated equivalent lines, the accuracy of this approach is limited. (It needs to be stated that all network equivalencing techniques generate equivalent lines with no line limits and, consequently, this limitation is ubiquitous.) A solution to the line limit problem for the bus aggregation technique was proposed in [34]. In this method, buses are aggregated based on the congestion profile of the original network and the congested lines in the original system are preserved in the equivalent as are the lines parallel to the aggregated lines connecting zones. Along with the reduction method described in [32], the equivalent generates reasonably accurate LMPs and preserves the congestion pattern of the full model in the limited number of OPF studies conducted [32].

Typically when one thinks of network equivalents, one thinks of network reduction; however one often used equivalencing approach is to create a dc approximation of an ac network. The dc power flow has found favor in real-time market-based applications because of its robustness and speed [35], [36]. There has been a recent upsurge in the use of the dc power flow for electricity-market applications, such as auctions associated with transmission rights, real-time security-constrained dispatch, and day-ahead security-constrained unit commitment. Considering the pervasive use of the dc power-flow models, the accuracy and feasibility of dc power-flow models is of great concern. Since LMPs are predicted based on congestion profile, if the dc model does not estimate the line flows accurately, the financial consequences can be substantial. However, the industry seems to be sanguine about the performance of dc power-flow models. A flurry of research aimed at improving and estimating the accuracy of dc power-flow formulations has occurred [36]-[42]. While some authors have shown impressive accuracy with dc power-flow formulations, others are not so sanguine about the dc power-flow's accuracy [42].

The number of dc power-flow formulations available is legion. Several of the more accepted dc power-flow models are described in [35], [39], [42]-[45]. The different formulations are characterized by different definitions of active power injections, loss estimation and branch admittances [42], [44]-[45].

One taxonomy for classifying dc power flow formulations starts by breaking the models into two categories: non-incremental models and incremental models. For non-incremental models, hot-start models and cold-start models are two major types. They are mostly used for the pre-contingency state in security-constrained applications. Hot-start models are constructed when a solved ac power-flow solution is available, while cold-start models are built when an ac solution is unavailable. Hot-start models, which have the same MW losses as the ac solution, are often

used to inform operation decisions and in short-term studies, e.g., real-time security constrained economic dispatch (SCED) [42], [47]. Cold-start models are often used in long-term planning studies, e.g., dc-model-based security constrained unit commitment [48].

The incremental model is used to compute changes from a base-case ac/dc power-flow solution [42]. Sparse models and sensitivity factor models are two major types of incremental models. The sparse model is used for the applications where a solved ac/dc base case is available. For the sensitivity factor model, sensitivity factors are generated from the sparse dc network. These models are used to calculate various quantities, including the PTDF (power transfer distribution factor), OTDF (outage transfer distribution factor) and LODF (line outage distribution factor). PTDF and OTDF are usually used for internal calculations for transmission loading relief (TLR). LODF factors are used for fast contingency screening, which are only updated when the network topology changes.

Another way for classifying dc power-flow formulations is to break the models into state-dependent and state-independent dc power-flow formulation [36], [42] and [44]. The state-dependent dc power-flow models take into consideration the system losses and bus voltage values at an initial solution state. The state-independent dc power-flow models assume a lossless network, one-per-unit voltage values, and small voltage angle differences [44]-[49].

1.3 Organization of the Report

In this report, the major content is partitioned into 5 additional chapters.

Chapter 2 analyzes different dc power flow formulations constructed based on different assumptions in detail.

Chapter 3 conducts numerical examples to test the feasibility and accuracy of the different dc models on the 10-bus system, IEEE 118-bus system and EI 62,000-bus system.

Chapter 4 proposes a new hot-start optimal dc power-flow model based on ac power transfer distribution factors and numerical examples are shown to demonstrate the process.

Chapter 5 presents the bus aggregation method based on the PTDFs and the methods of speeding up the reactance evaluation process for large-scale power system. The ERCOT system is used as the test system to verify the speeding-up process.

CHAPTER 2 . DC POWER-FLOW MODEL

Considering the pervasive use of the dc models, it is of interest to examine the influence of different assumptions so that better dc model can be developed. In this chapter, starting from a typical ac branch model, a general dc model is introduced. Then, detailed analysis toward the assumptions made for the dc model is conducted. Based on the analysis of general dc power-flow model and the assumptions involved in the dc model, three hot-start dc models with different loss compensation approaches and one cold-start dc models are discussed in detail.

2.1 General dc power-flow model

The dc-network-modeling process starts from the ac power-flow equations. For a transmission line spanning bus *i* and bus *j*, which is shown in Fig. 2.1, the net active power injection at bus *i* and bus *j* are defined as p_i and p_j.

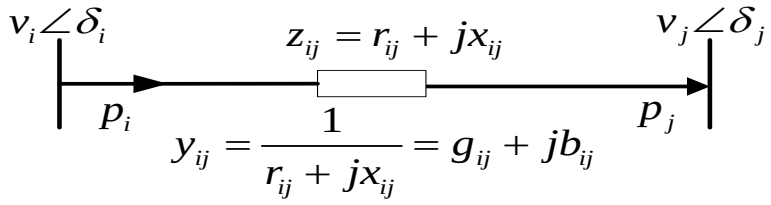

Fig. 2.1 A typical transmission line model connecting bus *i* and bus *j*

Variables p_i and p_j are defined by:

$$\begin{aligned} p_i &= \mathrm{Re}\left\{v_i\angle\delta_i\left[\left(g_{ij} + jb_{ij}\right)\left(v_i\angle\delta_i - v_j\angle\delta_j\right)\right]^*\right\} \\ &= g_{ij}\left(v_i^2 - v_i v_j\cos\left(\delta_i - \delta_j\right)\right) - v_i v_j b_{ij}\sin(\delta_i - \delta_j) \end{aligned} \tag{2.1}$$

$$p_j = -g_{ij}\left(v_j^2 - v_i v_j\cos(\delta_i - \delta_j)\right) - v_i v_j b_{ij}\sin(\delta_i - \delta_j) \tag{2.2}$$

where:

$r_{ij:}$ the resistance of branch *i-j*

$x_{ij:}$ the resistance of branch *i-j*

$z_{ij:}$ the impedance of branch *i-j*

$g_{ij:}$ the conductance of branch *i-j*

$b_{ij:}$ the susceptance of branch *i-j*

y_{ij}: the admittance of branch *i-j*

v_i: the per unit magnitude of bus voltage at bus *i*

v_j: the per unit magnitude of bus voltage at bus *j*

δ_i: the bus voltage angle at bus *i*

δ_j: the bus voltage angle at bus *j*

It is easy to show that the difference of the terms of (2.1) and (2.2) represent the line MW losses. Let us designate

$$l_i = g_{ij}\left(v_i^2 - v_i v_j \cos\left(\delta_i - \delta_j\right)\right)$$
$$l_j = g_{ij}\left(v_j^2 - v_j v_i \cos\left(\delta_i - \delta_j\right)\right) \quad (2.3)$$

where the branch series loss is l_i+l_j.

The second terms in (2.1) and (2.2) are the identical, which is:

$$p_{ij} = -v_i v_j b_{ij} \sin(\delta_i - \delta_j) \quad (2.4)$$

Then (2.1) and (2.2) can be rewritten as:

$$p_i = l_i + p_{ij} \quad (2.5)$$

$$p_j = -l_j + p_{ij} \quad (2.6)$$

Based on (2.4) - (2.6), an ac equivalent model of branch can be modeled as following:

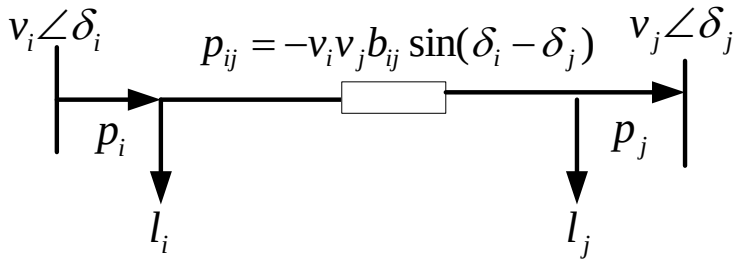

Fig. 2.2 ac equivalent model of branch

Since the dc power-flow formulations are linearly approximating (2.4) - (2.6), a bilateral dc equivalent branch model can be written as:

$$p_{ij} = h_{ij} \cdot \delta_{ij} \tag{2.7}$$

$$p_i = \alpha_i + p_{ij} \tag{2.8}$$

$$p_j = -\alpha_j + p_{ij} \tag{2.9}$$

Therefore, a general dc equivalent model can be modeled as:

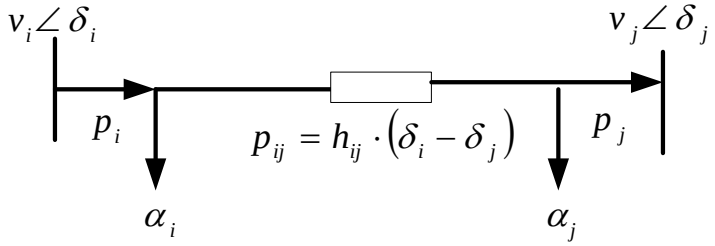

Fig. 2.3 dc equivalent model of branch

In Fig. 2.3, h_{ij} is defined as the dc equivalent branch admittance and α_i and α_j are defined as fixed injections. In this model, the sum of α_i and α_j can be used to approximate the branch loss at some chosen operating point. It is obvious that different definitions of active power injections (selections of α_i and α_j), loss estimation (sum of α_i and α_j) and branch admittance h_{ij} will affect the accuracy and feasibility of dc power-flow models' results. It seems that the selections of α_i, α_j and h_{ij} are quite arbitrary. For the classical dc model, it is traditional to select α_i=0, α_j=0 and

$h=1/x_{ij}$. While it is tempting to equate the α in the dc model with the l in the ac model. We will see that, depending on how we model the series component in the dc model, to get an exact match between the ac and dc models will require some flexibility. Also, it is tempting to equate b from the ac model with h_{ij} of the dc model (and this is one assumption that can be made) however the assignments of α and h_{ij} are arbitrary, with a relationship between them that, if obeyed, allows the dc solution to exactly match the ac solution for any arbitrary base case. Furthermore, by selecting these values in one particular way, the dc model performs better than in selecting them another way.

Depending on the application of the dc model and the type of base case, for the "best" linear fit of the dc to the ac model over a practical operating range, h_{ij}, α_i and α_i need to be evaluated at a "suitable" point [42]. Using the definitions above, Fig. 2.2 and Fig. 2.3, different dc power-flow models are discussed in the following section.

Based on (2.7) - (2.9) , the dc power flow equation in matrix form is written as:

$$\mathbf{P} = \mathbf{H} \cdot \boldsymbol{\theta} \qquad (2.10)$$

where

P: the vector of nodal power injections;

Θ is the vector of nodal phase angles;

H: the nodal susceptance matrix;

After solving the bus voltage angels by (2.10), the branch flows are obtained by (2.8) and (2.9).

2.2 Classical dc power-flow model

The classical dc model assumes a lossless network, one-per-unit bus voltage values, and small voltage angle differences. In order to obtain the classical dc power-flow model, a number

of assumptions are made. After a sequence of approximations, the classical dc power-flow model could be derived step by step from the sending end MW flow on the line which is shown as (2.1).

First, by assuming that the resistances on the line are ignored, then sending end MW flow p_i on the line could be written as:

$$p_i = v_i v_j \sin(\theta_i - \theta_j) / x_{ij} \qquad (2.11)$$

Second, if all voltage magnitudes are identical to one per unit, then p_i can be written as:

$$p_i = \sin(\theta_i - \theta_j) / x_{ij} \qquad (2.12)$$

Third, if small voltage angle differences are assumed, then p_i can be written as:

$$p_i = (\delta_i - \delta_j) / x_{ij} \qquad (2.13)$$

According to the general dc power-flow model shown in Fig. 2.3, in this model, α_i and α_j are set to be zero. Traditionally, h is selected as $1/x_{ij}$. After solving the (2.10) for the bus angels, the branch flows can be given by (2.8) and (2.9). Since the classical dc model is only a function of the network topology and branch reactances, the classical dc model is state-independent.

It seems that these assumptions may lead to huge errors into the dc model. It would be interesting to figure out the true impact of these approximations and where the errors in the derivation occure.

For the assumption of a lossless network, the errors introduced for a large-scale system may yield MW flows that significantly deviate from the actual MW flow due to lack of MW losses in the model, especially the branches located in the reference (slack) bus's neighborhood where system losses may be supplied.

For the assumption of one-per-unit voltage value, high voltages (like 1.1 p.u.) can be observed at the places where large reactive power resources are engaged. If the voltage magnitudes of both ends of the branch are 1.1, then the absolute error for this one-per-unit

approximation reaches 0.21 p.u., whose error in percentage is 21%. When such voltages occur in a large-scale power system, deviation of flows can lead to even larger and larger errors. For example, the voltage magnitudes of the typical NERC-MMWG models are in the range 0.75 to 1.4 per-unit. These extraordinary errors occur because of MVA base changes between two sections of the model. The errors introduced by the voltage magnitudes of this system are correspondingly large.

For the assumption of small voltage angle differences, large angle differences may be found on some long transmission lines in a large-scale system. If the angle difference δ is at 45 degrees (rare, but this has been seen in the MMWG—EI model under contingency conditions,) the difference between $sin\delta$ and δ in percentage is about 11.1%.

These different assumptions have been analyzed and evaluated for accuracy acceptably assuming high X/R ratios and small voltage deviations from one per unit [39]. Clearly, the assumptions made will affect the accuracy of dc power-flow models' results.

2.3 Hot-start dc power-flow models

Hot-start dc models are constructed when a solved ac power-flow solution is available. By constructing the hot-start dc power-flow model based on the known ac power-flow solution, they can be made to model the same MW losses as the ac base-case power-flow solution. Since the base-case ac power-flow solution is known, the series and shunt MW losses and ZIP loads are evaluated from the base point ac solution and modeled as constant P in the dc model. Hot-start dc models are often used in short-term operation and studies, e.g., real-time security constrained economic dispatch (SCED) [42], [47].

2.3.1 dc power-flow model with net loss dispersal

For this dispersed-loss dc power-flow model, the network-modeling assumptions are the same as those for the classical dc model. In order to take into account the MW losses, a single multiplier λ is applied to each load. By scaling up the entire loads in the system, the losses are distributed throughout the entire model. This single multiplier λ is defined as the ratio of the total generation to total load for the base case, shown as:

$$\lambda = \frac{\sum P_G}{\sum P_L} \tag{2.14}$$

Where

$\sum P_G$ and $\sum P_L$ are the total generation and total load in the system, respectively.

Since the MW losses of the system are obtained from the base-case solution, the total MW losses of this model are same as the base-case power-flow solution. Considering its state-dependent feature, clearly there are pros and cons to selecting the losses using a base case that may or may not be close to the conditions of interest.

2.3.2 dc power-flow model with halved localized loss compensation

Instead of scaling the loads globally to compensate for the MW losses, this dc power-flow model disperses the MW losses locally to each branch. Since the MW loss of each branch is known from the solved ac base, the most convenient way of loss modeling is to take 50% each of the initial branch loss as equivalent injections at the sending and receiving end of this branch.

As defined in the general dc power-flow model shown in Fig. 2.3, α_i and α_j are defined as two equivalent injections, whose sum can be used to represent the MW losses over the branch *i-j*. This additional injection vector, P_{loss}, is added to the original bus injection vector $\boldsymbol{P}$ in (2.10). Then the bus angels can be solved for and branch flows can be calculated using (2.8) and (2.9).

2.3.3 α-matching dc power-flow model

When operating in a real-time environment where the present state of the system is known relatively accurately, the α-matching power-flow dc model is constructed by first specifying the branch parameter h_{ij}. Second, α_i and α_i components are assigned so that the real power flows at the end of each line (including losses) exactly match [42]. A more detailed description of this follows.

- Modeling of transmission line

In tems of the general dc power-flow model, h_{ij} can be defined by matching the p_{ij} in (2.4) and (2.7).

The active power at the sending end and the receiving end are

$$p_i^0 = \alpha_i + h_{ij}\left(\delta_i^0 - \delta_j^0\right) \tag{2.15}$$

$$p_j^0 = -\alpha_j + h_{ij}\left(\delta_i^0 - \delta_j^0\right) \tag{2.16}$$

The superscript 0 is used to indicate the base-case operating point.

After matching p_i and solving (2.15) and (2.8) , α_i can be obtained. Similarly, α_i can be obtained by matching p_j in (2.9) and (2.16). h_{ij}, α_i and α_j equations are summarized as follows:

$$h_{ij} = -v_i^0 v_j^0 b_{ij} \sin(\delta_i^0 - \delta_j^0)/(\delta_i^0 - \delta_j^0) \tag{2.17}$$

$$\alpha_i = g_{ij}\left(v_i^{0^2} - v_i^0 v_j^0 \cos\left(\delta_i^0 - \delta_j^0\right)\right) \tag{2.18}$$

$$\alpha_j = g_{ij}\left(v_j^{0^2} - v_i^0 v_j^0 \cos\left(\delta_i^0 - \delta_j^0\right)\right) \tag{2.19}$$

where:

v_i^0 : the magnitude of bus voltage at bus *i* at the base case

v_j^0 : the magnitude of bus voltage at bus *j* at the base case

δ_i^0 : the bus voltage angle at bus *i* at the base case

δ_j^0 : the bus voltage angle at bus *j* at the base case

➢ Modeling of transformer/phase shifter

Considering the off-nominal transformer tap in the dc model, transformer/phase shifter is formulated differently from the transmission line. Generally, transformers/phase shifter is modeled as a standard Π transmission line model in series with an ideal phase shifting transformer. For the transformer, let the quantity $t_i \angle \tau_i$, a complex number, represent the tap ratio magnitude, t_i, and phase shift angle, τ_i, respectively. As shown in Fig.2.4 A general transformer model with off-nominal tap and (or) non-zero phase shift, it is located at the "from" end of the branch.

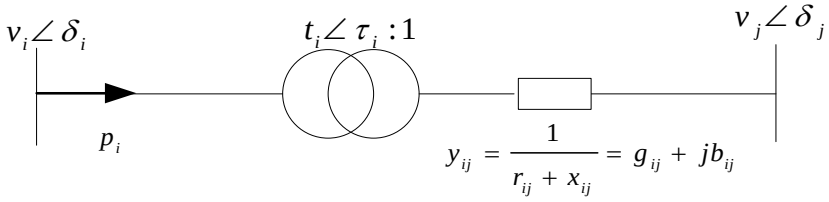

Fig.2.4 A general transformer model with off-nominal tap and (or) non-zero phase shift

The active power at the sending bus *i*:

$$\begin{aligned} p_i &= \mathrm{Re}\left\{\left(v_i \angle \delta_i / t_i \angle \tau_i\right)\left[\left(g_{ij} + jb_{ij}\right)\left(v_i \angle \delta_i / t_i \angle \tau_i - v_j \angle \delta_j\right)\right]^*\right\} \\ &= g_{ij}\left(\left(v_i / t_i\right)^2 - v_i v_j / t_i \cos\left(\delta_i - \delta_j - \tau_i\right)\right) - v_i v_j b_{ij} \sin(\delta_i - \delta_j)/t_i \end{aligned} \tag{2.20}$$

Therefore, based on a solved ac base-point solution, the branch admittance, α_i and α_j components for a transformer are derived as:

$$h_{ij} = -v_i^0 v_j^0 b_{ij} \sin(\delta_i^0 - \delta_j^0 - \tau_i^0)/t_i^0(\delta_i^0 - \delta_j^0) \tag{2.21}$$

$$\alpha_i = g_{ij}\left(\left(v_i^0 / t_i^0\right)^2 - v_i^0 v_j^0 / t_i^0 \cos\left(\delta_i^0 - \delta_j^0 - \tau_i^0\right)\right) \tag{2.22}$$

$$\alpha_j = g_{ij}\left(\left(v_j^0\right)^2 - v_i^0 v_j^0 / t_i^0 \cos\left(\delta_i^0 - \delta_j^0 - \tau_i^0\right)\right) \tag{2.23}$$

2.4 Cold-start dc power-flow models

Cold-start dc power-flow models are built when an initial solved ac power flow solution is unavailable. Due to the absence of a reliable base case, the construction of cold-start dc power-flow models is more difficult than the hot-start dc model. Sometimes a power-flow solution of a

simplified ac power flow problem is used for the dc power flow modeling. Cold-start models are often used in long-term planning studies, e.g., dc-model-based security constrained unit commitment [48].

2.4.1 Fixed-voltage ac power flow solution

Sometimes, due to the lack of good voltage/VAr data from a solved case, a fixed-voltage ac power-flow solution can be used for the dc power flow modeling for loss estimation. Starting with a power flow traditional ac power flow model, all buses are set to be PV buses with no VAr limits. That is to say, the magnitudes of all the buses and taps of transformers are fixed at one-per-unit values. Obviously, in this case, the VAr flows of this ac solution are very poor approximations. Further, if the loss estimation is based on fixed-voltage ac power flow solution, the following may also not be approximated well: MW flows, net losses and loss distributions.

2.5 Comparison of models

In Fig. 2.5, the relationship between the bus angle differences δ_{ij} and the real power injection p_i at bus i are shown. This is the solid line in the figure. The variables p_i^0 and δ_{ij}^0 represent the power injected at the sending end bus i and the bus-voltage-angle difference between the ends of the line at the base-case operating point, respectively. Line 1 indicates the behavior of the classical dc model. Due to the assumptions made in this model, it is not surprising these models are far from the exact ac power-flow model. Line 2 indicates the dispersed-loss dc power-flow model. Note that the behavior of the p_i v.s. δ_{ij} model with dispersed loss compensation should not intersect the origin, which indicates the loss compensation by escalating loads to model losses. However, it is not clear how to allocate the MW losses compensation to each branch attached to this bus. In this model, the losses are distributed throughout the system and this will lead to better performance than the classical model, as shown in the numerical experiments presented in

a subsequent chapter. Line 3 indicates the localized-loss dc power-flow model. Since the MW losses are calculated and compensated locally for each branch, the "halved localized-loss dc power-flow model" may perform better than the global loss compensation. Compared to the previous three lines, line 4 represents the α-matching dc power-flow model, which passes through the base-case operating point directly. As long as the changes to the operating point are within a limited range, the α-matching dc model is expected to perform the best among the three dc power-flow models, even though the α-matching model is state-dependent. However, how large this limited range might be is unclear.

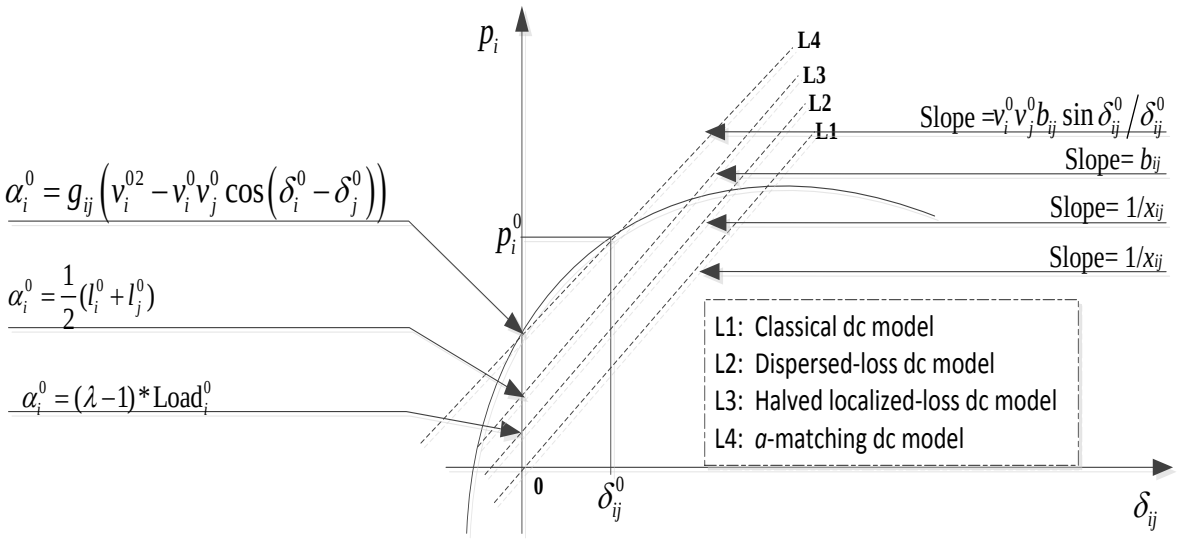

Fig. 2.5 dc power-flow model approximation

2.6 Summary

In this chapter, several dc power-flow models are discussed in detail.

The state-independent dc power-flow models assume a lossless network, one-per-unit voltage values, and small voltage angle differences. As mentioned before, this model is only a function of the network topology and branch reactance which indicates a state-independent dc model. In

order to estimate the true impact of these approximations and how errors accumulate during the deriving process, the assumptions had been analyzed and evaluated in section 2.2.

The state-dependent dc power-flow models are constructed based on an initial ac solution. Based on a reliable base-case solution, the lack of MW losses in the dc solution can be reasonably compensated for by increasing the dc load by the amount of ac MW losses. In terms of different loss compensation method, global loss compensation, halved localized loss compensation and base-point matching can be constructed. For the global loss compensation method, by scaling up all the loads in the system, the dispersed dc models compensate the MW losses globally. For the halved localized loss compensation method, by taking 50% each of the initial branch loss as equivalent injections at both sides of the branch, a localized-loss dc model can be constructed. For base-point matching, by specifying the branch admittance h and solving the matching values α_i, α_j, the α-matching dc model can be constructed and match the base-case perfectly. However, the absence of an initial ac power flow solution makes the construction of dc power-flow more complicated. Usually, a fixed-voltage ac solution is used to construct cold-start dc power flow models. Based on the per-unit voltage ac solution, a dispersed-loss dc power-flow model can be constructed.

Clearly, the assumptions made will affect the accuracy of dc power-flow models' results. If anything, investigations into the accuracy of any formulation have shown that such analysis is not amenable to theoretical efforts, but must be assessed empirically, assessment that is system and case dependent.

CHAPTER 3 . EXPRIMENTAL STUDIES ON DC POWER FLOW MODELS

Given the limits of theory and applied mathematics in formulation-acceptability analysis, this chapter conducts numerical experiments to show the impact of the assumptions on the accumulation of errors. Also, this chapter experimentally examines the accuracy of dc power-flow models discussed in CHAPTER 2 . Errors introduced by these dc power-flow models in the power-flow results and LMP calculations are quantified and compared. The simulations reported upon here use MATLAB, MATPOWER and PowerWorld for modified 118-bus IEEE system and the 62,000-bus Eastern Interconnection (EI) system. In order to conduct an OPF study on the IEEE 118-bus system, the IEEE 118 bus system with branch limits added, as found on the PowerWorld web site, was used.

In addition, contingency analysis is performed to evaluate the change in accuracy of these models for operating conditions that deviate from the base case.

In these test-case studies, automatic generation control (AGC), LTC transformer control, phase-shifter control and switched-shunt control have been disabled. Two metrics were chosen to measure the accuracy of the dc model. The first is the absolute value of the difference between the dc and ac branch flows (MW) normalized by the MVA limit of each respective line. The second metric involves a comparison of the congestion pattern and the differences of average LMPs between the dc and ac OPF solutions.

3.1 Impact of assumptions on classical dc model

The classical dc model assumes a lossless network, one-per-unit voltage values, and small voltage angle differences. In this chapter, in order to quantify the impact of these assumptions, three simplified ac power-flow models are introduced:

1) Model 1: ac power-flow formulation with one-per-unit bus voltage magnitude at each bus;
2) Model 2 : ac power-flow formulation with no resistance (R=0);
3) Model 3: ac power-flow formulation with fixed bus voltage (V=1) and no resistance (R=0).

Numerical experiments are conducted on the modified IEEE 118-bus system. For each of the three simplified ac power flow formulations, the power flow problem is solved and the results compared with the original ac PF solution. Fig. 3.1.summerizes the numerical experiments conducted.

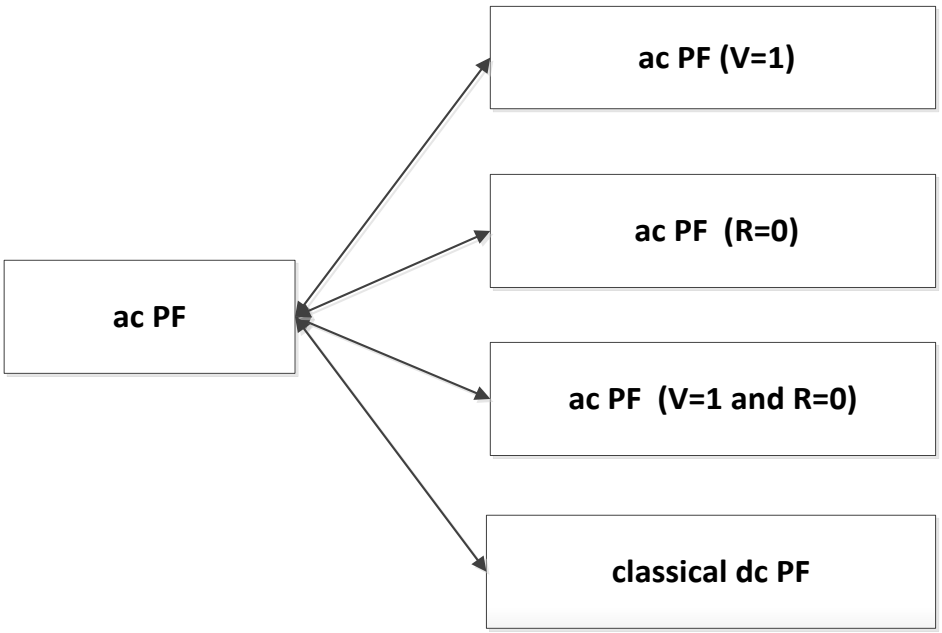

Fig. 3.1 Numerical simulation conducted

For the IEEE 118-bus system, the simulation results showing the comparison of the branch MW-flows between the full ac PF model and the simplified ac PF models are presented below:

A) ac PF vs. ac PF (V=1)

In this part, the branch MW-flows comparison between the full ac PF and the ac PF (V=1) is shown in Fig. 3.2. The upper part of the figures shows the actual branch-MW flows of these two models while the lower part shows the difference (errors) in the branch MW-flow by using the full ac PF solution.

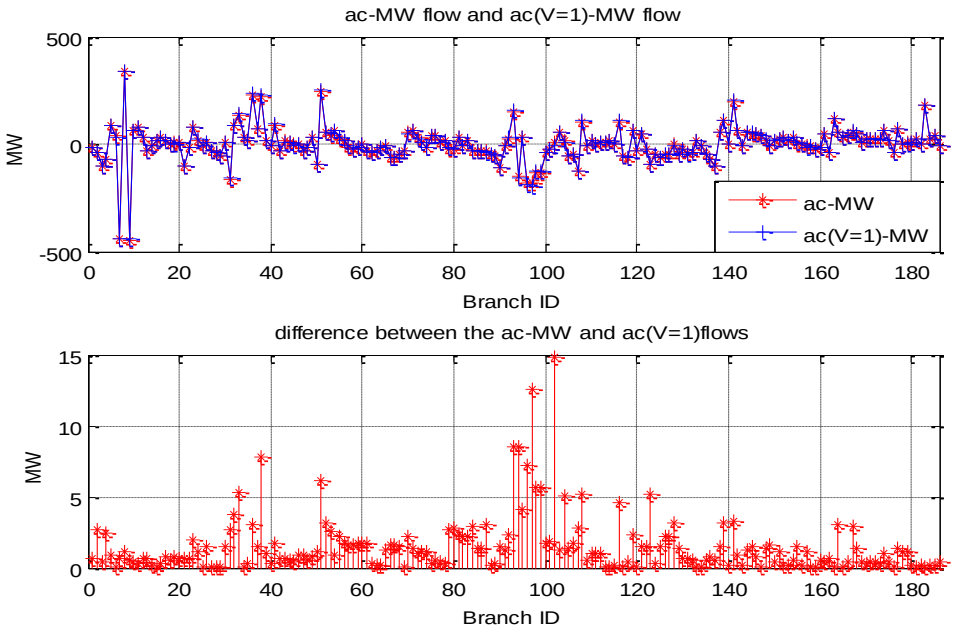

Fig. 3.2 Branch MW-flows and MW-flow differences between ac and the ac PF (V=1) models

As shown in Fig. 3.2, the largest error in the branch PFs is about 14.8 MW. The average error is calculated to be 1.2 MW based on ((3.1)),

$$Difference_{Avg} = \frac{\sum_{i=1}^{N} \left| Pf_i^{ac} - Pf_i^{ac\_simplified} \right|}{N} \tag{3.1}$$

where Pf_i^{ac} and $Pf_i^{ac\_simplified}$ represent the PF on the i^{th} branch based on the ac PF and simplified ac PF models, respectively; N is the total number of branches examined.

The maximum branch MW-flow error, for any branch, in percentage is 4.2% calculated as following:

$$Difference_i = \frac{\left| Pf_i^{ac} - Pf_i^{dc} \right|}{MVA_i} \times 100\% \tag{3.2}$$

where MVA_i is the MVA rating of line i.

Based on (3.2), the average value of the flow error in percentage is 0.4%.

B) ac PF vs. ac PF (R=0)

In this part, the branch MW-flows comparison between the full ac PF and the ac PF (R=0) is shown in Fig. 3.3. The maximum error of the branch MW-flows is 60.3 MW, and the average error is calculated to be 3.4MW. The maximum percentage errors in the branch MW-flow is found to be 15.7%. The average percentage error is calculated to be 0.94%.

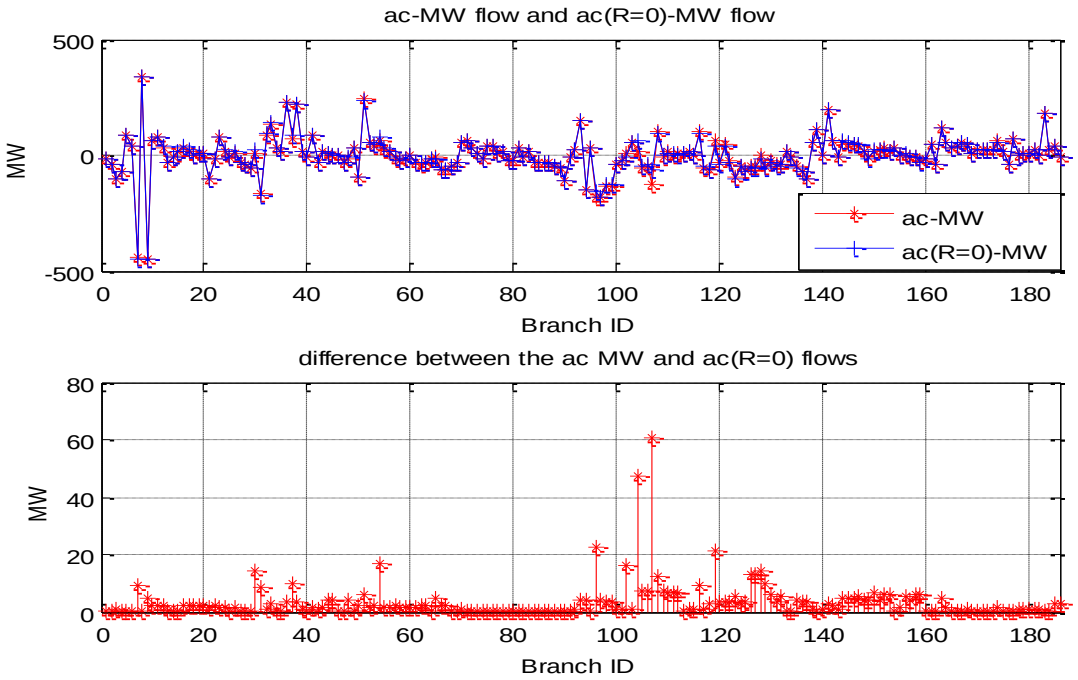

Fig. 3.3 Branch MW-flows and MW-flow differences between ac and the ac PF (R=0) models

By looking at the simulation results and Fig. 3.3, it is shown that the branches with the large errors are in the neighborhood of slack bus. Recall the discussion about the lossless network in section 2.2, these results verified that the huge errors of the MW flows over the branches exist in the slack bus's vicinity.

C) ac PF vs. ac PF (V=1 and R=0)

In this part, the branch MW-flows comparison between the full ac PF and the ac PF (V=1 and R=0) is shown in Fig. 3.4. In this case, the maximum error in the branch MW-flows is 59.5MW, and the average error is calculated to be 3.4 MW. The maximum percentage errors in the branch MW-flow is found to be 15.4%. The average percentage error is calculated to be 0.98%.

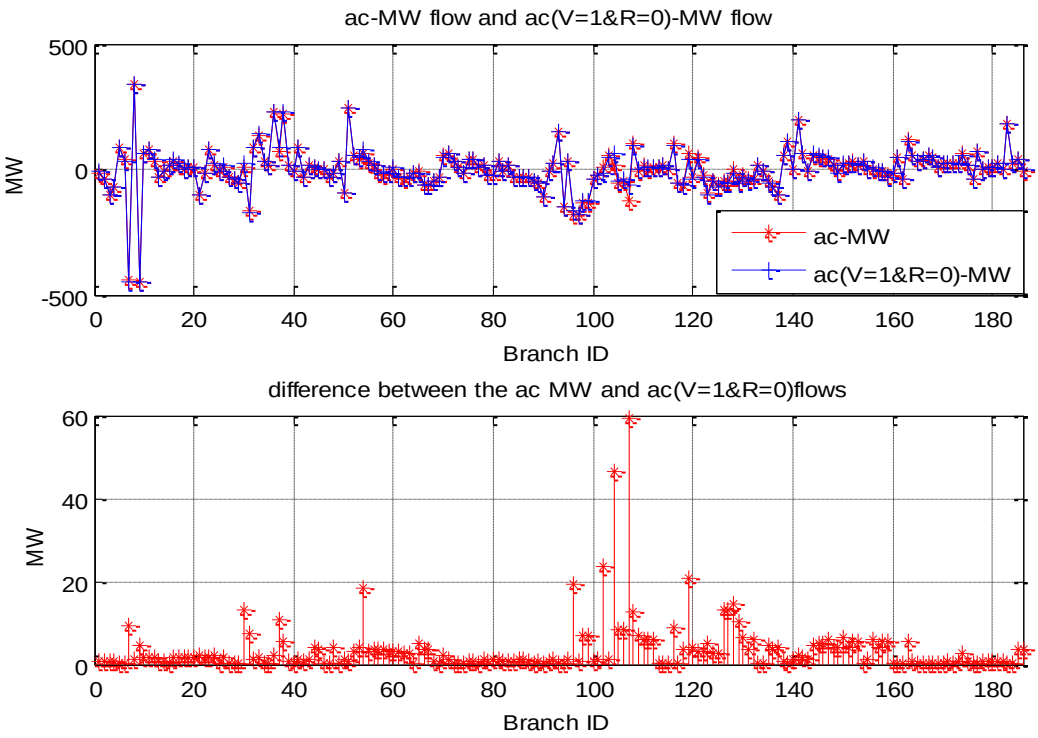

Fig. 3.4 Branch MW-flows and MW-flow difference between ac and the ac PF (R=0) models

As we discussed in section 2.2, the only difference between this model and the classical dc model is the difference between $\sin\delta$ and δ.

D) ac PF vs. classical dc model

In this part, the branch MW-flows comparison between the full ac PF and the classical dc model is shown in Fig. 3.4. As expected, the performance of classical dc model and ac model (R=0 and V=1) are very similar. The maximum error in the branch MW-flows is 59.5MW, and

the average error is calculated to be 3.5 MW. The maximum percentage errors in the branch MW-flow is found to be 15.4%. The average percentage error is calculated to be 0.98%.

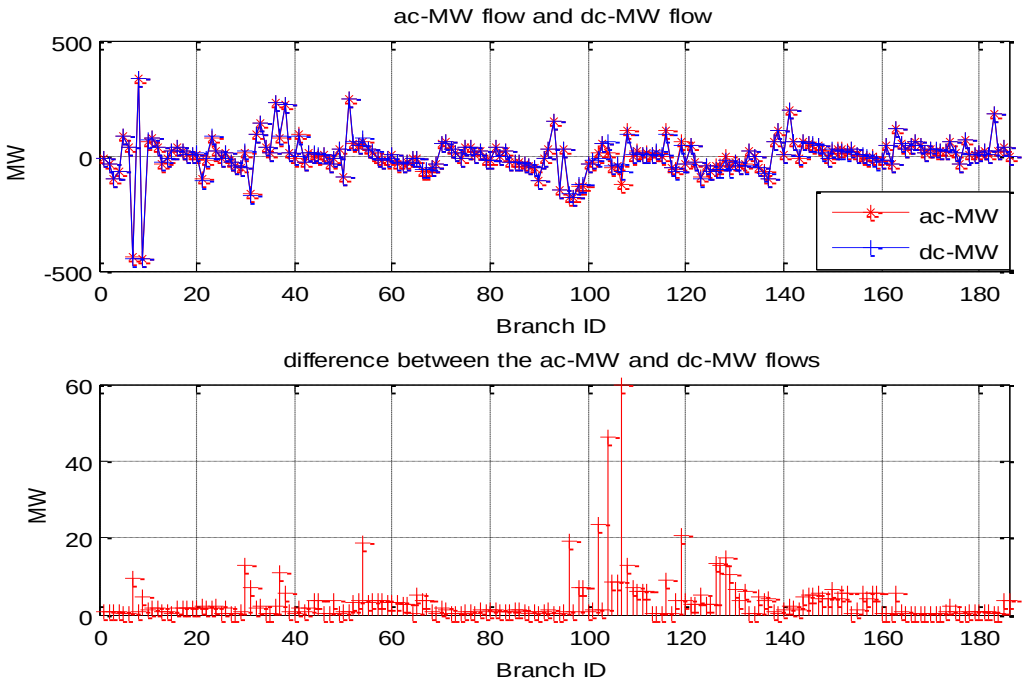

Fig. 3.5 Branch MW-flow differences and MW-flow between ac and classical dc model

Toward this end, four models constructed on different assumptions used for classical dc model were examined, namely ac model with flat voltage profile, the ac model with no resistance, ac model with no resistance and flat voltage profile and classical dc PF model. These four models were tested on the IEEE 118-bus system, respectively. In this test, the PF solutions from the five PF models were compared to the ac PF solutions for each of the aforementioned systems. Fig. 3.6 shows the branch MW-flows errors between each of the four PF models and the ac model for the 118-bus test system. The test results are summarized into Table 3.1 and Fig. 3.6.

Table 3.1 Simulation results for the analysis of the impact of assumptions

	ac model with V=1	ac model with R=0	ac model with R=0 & V=1	Classical dc model
Max difference(MW)	14.8	60.3	59.5	59.5
Average difference (MW)	1.5	3.4	3.4	3.5
Max difference (%)	4.2%	15.7%	15.4%	15.4%
Average difference (%)	0.4%	0.94%	0.98%	0.98%

In Fig. 3.6, the upper part of the figure shows the difference in the branch MW-flow by using the ac PF solution, while the lower part shows the difference in percentage in the branch MW-flow.

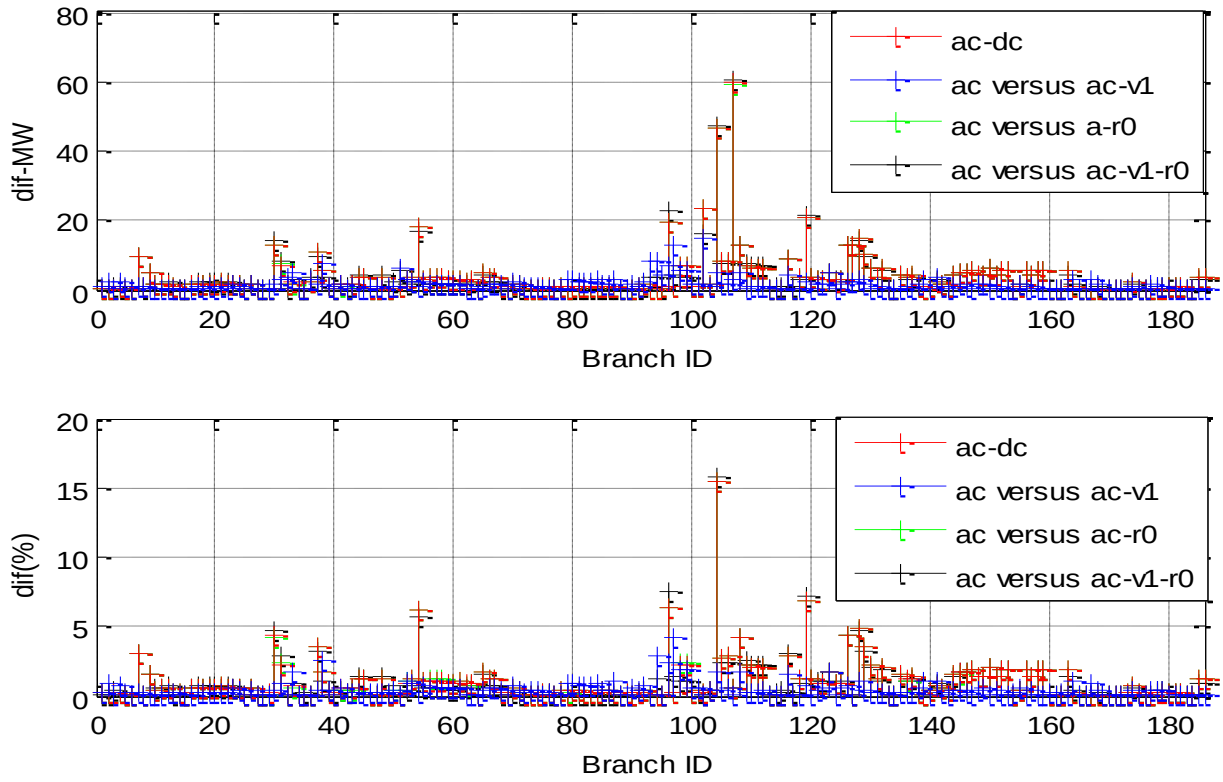

Fig. 3.6 MW branch-flow errors between the ac PF and simplified ac and dc PF for the 118-bus system

According to Table 3.1 and Fig. 3.6, the simulation results verified the theoretical analysis in Chapter 2.2. The ac solution with the fixed-voltage did not deviate from the full ac solution far. The actual errors tend to be much lower than would be expected. The voltage magnitudes of the

IEEE 118-bus system model are in the range 0.94 to 1.05 per-unit. The maximum error that can be introduced is about 10.4% under the base case while the actual maximum error is about 4.2%.

For the ac model without resistance, the MW errors are due to the lossless network. It seems that the branch resistance has a larger impact than the bus voltage on the accuracy of branch MW-flows. Obviously, the dc model with loss compensation would perform much better than the classical dc model.

3.2 Numerical experiments towards the hot-start model accuracy

As discussed in chapter 2.3, hot-start dc models are constructed based on a well-solved ac power-flow solution. In this section, a dc power-flow formulation with net loss dispersal, dc power-flow with halved localized loss compensation and alpha-matching dc power-flow model discussed in the previous chapter are constructed on a base-case ac solution. The performances of these three dc models in the power-flow calculation and LMP calculation are evaluated on the modified 118-bus system. Due to the limit of the calculation capacity and memory, for EI (Eastern Interconnection) 62,000-bus system, only the power flow comparisons are conducted.

summarizes the numerical experiments conducted.

- Branch power-flow comparison

The detailed simulation results for the modified IEEE 118 bus system are summarized in Table 3.2 and Fig. 3.7. Clearly, these three dc models perform much better than the classical dc model. It is obvious that loss compensation is essential in the dc case. By scaling loads at each bus in terms of a single multiplier to compensate the MW losses in the system, the maximum difference of the dispersed-loss dc model is about 14.8 MW. As expected, the localized-loss dc model has a better performance than the dispersed-loss dc model under the base case by compensating the MW losses locally. As shown in Table 3.2, the maximum MW difference of

the localized-loss dc model is around 13.2 MW, while the maximum error for α-matching is essentially 0 MW. For the base point, the accuracy of α-matching dc power-flow model is the best among these three dc power-flow models. By exactly matching the ac base case, the α-matching dc power-flow model provides essentially an exact fit to the ac power-flow model, as it should.

Table 3.2 Simulation results for the modified IEEE 118 system

	Hot-start dispersed-loss dc model	Hot-start localized-loss dc model	Hot-start alpha-matching dc model	Classical dc model (for reference)
Max difference(MW)	16.4	13.2	1.2e-11	59.5
Average difference (MW)	1.6	1.0	6.5e-13	3.5
Max difference (%)	4.95%	2.84%	0%	15.4%
Average difference (%)	0.43%	0.28%	0%	0.98%

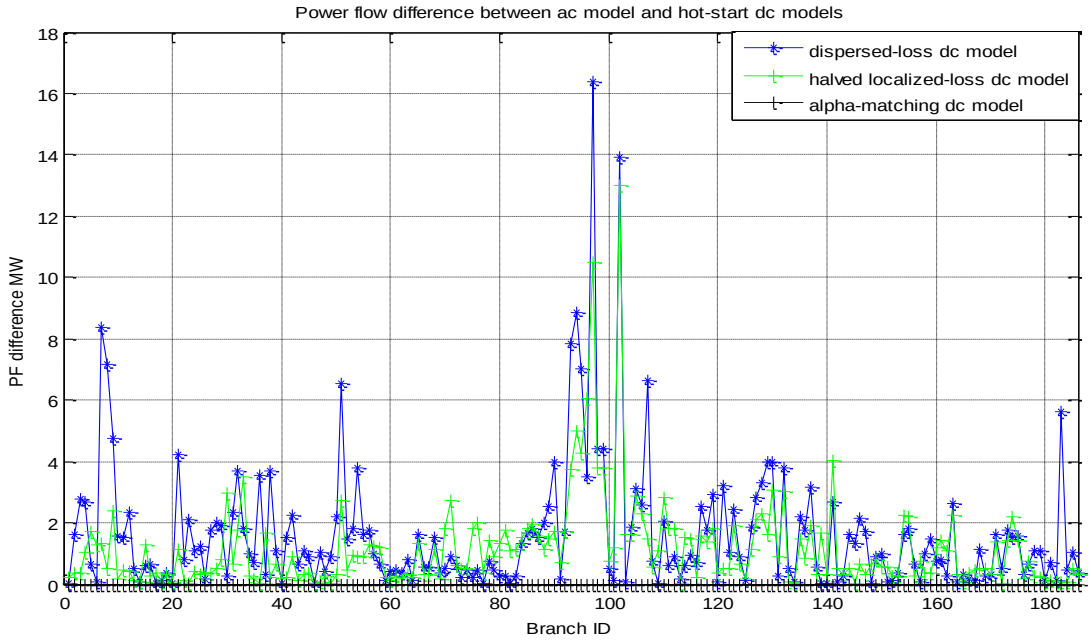

Fig. 3.7 MW branch-flow errors between the ac PF and the hot-start dc PFs for the 118-bus system

Further, comparisons are conducted on 62,000-bus Eastern Interconnection (EI). The simulation results are summarized in Table 3.3.

Table 3.3 Simulation results for the EI system

	Hot-start dispersed-loss dc model	Hot-start halved localized loss dc model	Hot-start Alpha-matching dc model	Classical dc model (for reference)
Max difference(MW)	378.8	57.8	0.9	1525.7
Average difference (MW)	3.51	1.2	0.01	11.3
Max difference (%)	57.7	1.6	0.3	173.2
Average difference (%)	1.70	0.33	0.0058	4.5

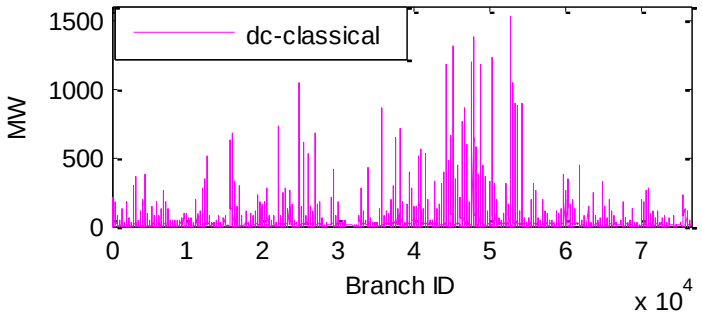

Fig. 3.8 MW branch-flow errors between the classical dc model and ac model

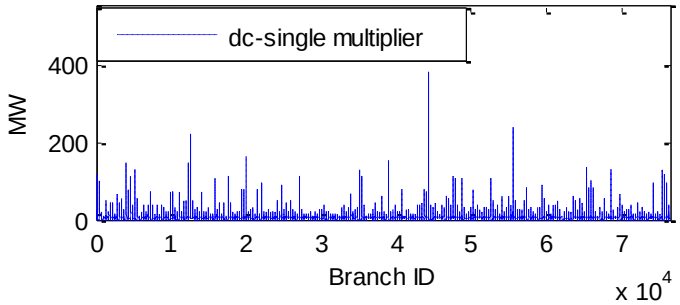

Fig. 3.9 MW branch-flow errors between the dc model with single multiplier and ac model

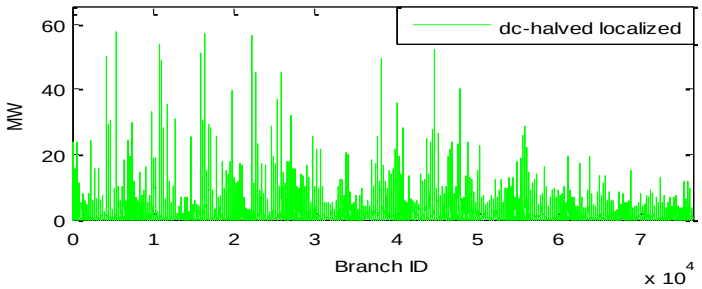

Fig. 3.10 MW branch-flow errors between the dc model with halved localized loss compensation and ac model

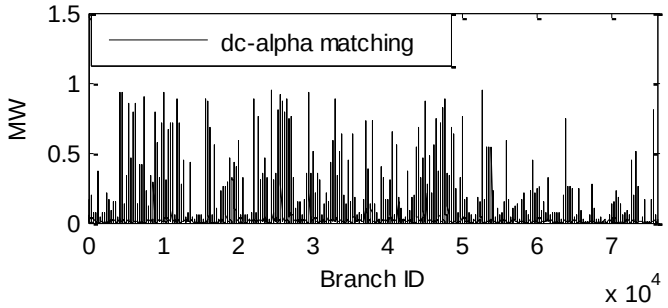

Fig. 3.11 MW branch-flow errors between the α-matching dc model and ac model

The errors in percentage only include lines that had MVA limits in the data set. Compared to the pervious test cases, even though the percentage losses do not vary wildly between test systems, the total active losses of the EI system is considerably larger due to its size. As mentioned before, the classical dc model without loss compensation has the worst performance among these three dc power-flow model studies; one cause is the need for the slack bus to compensate for the absence of losses in the dc case. By compensating for losses by scaling loads at each bus, the dc power-flow model with loss compensation performs significantly better than the classical model, something not seen in the modified 118-bus system, giving credence to the claim that the model accuracy is system dependent. Further, the errors introduced by the dc model with localized loss compensation are reduced by compensating the MW losses locally. By exactly matching the ac base case, the α-matching dc power-flow model provides essentially an exact fit to the ac power-flow model, as it should.

3.3 Numerical experiments towards the cold-start model accuracy

Cold-start dc power-flow models are built when an initial solved ac power flow solution is unavailable. In this section, the cold-start dc model based on a fixed-voltage ac power-flow solution is examined. Fig. 3.12 summarizes the numerical experiments conducted.

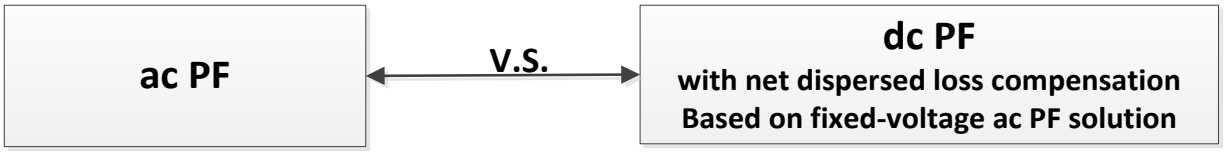

Fig. 3.12 Numerical simulations conducted

- Branch power-flow comparison

Comparing the performance of the hot-start dispersed-loss dc model and the cold-start dispersed-loss dc model, the performances are very similar. As shown in section 3.1, the fixed-voltage ac solution is not far from the full ac solution. The loss estimation based on this cold-start model is obviously acceptable. The power flows calculated based on the cold-start dispersed-loss dc model are compared to the original ac PF solution. The simulation results are summarized in Table 3.4 and Fig. 3.13.

Table 3.4 Simulation results for the comparison between cold-start dc model and ac model

	Cold-start dispersed-loss dc model	Classical dc model (for reference)
Max difference(MW)	16.3	59.5
Average difference (MW)	1.6	3.5
Max difference (%)	4.93%	15.4%
Average difference (%)	0.43%	0.98%

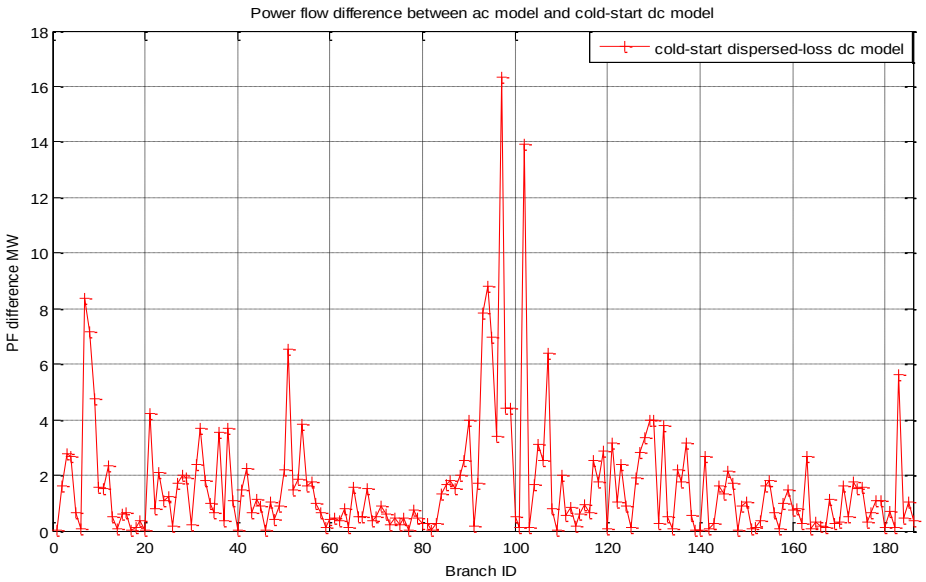

Fig. 3.13 MW branch-flow errors between the ac PF and the cold-start dc PF for the 118-bus system

3.4 Numerical experiments in LMP calculation

Considering the pervasive use of the dc models in the electricity market, dc models are further compared in terms of their LMP calculation and the congestion pattern results. The congestion pattern is indicated by the branch binding constraints in the OPF study. The simulation results are summarized in Table 3.5 and Fig. 3.14.

Table 3.5 OPF solutions for the modified IEEE 118-bus system

Model	Total cost ($/hr)	Binding constraints [Branch]		Average LMP ($/MWh)
		From bus	To bus	
ac model	130060.61	8	9	39.56
		9	10	
Hot-start dispersed-loss dc model	131748.45	8	9	40.01
		9	10	
Hot-start halved localized loss dc model	131751.98	None	None	40.06
Hot-start alpha-matching dc model	13175.98	None	None	40.06
Cold-start dispersed-loss dc model	131705.92	8	9	39.97
		9	10	
Classical dc model	126434.23	8	9	39.86
		9	10	

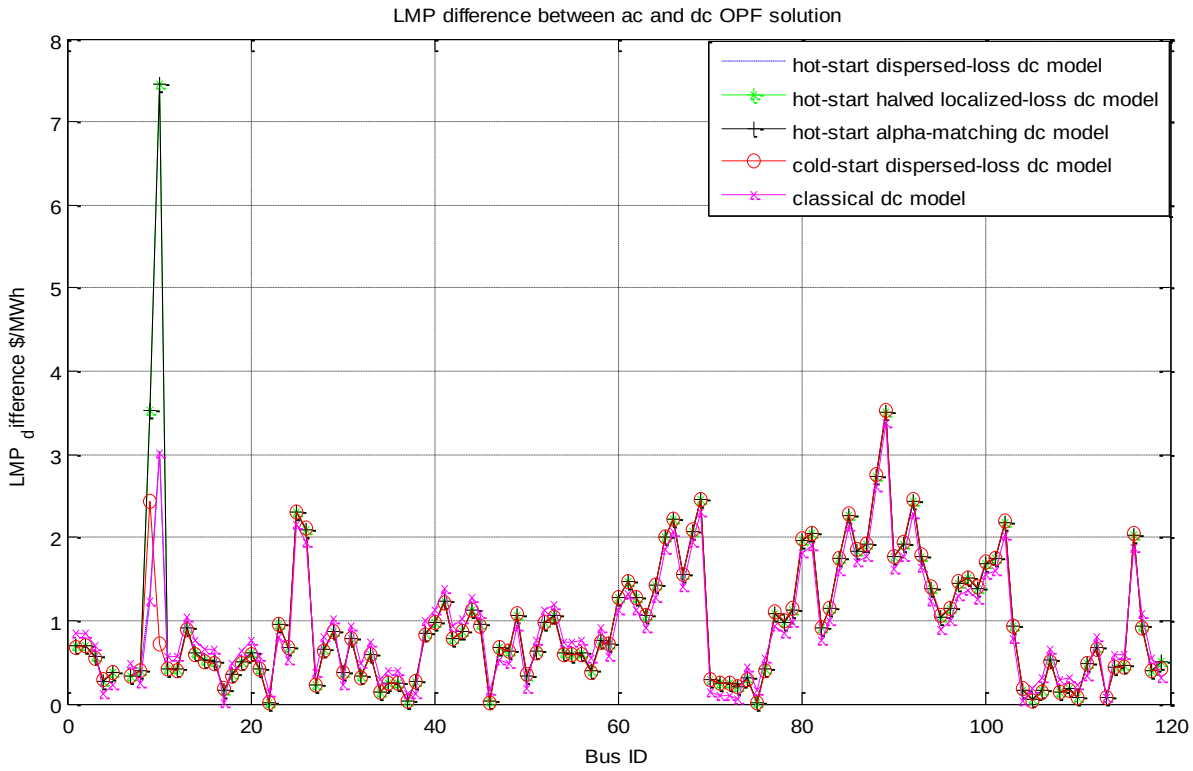

Fig. 3.14 LMP comparisons for modified IEEE118 system

The total cost of each of the loss-compensated dc models is similar to the total cost of the ac model. Also, the overall agreement of LMPs is good. However, for the hot-start alpha-matching dc model and the hot-start halved localized-loss dc model, since they have no binding constraints, the deviations of LMP at some individual buses (related to the congested lines in ac solution) were significant. On the other hand, for the classical dc model, the hot-start dispersed-loss dc model and the cold-start dispersed-loss dc model, the binding constrains in those three models are same as ones shown in the ac OPF results. Although those dc models that did not perform well in the power-flow comparison, they did a good job of revealing the congestion patterns that would actually occur using the full ac system. But, for hot-start alpha-matching dc model and hot-start halved localized-loss dc model, the branch power flows of the binding constraints shown in other dc models are 2 to 5MW less than 300MW (line limit for these two branches),

which shows how close these models also are to predicting the same congestion pattern.

3.5 Effect of contingencies on accuracy

In order to evaluate the change in accuracy of these models for operating conditions that deviate from the base case, *N*-1 contingency analysis is performed in this section. For the generator outages, the extra slack is picked up by the system slack bus. For line outages, no adjustments in the loss compensation are made, even though system losses change.

- Modified IEEE 118-bus system

In this case, all the possible contingencies, which include outages on all 186 branches and 54 generators, are modeled as change-cases. For each dc model, the dc PF results were calculated and compared to the full ac PF result under all the possible outages. The simulation results conducted on the modified IEEE 118-bus system are summarized in Table 3.6.

Table 3.6 Summary of contingencies in the modified IEEE 118-bus system comparing to ac PF

	Classical dc model	Hot-start dispersed-loss dc model	Hot-start halved localized-loss dc model	Hot-start alpha-matching dc model	Cold-start dispersed-loss dc model
Max Difference (MW)	77.4	24.9	26.5	21.5	26.7
Average Difference (MW)	3.67	1.02	1.6	0.19	1.6
Max Difference (%)	22.6%	8.3%	8.3%	7.2%	8.5%
Average Difference (%)	1.04%	0.29%	0.44%	0.05%	0.44%

Since the classical dc model is state-independent and because its accuracy is so poor even for the base case, its performance does not degrade much under contingency conditions (c.f. Table 3.2 and Table 3.6) due to the change in operating point. Similarly the performance of the dc power-flow model with loss compensation, which is state-dependent, does not deteriorate much the base case (c.f. Table 3.2 and Table 3.6). It is somewhat surprising that even though the halved localized-loss model assigns the losses on each branch to that branch, the performance of

the halved localized-loss dc model performs worse than the dispersed-loss dc model. The α-matching model has the best performance. Since the α-matching model is constructed to match the based-case exactly, and since the contingency condition will often not be extremely different from the base case, it is expected that those errors will be smaller than those of the other models.

For large-scale power systems, contingency analysis is rather limited due to the computational demands, though contingency ranking algorithms can screen contingencies so that fewer need be considered. For the EI system, a number of random lines and generators (10 lines and 10 generators) at different voltage levels are selected to be outaged for testing the equivalents for change-cases. For the generator outages, the extra slack is picked up by the system slack bus. For line outages, no adjustments are made, even though system losses change. The simulation results are summarized in Table 3.7. In this table, the maximum error is the maximum branch power flow error that occurs over any branch for all the contingencies.

Table 3.7 Summary of contingencies in the EI system compared to an ac PF model

	Classical dc model	Hot-start dispersed-loss dc model	Hot-start localized-loss dc model	Hot-start alpha-matching dc model
Max Difference (MW)	1525.5	379.4	382.5	9.23
Average Difference (MW)	11.35	3.5	3.8	0.02
Max Difference (%)	174.4	57.7	60.1	2.3
Average Difference (%)	4.6	1.7	2.3	0.18

As shown in Table 3.7 and Table 3.3, the α-matching model still performs best. The average error is similar to its performance in the base case. Since the α-matching model is constructed to match the based-case exactly, and since the contingency condition will often not be extremely different from the base case, it is expected that these errors will be smaller than those of the other models. However, since this contingency analysis is only conducted on 20 random elements, the experiments in this data set may not enough to draw a general conclusion. As we can see from

Table 3.7, the maximum error of the α-matching dc model grows about 10 times larger than is seen in the base case. It is possible that α-matching dc model may perform worse than other dc models when it comes to some specific contingencies. For other dc models, their performances in the contingency analysis are rather similar to their performances in the base-case, which are consistent with their models performances in the 118-bus system.

3.6 Summary

Considering the pervasive use of the dc power-flow model, the accuracy of dc power-flow models is of great concern. In this chapter, accuracy tests are conducted on several state-dependent and state-independent dc models. The state-dependent dc power-flow models take into consideration the system losses and bus voltage values at a suitable state. The state-independent dc power-flow models assume a lossless network, one-per-unit voltage values, and small voltage angle differences.

For the state-independent dc model, the large MW power-flow errors of the classical model occur on the lines that are located near the slack bus, which is expected since all of losses (not accounted for) in the classical model must be compensated by reduced generation at the slack bus, a reduction that can become quite large for large systems. This reduced generation will change the branch flows radically near the slack bus. For the state-dependent dc models, this chapter examines the hot-start dc model and cold-start dc model. The performance of the hot-start dc models, including the dc power-flow model with net dispersed loss compensation, dc model with halved localized loss compensation and α-matching dc power-flow model are compared with that of a full ac PF solution. For the cold-start dc model, dc power-flow model with net dispersed loss compensation is constructed.

Accuracy tests using these four dc models, including classical dc model, hot-start dispersed-loss dc model, hot-start localized-loss dc model and hot-start alpha-matching dc model,are conducted on two test power systems: the modified IEEE 118-bus system and the 62,000-bus Eastern Interconnection system. For the 118-bus system, errors introduced by these dc power-flow models in the power-flow results and LMP calculations are quantified and compared. For the EI 62,000-bus system, only the power-flow comparisons are conducted. Also, contingency analysis is performed to evaluate the change in accuracy of these dc models for operating conditions that deviate from the base case. For 118-bus system, the reestablished operating points to all of the possible contingencies are quantified and compared with the full ac solution; whereas, considering the computational demands of all the contingencies for EI system, only 20 random elements are outaged to test for the changed cases.

The classical dc model is state-independent and simple to construct. However, the accuracy of the classical model will not be satisfactory in most applications. Although the net dispersed loss-compensated dc model performs similarly to the classical model in the 118-bus system case, its performance is much better than the classical model in the 62,000-bus system. Clearly, something in the 62,000-bus system not seen in the 118-bus system gives credence to the claim that the model accuracy is system dependent.

In the base-case comparison, the halved localized loss-compensated dc model has better performance than the dc model with net loss dispersal Furthermore, since the α-matching dc model is structured to match the base case exactly, it performs the best among these four for the base case, as expected. It localizes the losses and calculates the branch admittance to exactly match the base case.

However, in the OPF result comparisons, the localized loss-compensated dc model and the α-matching dc model do not reveal the congestion pattern for the modified IEEE 118-bus system well. At this point, it is not clear whether those two models with acceptable accuracy would be good candidates for the electricity market and system planning studies. Further experiments are needed to explore their performances in the LMP-based market studies.

In the PF comparisons, we expected that there would be an accuracy gap between the hot-start and cold-start models. However, the difference between the cold-start loss-dispersed dc model and the hot-start loss-dispersed dc model is not large. In contingency analysis, the performance of classical and the loss-compensated models are similar. The α-matching model performs the best as expected.

CHAPTER 4 . PTDF-BASED DC PF MODEL BASED ON AC PTDFS

It is known that ac PTDF provides a more accurate allocation of the MW loading on the transmission line than classical dc model. In order to obtain a more accurate reduced equivalent system for power market analysis and investment planning studies, a hot- start optimal dc power-flow model based on ac power transfer distribution factors (PTDFs) is proposed in this chapter.

4.1 Introduction

Generally, considering the unknown accuracy of the dc PTDFs due to the assumptions involved in the dc power-flow models, dc PTDF calculations may contain serious errors when it comes to the large deviations from the flat voltage profile, small X/R ratio or large voltage angle differences; whereas, the ac PTDF yields more accurate sensitivities of flows to bus injections by taking into account resistance, voltage magnitudes as well as angles. Therefore, the equivalent reactances evaluated based on ac PTDFs provide a better network that can preserve the essential characteristics of the original ac network.

There are two steps involved in finding an optimal-reactance-only dc model from a full ac model: translating ac PTDFs into equivalent dc PTDF's for the full model and then using these dc PTDFs to find a reactance-only model that optimally matches dc PTDF's for the model.

For the first part, ac PTDFs are calculated at the base-case load flow result. Then, considering the nonlinear properties of the ac power-flow equation, a linear least squares state (LLS) estimation process is applied to get equivalent dc PTDFs based on ac PTDFs. By applying a reactance evaluation algorithm, an optimal dc network can be obtained for the full system based on the equivalent dc PTDFs.

The third step (if needed) is to generate a reduced optimal dc equivalent for the full model. In this part, the bus clustering is obtained by using k-means++ method based on the dc PTDFs. Based on the bus clustering result, the generators and loads are aggregated within each zone. Then, the reactance of the equivalent lines for the reduced system is evaluated by using a weighted least squares (WLS) state estimation process.

The flowchart of the whole process is summarized in Fig.4.1. The left-hand side shows the process of evaluating the equivalent dc network starting from an ac network. The right-hand side shows the process of network reduction starting from a dc network.

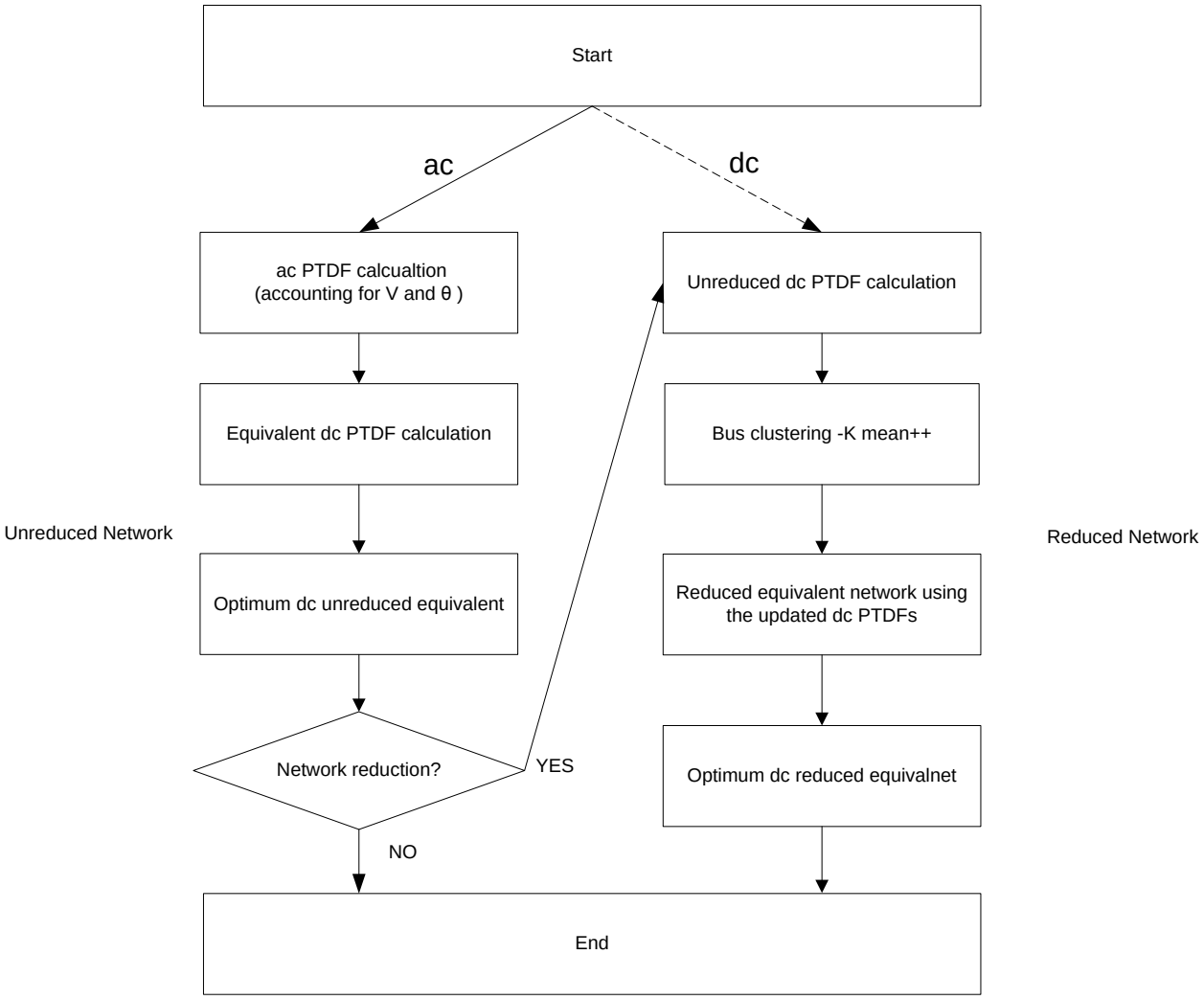

Fig.4.1 General process of network reduction

4.2 PTDF calculations

4.2.1 dc PTDF calculation

In the dc PF model, since dc PTDFs are calculated based on the assumptions of a lossless network, one-per-unit voltage values, and small voltage angle differences, the power injection and branch power flow are linearly related to the bus voltage angle, which can be written, for an *N+1* bus system with *L* branches, as:

$$\boldsymbol{P}_{inj} = \boldsymbol{B}_{bus}\boldsymbol{\theta} \tag{4.1}$$

$$\boldsymbol{P}_{flow} = \boldsymbol{B}_{branch}\boldsymbol{\theta} \tag{4.2}$$

Where

$\boldsymbol{P}_{inj}$: Bus net injection vector with the dimension of *N* by 1;

$\boldsymbol{P}_{flow}$: Branch power flow vector with the dimension of *L* by 1;

$\boldsymbol{B}_{bus}$: Bus susceptance matrix with the dimension of *N* by *N*;

$\boldsymbol{B}_{branch}$: Branch susceptance matrix with the dimension of *L* by *N*;

$\boldsymbol{\Theta}$: Bus voltage angle vector with the dimension of *N* by 1.

Combing (4.1) and (4.2), the branch power flow is:

$$\boldsymbol{P}_{flow} = \boldsymbol{B}_{branch}\boldsymbol{B}_{bus}^{-1}\boldsymbol{P}_{inj} \tag{4.3}$$

Then, the system dc PTDF is written as:

$$\boldsymbol{\Phi} = \boldsymbol{B}_{branch}\boldsymbol{B}_{bus}^{-1} \tag{4.4}$$

Since the bus susceptance matrix $\boldsymbol{B}_{bus}$ and the branch susceptance matrix $\boldsymbol{B}_{branch}$ can be calculated in terms of node-branch incidence matrix $\boldsymbol{C}$ and the branch reactance vector $\boldsymbol{x}$ is given as:

$$\boldsymbol{B}_{bus} = \boldsymbol{C}^T diag(1/\boldsymbol{x})\boldsymbol{C} \tag{4.5}$$

$$\boldsymbol{B}_{branch} = diag(1/\boldsymbol{x})\mathbf{C} \tag{4.6}$$

where

$$\text{where } diag(1/\mathbf{x}) = \begin{bmatrix} 1/x_1 & 0 & \cdots & 0 \\ 0 & 1/x_2 & & \\ \vdots & & \ddots & \\ 0 & & & x_L \end{bmatrix} \text{ and } \mathbf{x} = \begin{bmatrix} x_1 \\ x_2 \\ \vdots \\ x_L \end{bmatrix} \tag{4.7}$$

Then, the dc PTDF matrix can be expressed as:

$$\boldsymbol{\Phi} = diag(1/\boldsymbol{x})\boldsymbol{C}[\boldsymbol{C}^T diag(1/\boldsymbol{x})\boldsymbol{C}]^{-1} \tag{4.8}$$

4.2.2 Linearized ac PTDF calculation

Power transfer distribution factors (PTDF) are defined as the MW change in a branch flow due to 1 MW exchange between a bus and the reference bus. The PTDF matrix represents the sensitivities of power flows to bus injections can be defined as:

$$PTDF_k^n = \left.\frac{\partial P_{ij}}{\partial P_n}\right|_{x=x^0} \tag{4.9}$$

where

P_{ij} is the power flow through branch *i*-*j*;

P_n is the power injected at bus *n*;

$\boldsymbol{x}^0$ is the operating point of the system;

Superscript *n* indicates that the bus *n* is the sending end bus;

Subscript *k* indicates that branch *k* connects bus *i* and bus *j*.

The ac PTDFs are derived using sensitivity properties of Newton-Raphson power flow at a base-case load-flow result. The ac PTDF are determined by branch parameters, the operating conditions and the network topology. Any changes of network topology or network parameters such

as line impedances will affect these sensitivities. Recall the discussion in section 2.2 about the assumptions of the classical dc PF model: the dc PTDF is evaluated assuming flat voltage profile using the decoupling assumptions. Therefore the dc PTDF depends only on the network topology and the network reactances.

- Polar form of ac PF equations

Recall that for the typical transmission line model connecting bus *i* and bus *j* shown in Fig. 2.1, the real and reactive power balance equations at bus *i* are:

$$P_i = V_i \sum_j \left[G_{ij} \cos(\delta_i - \delta_j) + B_{ij} \sin(\delta_i - \delta_j) \right] V_j \qquad (4.10)$$

$$Q_i = V_i \sum_j \left[G_{ij} \sin(\delta_i - \delta_j) - B_{ij} \cos(\delta_i - \delta_j) \right] V_j \qquad (4.11)$$

where

P_i :the real power injected into bus *i*, which is P_i^G-P_i^L;

Q_i : the reactive power injected into bus *i*, which is Q_i^G-Q_i^L.

P_i^G, Q_i^G : the real and reactive power of generators injected at bus *i;*

P_i^L, Q_i^L: the real and reactive power of load withdrawn at bus *i*.

The process of solving the power flow equations is iterated by using the following equation:

$$\begin{bmatrix} \Delta \mathbf{P} \\ \Delta \mathbf{Q} \end{bmatrix} = \begin{bmatrix} \dfrac{\partial \mathbf{P}}{\partial \boldsymbol{\delta}} & \dfrac{\partial \mathbf{P}}{\partial \mathbf{V}} \\ \dfrac{\partial \mathbf{Q}}{\partial \boldsymbol{\delta}} & \dfrac{\partial \mathbf{Q}}{\partial \mathbf{V}} \end{bmatrix} \begin{bmatrix} \Delta \boldsymbol{\delta} \\ \Delta \mathbf{V} \end{bmatrix} \qquad (4.12)$$

Where

$\begin{bmatrix} \dfrac{\partial \mathbf{P}}{\partial \boldsymbol{\delta}} & \dfrac{\partial \mathbf{P}}{\partial \mathbf{V}} \\ \dfrac{\partial \mathbf{Q}}{\partial \boldsymbol{\delta}} & \dfrac{\partial \mathbf{Q}}{\partial \mathbf{V}} \end{bmatrix}$: Jacobian matrix with the dimension of (2*N*-*m*) by (2*N*-*m*), where *m* is the number of PV buses;

$\begin{bmatrix} \Delta\mathbf{P} \\ \Delta\mathbf{Q} \end{bmatrix}$: Power mismatch matrix with the dimension of (2*N*-*m*) by 1;

$\begin{bmatrix} \Delta\boldsymbol{\delta} \\ \Delta\mathbf{V} \end{bmatrix}$: Bus voltage and angle mismatch matrix with the dimension of (2*N*-*m)* by 1.

The derivatives are calculated as follows:

$$
\begin{aligned}
&\frac{\partial P_i}{\partial \delta_j} = V_i\, V_j [G_{ij}\sin(\delta_i - \delta_j) - B_{ij}\cos(\delta_i - \delta_j) = H_{ij} \{i \neq j\} \\
&\frac{\partial P_i}{\partial \delta_i} = -Q_i^{calc} - B_{ii}V_i^2 = H_{ii} \{i = j\} \\
&\frac{\partial Q_i}{\partial \delta_j} = -V_i\, V_j [G_{ij}\cos(\delta_i - \delta_j) + B_{ij}\sin(\delta_i - \delta_j)] \{i \neq j\} \\
&\frac{\partial Q_i}{\partial \delta_i} = P_i^{calc} - G_{ii}V_i^2 \{i = j\} \\
&\frac{\partial P_i}{\partial V_j} = V_i [G_{ij}\cos(\delta_i - \delta_j) + B_{ij}\sin(\delta_i - \delta_j)] \{i \neq j\} \\
&\frac{\partial P_i}{\partial V_i} = \frac{P_i^{calc}}{V_i} + G_{ii}V_i \ \{i = j\} \\
&\frac{\partial Q_i}{\partial V_j} = V_i [G_{ij}\sin(\delta_i - \delta_j) - B_{ij}\cos(\delta_i - \delta_j)] \{i \neq j\} \\
&\frac{\partial Q_i}{\partial V_i} = \frac{Q_i^{calc}}{V_i} - B_{ii}V_i \ \{i = j\}
\end{aligned}
\qquad (4.13)
$$

where

$$Q_i^{Calc} = V_i \sum_j \left[G_{ij}\sin(\delta_{ij}) - B_{ij}\cos(\delta_{ij}) \right] V_j^0$$

$$P_i^{Calc} = V_i \sum_j \left[G_{ij}\cos(\delta_{ij}) + B_{ij}\sin(\delta_{ij}) \right] V_j^0$$

- Sensitivities of voltage magnitude and angle

In order to indicate a MW transfer in the system, a vector that describes the seller and buyer is defined as matrix $\Delta\mathbf{P}_{source}$ with the dimension of *N* by 1, which is constructed based on the following guidelines:

- It contains only 0's and 1's;
- Element $\Delta\mathbf{P}_{source}$ (i, 1) at row i is 1 if, in the power system bus i is the source bus;
- Element at row i is 0 if, in the power system bus i is not the source bus;
- For convenience, bus N+1 is always designated to be the sink bus.

Therefore, if bus k is the source bus, $\Delta\mathbf{P}_{source}$ will be:

$$\Delta P_{\text{source}} = [\overbrace{0 \quad \cdots \quad 0 \quad 1 \quad 0 \quad \cdots \quad 0}^{\text{N elements}}]^T \qquad (4.14)$$

(1 at the k^{th} position)

Then, the Jacobian matrix at the present operating point is used to calculate bus voltage magnitude and angle sensitivities:

$$\begin{bmatrix} \Delta\boldsymbol{\delta} \\ \Delta\mathbf{V} \end{bmatrix} = \begin{bmatrix} \dfrac{\partial\mathbf{P}}{\partial\boldsymbol{\delta}} & \dfrac{\partial\mathbf{P}}{\partial\mathbf{V}} \\ \dfrac{\partial\mathbf{Q}}{\partial\boldsymbol{\delta}} & \dfrac{\partial\mathbf{Q}}{\partial\mathbf{V}} \end{bmatrix}^{-1} \begin{bmatrix} \Delta\mathbf{P} \\ \Delta\mathbf{Q} \end{bmatrix} = \mathbf{J}^{-1} \begin{bmatrix} \Delta\mathbf{P} \\ \Delta\mathbf{Q} \end{bmatrix} \qquad (4.15)$$

Therefore, the voltage magnitude and angle sensitivity of the source sending real power to the slack bus can be determined as:

$$\begin{bmatrix} \Delta\boldsymbol{\delta} \\ \Delta\mathbf{V} \end{bmatrix} = [\mathbf{J}^{-1}] \begin{bmatrix} \Delta\mathbf{P}_S \\ \mathbf{0} \end{bmatrix} \qquad (4.16)$$

- ac PTDF calculation

For a transmission line spanning bus i and bus j, real power (P_{ij}) and reactive power (Q_{ij}) in a line-k connected between bus i and bus j can be written:

$$P_{ij} = V_i V_j \left[G_{ij} \cos(\delta_i - \delta_j) + B_{ij} \sin(\delta_i - \delta_j) \right] + V_i^2 G_{ii} \quad (4.17)$$

$$Q_i = V_i V_j \left[G_{ij} \sin(\delta_i - \delta_j) - B_{ij} \cos(\delta_i - \delta_j) \right] - V_i^2 B_{ii} \quad (4.18)$$

Considering that the branch power flows are functions of the voltage magnitude and voltage angles, ac PTDFs are functions of those voltage magnitudes and angles. Therefore, the derivatives of the branch power flow with respect to the voltages and angles can be calculated as:

$$\Delta P_{ij} = \frac{\partial P_{ij}}{\partial \delta_i} \Delta \delta_i + \frac{\partial P_{ij}}{\partial \delta_j} \Delta \delta_j + \frac{\partial P_{ij}}{\partial V_i} \Delta V_i + \frac{\partial P_{ij}}{\partial V_j} \Delta V_j \quad (4.19)$$

$$\Delta Q_{ij} = \frac{\partial Q_{ij}}{\partial \delta_i} \Delta \delta_i + \frac{\partial Q_{ij}}{\partial \delta_j} \Delta \delta_j + \frac{\partial Q_{ij}}{\partial V_i} \Delta V_i + \frac{\partial Q_{ij}}{\partial V_j} \Delta V_j \quad (4.20)$$

Also, (4.19) and (4.20) can be rewritten as:

$$\Delta P_{ij} = a_{ij} \Delta \delta_i + b_{ij} \Delta \delta_j + c_{ij} \Delta V_i + d_{ij} \Delta V_j \quad (4.21)$$

$$\Delta Q_{ij} = a'_{ij} \Delta \delta_i + b'_{ij} \Delta \delta_j + c'_{ij} \Delta V_i + d'_{ij} \Delta V_j \quad (4.22)$$

where

$$a_{ij} = V_i V_j [-g_{ij} \sin(\delta_i - \delta_j) + b_{ij} \cos(\delta_i - \delta_j)]$$

$$b_{ij} = V_i V_j [g_{ij} \sin(\delta_i - \delta_j) - b_{ij} \cos(\delta_i - \delta_j)]$$

$$c_{ij} = V_j [g_{ij} \cos(\delta_i - \delta_j) + b_{ij} \sin(\delta_i - \delta_j)] + 2 V_i g_{ii}$$

$$d_{ij} = V_i [g_{ij} \cos(\delta_i - \delta_j) + b_{ij} \sin(\delta_i - \delta_j)]$$

$$a'_{ij} = V_i V_j [-g_{ij} \sin(\delta_i - \delta_j) - b_{ij} \cos(\delta_i - \delta_j)]$$

$$b'_{ij} = V_i V_j [g_{ij} \sin(\delta_i - \delta_j) + b_{ij} \sin(\delta_i - \delta_j)]$$

$$c'_{ij} = V_j [g_{ij} \cos(\delta_i - \delta_j) - b_{ij} \sin(\delta_i - \delta_j)] - 2 V_i b_{ij}$$

$$d'_{ij} = V_i [g_{ij} \cos(\delta_i - \delta_j) - b_{ij} \sin(\delta_i - \delta_j)]$$

Since $\Delta \delta_i$, $\Delta \delta_j$, ΔV_i and ΔV_j have already been calculated before, ac PTDFs are calculated by (4.19). The *L*-by-*N* ac PTDF matrix is shown as follows:

$$\boldsymbol{\Phi}_{ac} = \boldsymbol{\Phi}' = \begin{bmatrix} \boldsymbol{\varphi}'^{1} & \boldsymbol{\varphi}'^{2} & \cdots & \boldsymbol{\varphi}'^{N} \end{bmatrix} = \begin{bmatrix} \varphi'_{11} & \varphi'_{12} & \cdots & \varphi'_{1N-1} & \varphi'_{1N} \\ \vdots & \vdots & \ddots & \vdots & \vdots \\ \varphi'_{i1} & \varphi'_{i2} & \cdots & \varphi'_{iN-1} & \varphi'_{iN} \\ \vdots & \vdots & \ddots & \vdots & \vdots \\ \varphi'_{j1} & \varphi'_{j2} & \cdots & \varphi'_{jN-1} & \varphi'_{jN} \\ \vdots & \vdots & \ddots & \vdots & \vdots \\ \varphi'_{1k1} & \varphi'_{1k2} & \cdots & \varphi'_{1kN-1} & \varphi'_{1kN} \\ \vdots & \vdots & \ddots & \vdots & \vdots \end{bmatrix} \tag{4.23}$$

4.3 Equivalent dc PTDF calculation

Considering the inconsistency of the ac PTDFs due to the MW losses in the power system, the equivalent dc PTDFs will be evaluated using a linear least squares (LLS) formulation. During this process, ac PTDFs are used as measurements to evaluate dc PTDFs.

Assuming the equivalent *L*-by-*N* dc PTDF matrix is written as:

$$\boldsymbol{\Phi}_{dc} = \boldsymbol{\Phi} = \begin{bmatrix} \boldsymbol{\varphi}^{1} & \boldsymbol{\varphi}^{2} & \cdots & \boldsymbol{\varphi}^{N} \end{bmatrix} = \begin{bmatrix} \varphi_{11} & \varphi_{12} & \cdots & \varphi_{1N-1} & \varphi_{1N} \\ \vdots & \vdots & \ddots & \vdots & \vdots \\ \varphi_{i1} & \varphi_{i2} & \cdots & \varphi_{iN-1} & \varphi_{iN} \\ \vdots & \vdots & \ddots & \vdots & \vdots \\ \varphi_{j1} & \varphi_{j2} & \cdots & \varphi_{jN-1} & \varphi_{jN} \\ \vdots & \vdots & \ddots & \vdots & \vdots \\ \varphi_{1k1} & \varphi_{1k2} & \cdots & \varphi_{1kN-1} & \varphi_{1kN} \\ \vdots & \vdots & \ddots & \vdots & \vdots \end{bmatrix} \tag{4.24}$$

where Φ_j^i: dc PTDF at branch *j* due to injection at bus *i*.

The evaluation process is an iterated process, which is shown in Fig. 4.2.

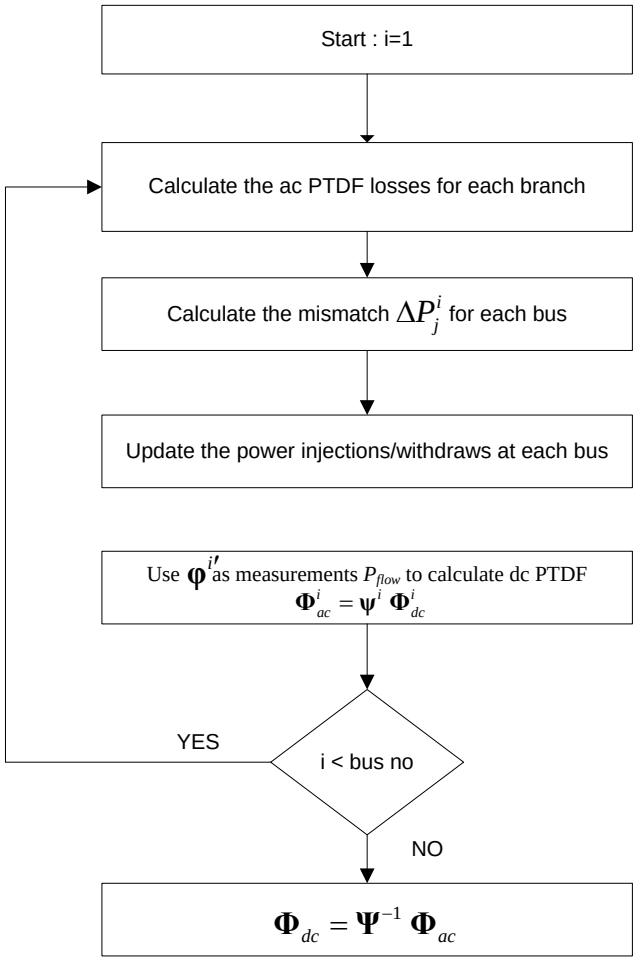

Fig. 4.2 Flowchart for dc PTDF evaluation process

The first step is to extract one column from of the ac PTDF matrix $\boldsymbol{\Phi}$, for example column, *i*, ($\boldsymbol{\varphi}^{\prime i}$), which represents the power division (shift factor) due to the power injection at bus *i*. Since the ac PTDF at the sending end is different from one at the receiving end due to the branch losses, the difference between ac PTDF at the sending end and at the receiving end is defined as PTDF losses. These PTDF losses indicate the inconsistency property of ac PTDFs.

For the experiment related to bus *i*, these ac PTDFs are taken as the power flow measurements due to the injection at bus *i*. In order to match the power flow measurement over each branch, the loss over the each branch is treated as the power withdrawal at the receiving end. Since the sum of power injections and power withdraws at each bus should be equal to zero, the power mismatch

ΔP_j^i at each bus is calculated. After this process is repeated for all the buses, the power mismatch can be written in matrix form as $\Delta \mathbf{P}^i$. Then, the problem is formulated into equations in terms of the definition of PTDF. Therefore, dc PTDFs evaluation formulation for experiment *i* can be written as

$$\mathbf{\Phi}'^i = \mathbf{\Psi}^i \mathbf{\Phi} \tag{4.25}$$

where

$$\mathbf{\Psi}^i = \left[diag(\Delta P_1^i), \quad diag(\Delta P_2^i), \quad \cdots \quad diag(\Delta P_N^i) \right]$$

The previous steps for each column of ac PTDF matrix are repeated, then the following equation to obtain the equivalent dc PTDF is solved:

$$\mathbf{\Phi} = \mathbf{\Psi}^{-1} \mathbf{\Phi}' \tag{4.26}$$

where

$$\mathbf{\Psi} = \begin{bmatrix} \mathbf{\psi}_1 \\ \mathbf{\psi}_2 \\ \vdots \\ \mathbf{\psi}_N \end{bmatrix}$$

Also, (4.26) can be expanded as:

$$\begin{bmatrix} \varphi_1^i \\ \vdots \\ \varphi_i^i \\ \vdots \\ \varphi_j^i \\ \vdots \\ \varphi_k^i \\ \vdots \end{bmatrix} = \begin{bmatrix} \Delta P_1^i & 0 & \cdots & 0 & \Delta P_2^i & 0 & \cdots & 0 & \cdots & \Delta P_N^i & 0 & \cdots & 0 \\ 0 & \Delta P_1^i & \vdots & 0 & \Delta P_2^i & 0 & \vdots & \cdots & 0 & \Delta P_N^i & 0 & \vdots & \\ & \ddots & 0 & \vdots & 0 & \ddots & 0 & \cdots & \vdots & 0 & \ddots & 0 & \\ 0 & 0 & \Delta P_1^i & 0 & \cdots & \Delta P_2^i & \cdots & 0 & \cdots & 0 & \Delta P_N^i & & \end{bmatrix} \begin{bmatrix} \varphi_1^{1'} \\ \vdots \\ \varphi_{k1}^{1'} \\ \vdots \\ \varphi_{l1}^{2'} \\ \vdots \\ \varphi_{k1}^{2'} \\ \vdots \\ \varphi_{l1}^{N-1'} \\ \vdots \\ \varphi_{k1}^{N-1'} \\ \vdots \end{bmatrix} \tag{4.27}$$

As shown in (4.27), the equivalent dc PTDF matrix is evaluated in its entirety.

Or, (4.26) also can be expanded as (4.28) if the PTDF matrix is ordered in a different sequence:

$$\begin{bmatrix} \phi_1'^1 \\ \phi_2'^1 \\ \vdots \\ \phi_L'^1 \\ \phi_1'^2 \\ \phi_2'^2 \\ \vdots \\ \phi_L'^2 \\ \vdots \\ \vdots \\ \phi_1'^N \\ \phi_2'^N \\ \vdots \\ \phi_L'^N \end{bmatrix} = \begin{bmatrix} 1+\Delta P_1^1 & \Delta P_2^1 & \cdots & \Delta P_N^1 & & & & & \cdots & \cdots & & & \\ \Delta P_1^2 & 1+\Delta P_2^2 & \cdots & \Delta P_N^2 & & & \mathbf{0} & & \cdots & \cdots & & \mathbf{0} & \\ \vdots & \vdots & \ddots & \vdots & & & & & & & & & \\ \Delta P_1^N & \Delta P_2^N & \cdots & \Delta P_N^N & & & & & & & & & \\ & & & & 1+\Delta P_1^1 & \Delta P_2^1 & \cdots & \Delta P_N^1 & & & & & \\ & & & & \Delta P_1^2 & 1+\Delta P_2^2 & \cdots & \Delta P_N^2 & \cdots & \cdots & & & \\ & \mathbf{0} & & & \vdots & \vdots & \ddots & \vdots & & & & \mathbf{0} & \\ & & & & \Delta P_1^N & \Delta P_2^N & \cdots & \Delta P_N^N & & & & & \\ & \vdots & & & \vdots & & & & \ddots & \cdots & & \vdots & \\ & \vdots & & & \vdots & & & & \cdots & \ddots & & \vdots & \\ & & & & & & & & & & 1+\Delta P_1^1 & \Delta P_2^1 & \cdots & \Delta P_N^1 \\ & \mathbf{0} & & & \mathbf{0} & & & & \cdots & \mathbf{0} & \Delta P_1^2 & 1+\Delta P_2^2 & \cdots & \Delta P_N^2 \\ & & & & & & & & & & \vdots & \vdots & \ddots & \vdots \\ & & & & & & & & & & \Delta P_1^N & \Delta P_2^N & \cdots & \Delta P_N^N \end{bmatrix} \begin{bmatrix} \phi_1^1 \\ \phi_2^1 \\ \vdots \\ \phi_L^1 \\ \phi_1^2 \\ \phi_2^2 \\ \vdots \\ \phi_L^2 \\ \vdots \\ \vdots \\ \phi_1^N \\ \phi_2^N \\ \vdots \\ \phi_L^N \end{bmatrix} \tag{4.28}$$

As shown in (4.28), basically, each row of the PTDFs can be evaluated separately. However, this form of the evaluation is not convenient to add additional constraints to the evaluation process.

After the losses are modeled by fictitious loads at each bus in the equivalent dc model and the application of the linear least squares state estimation process, the equivalent dc PTDFs are more

consistent, at least consistent within each shift factor. The dc PTDF's are said to be consistent if the sum of the PTDFs into each bus is either 0 or 1.

4.4 Equivalent dc network reactance evaluation

The main objective is to obtain a set of transmission reactances for the equivalent model such that its power flows match the ac power flows of the original system as closely as possible. In this section, an optimization procedure is used to determine the equivalent transmission line reactances that best fit the PTDF matrix of the reduced equivalent network. The minimization of the Euclidean norm, denoted as ||·||, of the difference between the two power flow vectors is used.

This optimization problem is formulated as:

$$\begin{aligned} &\min \left\| \mathbf{P}_{flow}^{ac} - \mathbf{P}_{flow}^{dc} \right\| \\ &s.t. \quad x_i \neq 0, i = 1,2,\cdots N \end{aligned} \tag{4.29}$$

Recall from (4.8) that the dc PTDFs are calculated as $\boldsymbol{\Phi}=diag(\mathbf{1}/\boldsymbol{x})\boldsymbol{C}[\boldsymbol{C}^{\boldsymbol{T}}diag(\mathbf{1}/\boldsymbol{x})\boldsymbol{C}]^{-1}$. Then, multiplying both sides of this equation by the nonsingular matrix $\boldsymbol{C}^{\boldsymbol{T}}diag(\mathbf{1}/\boldsymbol{x})\boldsymbol{C}$ and rearranging yields:

$$(\mathbf{\Phi C}^{\mathbf{T}} - \mathbf{I})diag(\mathbf{1}/\mathbf{x})\mathbf{C} = \mathbf{0} \tag{4.30}$$

Rewrite node-branch incidence matrix $\boldsymbol{C}$ in terms of columns as

$$\mathbf{C} = [\mathbf{c_1}, \mathbf{c_2}, ..., \mathbf{c_N}] \tag{4.31}$$

where $\boldsymbol{c_i}$ entries represents the i^{th} column vector of $\boldsymbol{C}$.

Then, (4.30) can be re-written as the following set of equations:

$$(\mathbf{\Phi C}^{\mathbf{T}} - I)diag(\mathbf{1}/\mathbf{x})\mathbf{c_i} = \mathbf{0}, (i = 1, 2, ..., N) \tag{4.32}$$

Also, it can be shown that (4.32) is equivalent to:

$$(\mathbf{\Phi C}^T - \mathbf{I})diag(\mathbf{c_i})\left(1/\mathbf{x}\right) = \mathbf{0} \tag{4.33}$$

Hence, the set of equations used for evaluating the reactances are:

$$\mathbf{\Lambda}\left(1/\mathbf{x}\right) = \mathbf{0} \tag{4.34}$$

where

$$\mathbf{\Lambda} = \begin{bmatrix} (\mathbf{\Phi C^T} - \mathbf{I})diag(\mathbf{c_1}) \\ (\mathbf{\Phi C^T} - \mathbf{I})diag(\mathbf{c_2}) \\ \vdots \\ (\mathbf{\Phi C^T} - \mathbf{I})diag(\mathbf{c_N}) \end{bmatrix} \tag{4.35}$$

For (4.34), 1/***x***=**0** is an obvious solution to this equation. However, this is not a desirable answer for this equation because it represents the case where each bus is isolated from each other. Recognizing that the dc network acts as a current divider network, the branch reactance can be arbitrary scaled if an identical scalar is used to multiply each branch reactance. Therefore, a constraint is added to make the set of branch reactances reasonable and mathematically unique. Since this model is constructed based on the ac load flow base case, this constraint is constructed based on the original ac PF solution. Two bus voltage angles are chosen and denote them by δ_i and δ_j. So, the difference of these two bus voltage angles is $\delta_{ij} = \delta_i - \delta_j$. Also, the original ac power flow over branch *i-j* is $P_{i->j}$ where the from or to power flow may be used Therefore, one extra constraint is added to (4.34), which is $1/x_{ij} = P_{i->j}/\delta_{ij}$, in which, x_{ij} is the desired magnitude of the equivalent branch reactance of the network connecting bus *i* and bus *j*. Besides this constraint, network topology may reduce the rank of **Λ** further. For example, there is a radial system shown as Fig.4.3. For this network with a radial lines, the rank of lambda matrix is 0. That is to say, all these branch reactances are arbitrary. This is not surprising since no current division takes place. Therefore, in order to get reasonable reactances for a system like this, three additional constraints are needed.

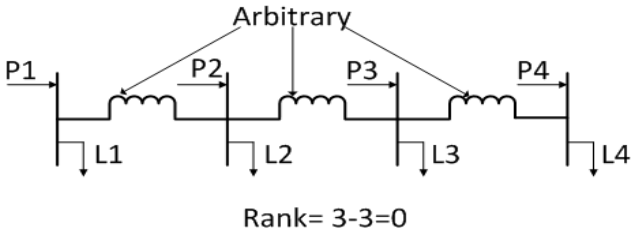

Fig.4.3 radial lines sample system

Assuming the more specific case where all radial lines are removed from the network, (4.34) becomes:

$$1/\mathbf{x} = \left[\left(\mathbf{\Lambda}^*\right)^T \mathbf{\Lambda}^*\right]^{-1}\left(\mathbf{\Lambda}^*\right)^T \begin{bmatrix} P_{i->j} \big/ \delta_{ij} \\ \mathbf{0} \end{bmatrix} \tag{4.36}$$

where $\mathbf{\Lambda}^* = \begin{bmatrix} \mathbf{N}_m \\ \mathbf{\Lambda} \end{bmatrix}$, in which $\boldsymbol{N_m}$ is a 1-by-L matrix with the branch i-j^{th} element 1 and all the other elements 0.

Since (4.36) is an over-determined problem, the reactance evaluation process is an error minimization process whose solution is straight forward.

4.5 Numerical example

In this section, the proposed optimal dc network is demonstrated on a 7-bus system and the IEEE 118-bus system. For the 7-bus system, the PF results from the normally loaded condition and the heavily loaded condition are compared to the original ac PF results. For the IEEE 118-bus system, the PF results for the normally loaded condition and the OPF results are compared to the original ac model.

In this section, once the dc-model reactances are found, the dc PF model with net loss dispersal (dc model with single multiplier) is used as a reference model.

4.5.1 7-bus system under normal loaded condition

This sample 7-bus test system is obtained from PowerWord, which is shown in Fig.4.4.

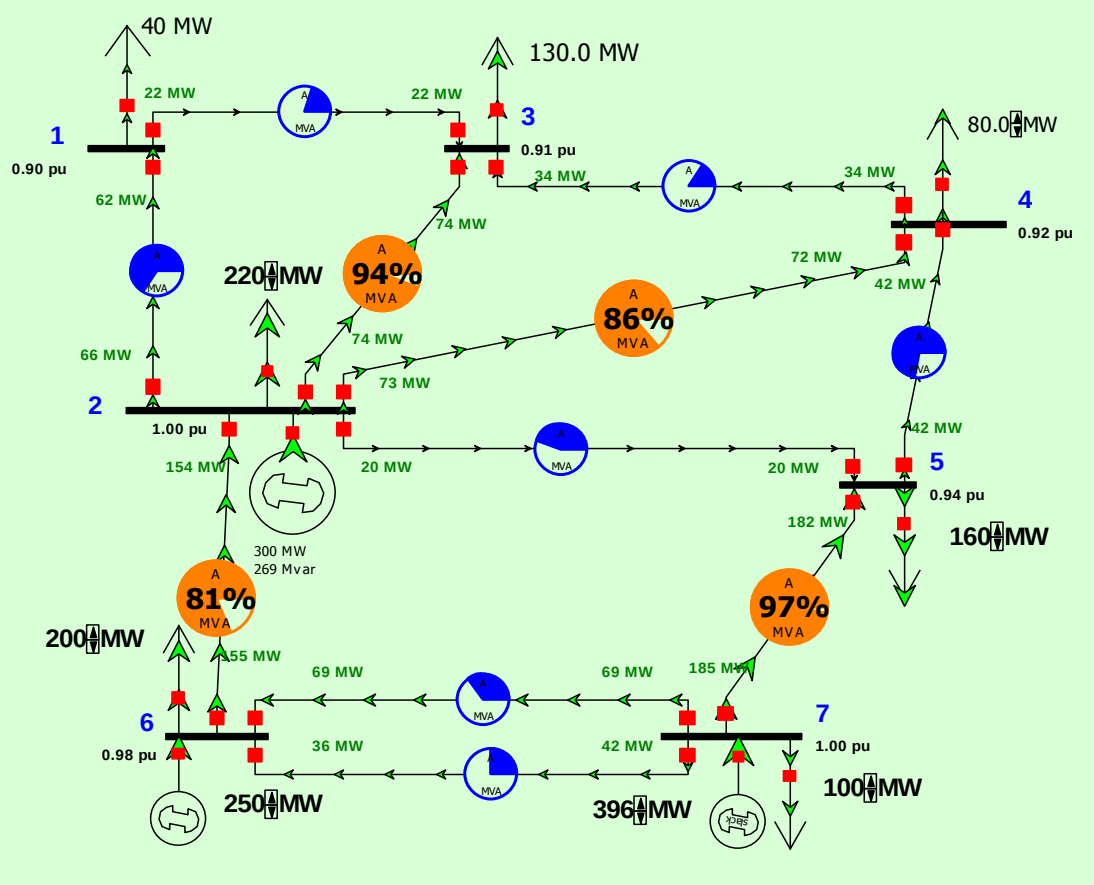

Fig.4.4 7-bus test system under normally loaded condition

The system parameters are shown in Table 4.1.

Table 4.1 7-bus system parameters and ac solutions under normally loaded condition

From Number	To Number	R	X	B	MW From	MW To
1	3	0.02	0.24	0	22.25493	-22.1252
1	2	0.06	0.15	0	-62.255	66.05361
2	6	0.005	0.06	0	-153.524	154.8468
2	5	0.01	0.12	0	20.1065	-19.8296
2	4	0.015	0.18	0	73.09677	-71.9798
2	3	0	0.18	0	74.26676	-74.2668
3	4	0.015	0.03	0	-33.6081	33.81943
4	5	0.02	0.24	0	-41.8396	42.26073
6	7	0.25	0.25	0	-35.5015	41.76386
6	7	0	0.25	0	-69.3453	69.34535
7	5	0.006	0.15	0	184.6926	-182.431

In terms of the method described in section 4.2.2, the ac PTDFs at the sending end and receiving end are calculated as follows:

- The ac PTDF matrix at the sending end:

branch\bus	1	2	3	4	5	6
1-3	0.3492	0.0169	-0.1473	-0.1102	-0.0153	0.0125
1-2	0.6508	-0.0169	0.1473	0.1102	0.0153	-0.0125
2-6	0.5421	0.5215	0.5059	0.4915	0.3425	-0.3529
2-5	0.3315	0.3592	0.2458	0.2114	-0.2493	0.2649
2-4	-0.0637	0.0573	-0.2528	-0.3265	-0.0426	0.0422
2-3	-0.0998	0.0440	-0.3355	-0.2546	-0.0335	0.0324
3-4	0.2459	0.0607	0.5188	-0.3636	-0.0486	0.0448
4-5	0.1876	0.1176	0.2793	0.3144	-0.0905	0.0867
6-7	0.1602	0.1542	0.1496	0.1453	0.1012	0.1865
6-7	0.3907	0.3759	0.3646	0.3543	0.2469	0.4548

- The ac PTDF matrix at the receiving end:

branch\bus	1	2	3	4	5	6
1-3	-0.3457	-0.0167	0.1457	0.1090	0.0151	-0.0123
1-2	-0.7101	0.0181	-0.1634	-0.1218	-0.0171	0.0133
2-6	-0.5510	-0.5300	-0.5142	-0.4995	-0.3481	0.3586
2-5	-0.3313	-0.3586	-0.2460	-0.2119	0.2471	-0.2645
2-4	0.0614	-0.0561	0.2459	0.3176	0.0413	-0.0414
2-3	0.0998	-0.0440	0.3355	0.2546	0.0335	-0.0324
3-4	-0.2490	-0.0614	-0.5252	0.3680	0.0492	-0.0453
4-5	-0.1914	-0.1198	-0.2849	-0.3208	0.0923	-0.0884
6-7	-0.2305	-0.2217	-0.2151	-0.2090	-0.1456	-0.2683
6-7	-0.3907	-0.3759	-0.3646	-0.3543	-0.2469	-0.4548

Based on the method described in section 4.3 above, the dc equivalent PTDFs are calculated:

branch\bus	1	2	3	4	5	6
1-3	0.343692	0.022125	-0.15418	-0.11531	-0.02545	0.015646
1-2	0.655901	-0.02034	0.150567	0.113116	0.021105	-0.01432
2-6	0.510483	0.528169	0.486689	0.480116	0.337389	-0.35253
2-5	0.308724	0.357557	0.236161	0.204872	-0.25033	0.266663
2-4	-0.06321	0.054748	-0.24213	-0.31842	-0.03839	0.04084
2-3	-0.0991	0.038721	-0.32596	-0.25096	-0.02308	0.029519
3-4	0.244067	0.060663	0.519759	-0.36668	-0.04903	0.045322
4-5	0.180493	0.11566	0.276448	0.314739	-0.08963	0.086584
6-7	0.151299	0.148344	0.149446	0.144573	0.107865	0.184748
6-7	0.357518	0.382484	0.332483	0.332579	0.223637	0.463172
7-5	-0.48824	-0.47455	-0.50982	-0.5177	-0.65918	-0.35428

Based on the equivalent dc PTDFs shown above, the equivalent reactances of this 7-bus system are calculated by using the reactance evaluation algorithm. Then the power flows for both the classical and single-multiplier dc PF models are calculated. The results are summarized in Table 4.2.

Table 4.2 Power flow and reactance results for optimal dc model and dc model with single multiplier under normally loaded case

	Optimal dc model		Classical dc model	
	X(p.u.)	PF (MW)	X(p.u.)	PF(MW)
1-3	0.159422	20.65183	0.24	20.48
1-2	0.101437	-62.616	0.15	-61.10
2-6	0.034342	-151.449	0.06	-160.61
2-5	0.074751	19.01595	0.12	25.21
2-4	0.122693	72.40434	0.18	72.67
2-3	0.130052	74.15471	0.18	78.22
3-4	0.021504	-35.364	0.03	-33.32
4-5	0.170232	-43.8344	0.24	-41.90
6-7	0.343763	-31.0811	0.25	-56.86
6-7	0.144073	-74.1606	0.25	-56.86
7-5	0.092899	186.2982	0.15	179.18

The dc power-flow results of the optimal-reactance dc model with single multiplier and classical dc model with single multiplier are compared with ac PF results, respectively. Both models take into

account the MW losses. In this section, the maximum branch MW-flow error, for any branch, in percentage is calculated as following:

$$Difference_i = \frac{\left| PF_i^{ac} - PF_i^{dc} \right|}{PF_i^{ac}} \times 100\% \qquad (4.37)$$

Fig.4.5 shows the power flow errors in percentage of each branch flow in these two models using the ac power from the sending bus as the base value. The largest percentage error for the classical dc power flow model (branch 9) is about 54%, while the percentage errors of optimal-reactance dc model for branch 9 is about 11%. It is shown that optimal dc model can provide a more accurate power flow distribution ("current division") than the classical dc model with single multiplier.

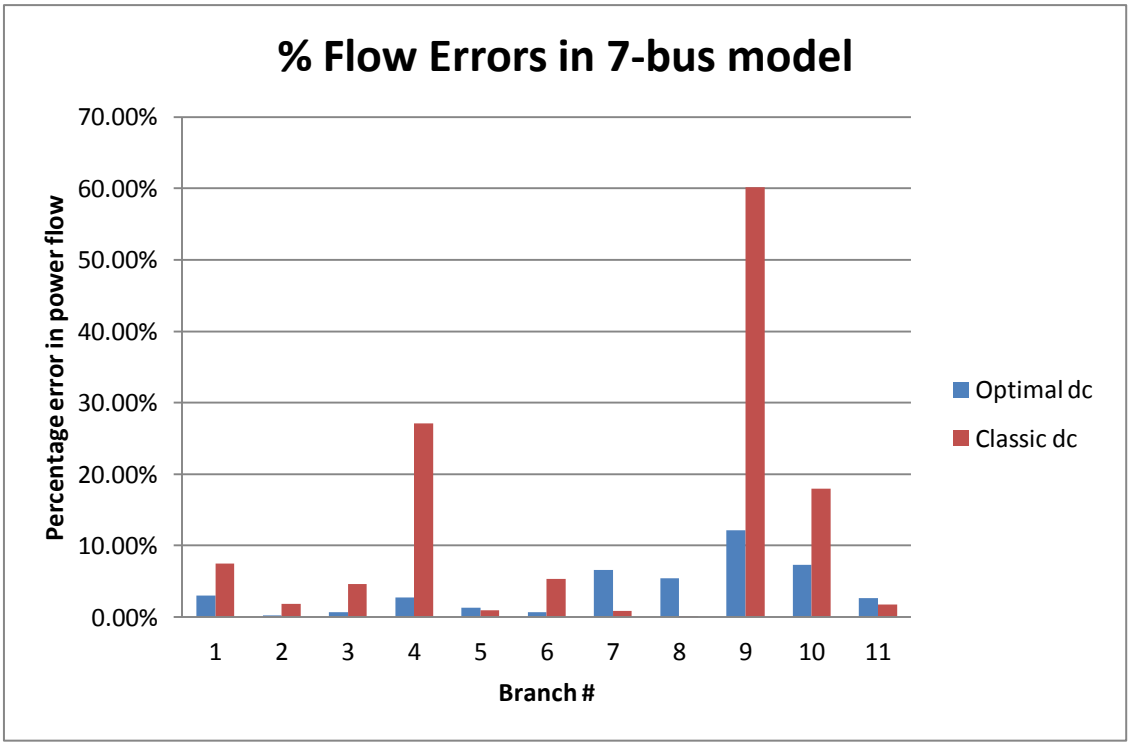

Fig.4.5 Percentage of power flow errors in 7-bus model

A summarized comparison of these results shown in Table 4.3.

Table 4.3 Comparisons of power flow results for optimal dc model and dc model with single multiplier under heavily loaded condition

	Optimal dc model	dc model with single multiplier
Maximum error (MW)	4.81	21.35
Average error(MW)	2.01	5.21
Maximum error (%)	12.45%	60.16%
Average error (%)	4.09%	11.66%

4.5.2 7-bus system under heavily loaded condition

For this heavily loaded case, the topology and the branch parameters of 7-bus system are the same as ones calculated under the normally loaded condition. (Note that the optimal reactance for the model will change with loading conditions since the magnitude and distribution of the losses will change, yielding different sets of ac PTDFs.) The loads at bus 3 and bus 5 are increased and the loads at other buses are adjusted correspondingly to get a converged PF solution.

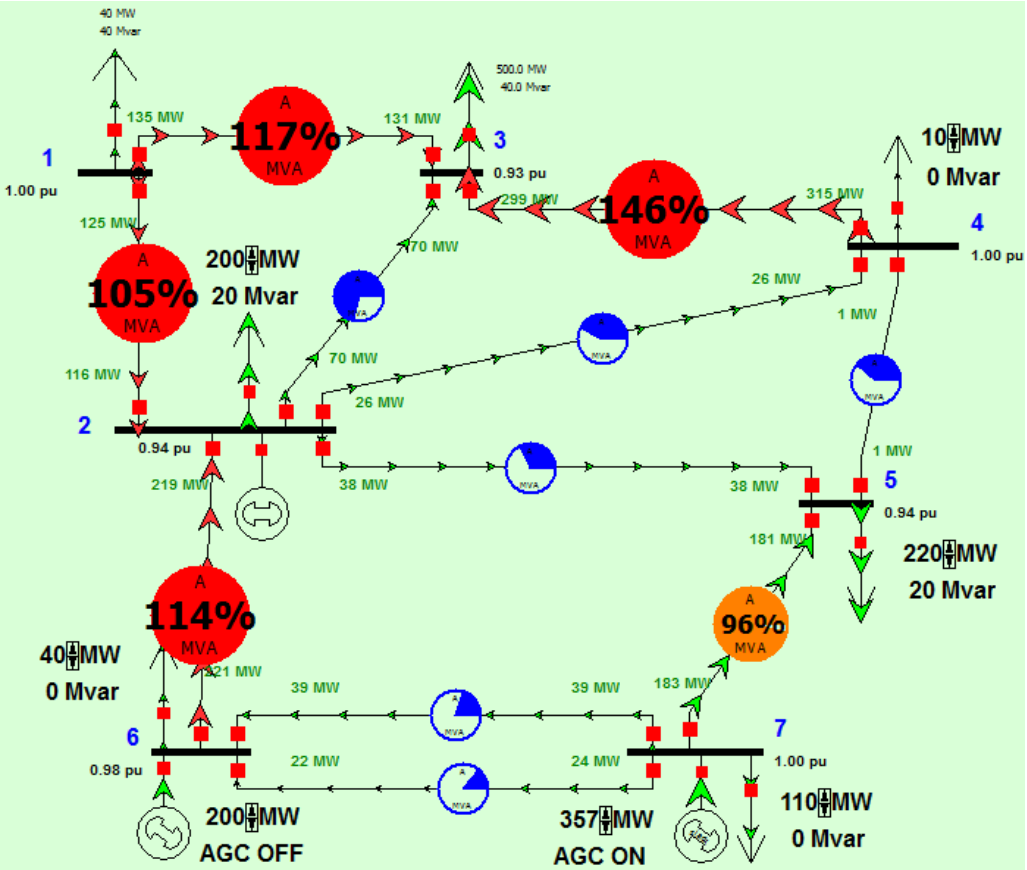

Fig.4.6 7-bus test system under heavily loaded condition

The dc power-flow results of the optimal-reactance dc model and dc model with single multiplier are compared with ac PF results, respectively. The power flow errors in percentage of each branch in these two models are shown in Fig. 4.7.

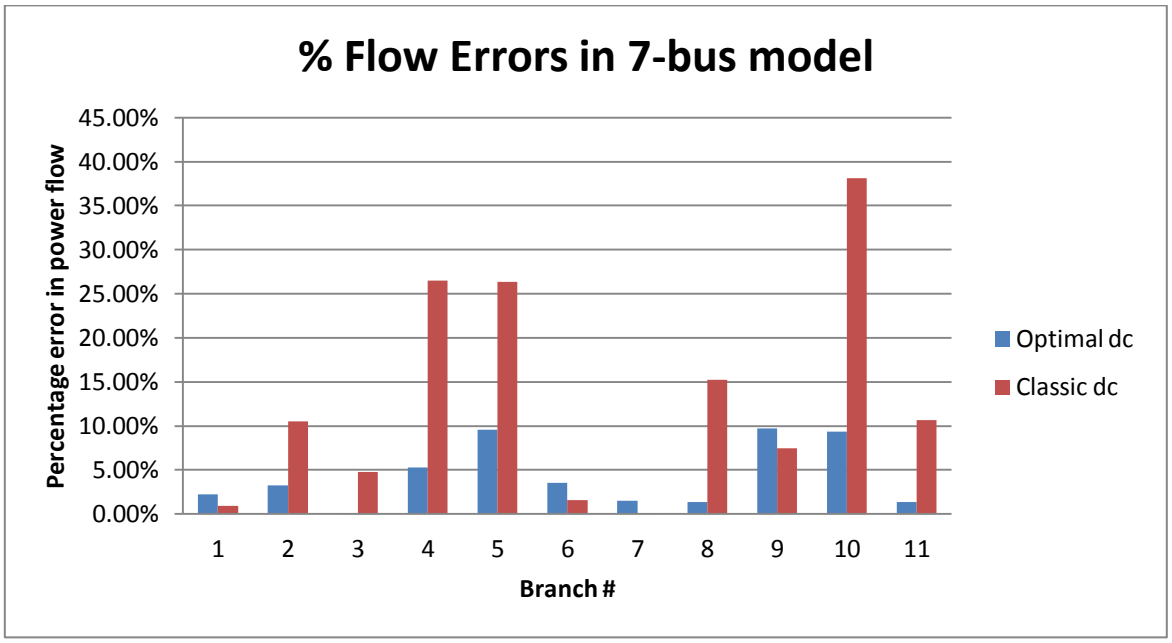

Fig. 4.7 Percentage of power flow errors in 7-bus model

The summarized comparison of these results are shown in Table 4.4.

Table 4.4 Comparisons of power flow results for optimal dc model and dc model with single multiplier under heavily loaded condition

	Optimal dc model (heavily loaded case)	dc model with single multiplier
Maximum error (MW)	4.45	19.25
Average error(MW)	2.63	7.89
Maximum error (%)	9.74%	38.1%
Average error (%)	4.3%	12.9%

4.5.3 118-bus system example

In this section, the (modified) IEEE 118-bus system under normal loaded condition is used to demonstrate the application of this method. The one-line diagram of the IEEE 118-bus system is

shown in Appendix A. The dc power-flow results of the optimal-reactance dc model and dc model, both with single multiplier are compared with the ac PF results, respectively. The comparison results are summarized in Table 4.5.

Table 4.5 Comparisons of power flow results for optimal dc model and dc model with single multiplier under normally loaded condition

	Optimal dc model with single multiplier	Classical dc model with single multiplier
Maximum error (MW)	5.09	17.37
Average error(MW)	0.78	3.12
Maximum error (%)	21.33%	170.75%
Average error (%)	2.46%	11.89%

The power flow errors in percentage of each branch in these two models are shown in Fig.4.8.

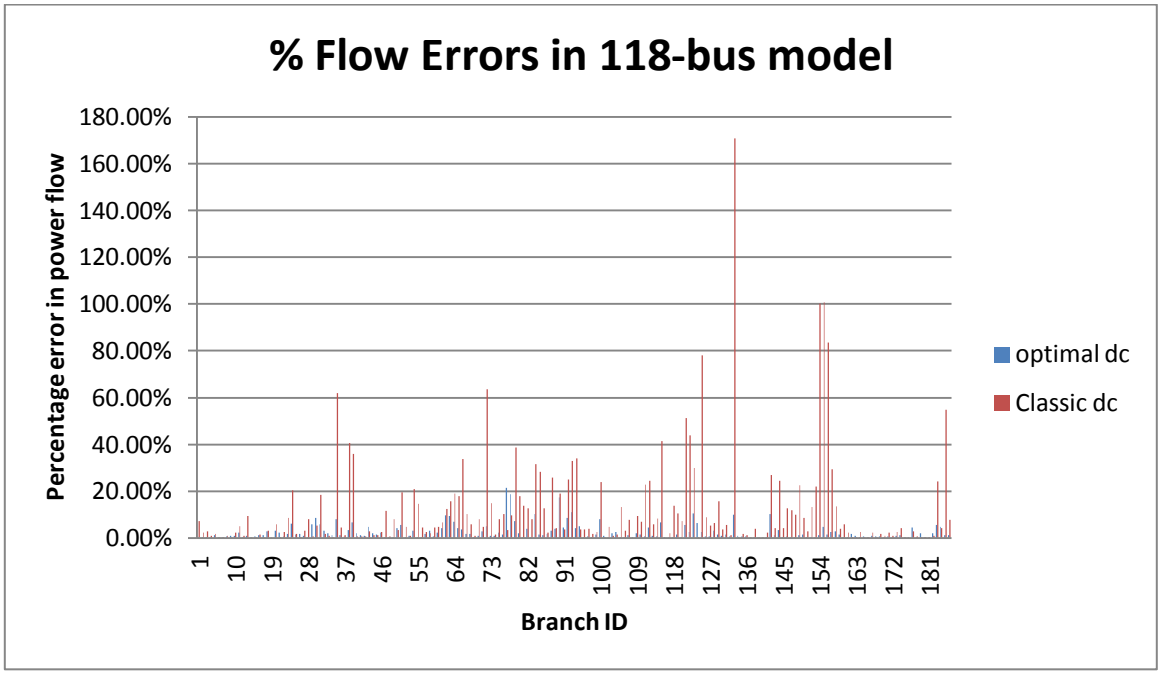

Fig.4.8 Percentage of power flow errors in 118-bus model

In order to further compare the distribution of the power flow errors in percentage, the error duration curve is shown in Fig.4.9. The left-handed plot shows all the results and the right-handed plot show the error duration curves between 0 and 0.1 for PF comparison.

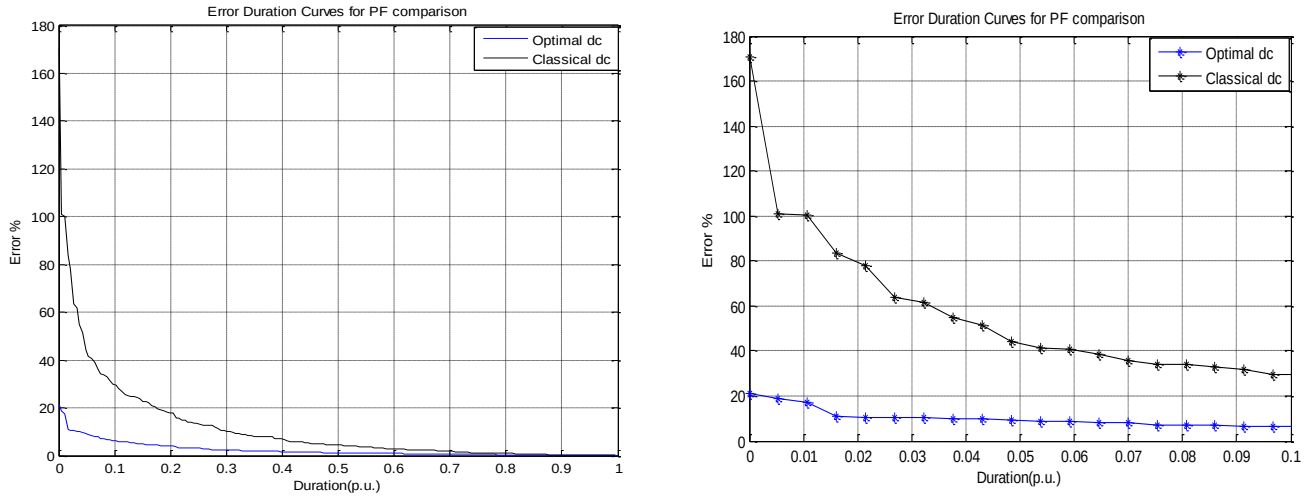

Fig.4.9 Error duration curve for 118-bus system

As with all the dc models that we discussed in the section 3.4, this optimal dc model is further tested by comparing the OPF results with the ac model. As shown in Table 4.6, the optimal-reactance dc model reveals the congestion patterns that actually occurred using the full ac system. The average LMP calculated by optimal-reactance dc model is similar to the average LMP calculated using the ac model.

Table 4.6 OPF results for optimal dc model and ac model

Model	Total cost ($/hr)	Binding Constraints [Branch]		Average LMP ($/MWh)
		From bus	To bus	
Optimal-reactance dc model	131726.13	8	9	39.99
		9	10	
ac model	130060.61	8	9	39.56
		9	10	
Classical dc model with single multiplier	131748.45	8	9	40.01
		9	10	

4.6 Conclusion

In this chapter, a hot-start optimal-reactance dc PF model based on ac power transfer distribution factors (PTDF) is proposed. Considering the questionable accuracy of the dc PTDFs

due to the assumptions involved in the dc PF models, ac PTDF that yields more accurate sensitivities of flows to bus injections is used to construct the optimal-reactance dc network.

The ac PTDFs are calculated based on a specific operating point of the system. Since the ac PTDFs include the losses, the ac PTDFs that result from these are not consistent. That is to say, for each bus, the net power into each bus may not be zero if the PTDFs are inconsistent.

In order to make ac PTDFs consistent, losses are modeled by fictitious loads at each bus in the equivalent dc model in order to calculate dc PTDFs that are consistent, at least within each shift factor. In light of the definition and desired characteristics of PTDFs, the linear least squares state estimation process is applied to get PTDFs that are more consistent. Then the reactance evaluation process is applied to the equivalent dc PTDFs to get the optimal-reactance full dc network.

The seven-bus system under different loading conditions and the IEEE 118-bus system are used as numerical examples to demonstrate this method. The metrics used to evaluate this dc model are PF and OPF result. Also, the dc model with single multiplier is used as a reference dc model. Comparing the simulation results in Table 3.2 and Table 3.5 this optimal-reactance dc model not only matches the ac PF solution well, but also preserves the congestion pattern obtain from the OPF results of the original ac model.

CHAPTER 5 . BUS-AGGREGATION TECHNIQUE

In thin chapter, the bus-aggregation technique that is used to preserve inter-zonal power flows is presented. This network equivalent preserves the main characteristics of the power system and will be used in the power market analysis and investment planning studies.

5.1 Basic idea

Considering the application of this network equivalent, the generators and loads as well as the inter-zonal power flows need to be retained in the equivalent. The process of generating the equivalent involves several steps:

First, the entire system is divided into different zones. The division process is based on the k-means ++ method by using the dc PTDFs in terms of their similar contributions to the designated inter-zonal power flows. Second, each zone is represented by a single bus. Within each zone, all the generators and loads are aggregated and retained at the equivalent bus. Also, all the intra-zonal transmission lines are ignored while the inter-zonal transmission lines are aggregated and represented by a single equivalent transmission line in the reduced equivalent. If there is one branch (at least) that directly connects the corresponding zones, the buses in the reduced equivalent will be connected by equivalent lines. After the topology of the reduced equivalent is determined, the reactance evaluation process mentioned in section 0 is used to determine the equivalent transmission line reactances that best fit the PTDF matrix of the reduced equivalent network.

5.2 Problem Formulation

The main objective of this network reduction is to obtain a set of transmission reactances for the reduced equivalent model such that its inter-zonal power flows matches the inter-zonal power

flows of the original system. In this optimization problem, the minimization of the Euclidean norm, denoted as ||·||, of the difference between the two inter-zonal power flow vectors is used.

The network reduction problem is formulated as:

$$\begin{aligned} &\min_{x_R} \quad \left\| \mathbf{P}_{flow}^{\text{inter-zonal}} - (\mathbf{P}_{flow}^{\text{inter-zonal}})_R \right\| \\ &s.t. \quad x_i^R \neq 0, i = 1, 2, \ldots, L_R \end{aligned} \tag{5.1}$$

In the full system, the inter-zonal power flows are calculated by summing up all the power flows on the transmission lines connecting the corresponding two zones using the following equation [33].

$$\mathbf{P}_{flow}^{\text{inter-zonal}} = \mathbf{\Pi}_{flow} \mathbf{P}_{flow} = \mathbf{\Pi}_{flow} \mathbf{\Phi} \mathbf{P}_{inj} \tag{5.2}$$

where

$\prod_{flow}$: Matrix used to sum up the line flows with the dimension of L_R by L

$\mathbf{P}_{flow}^{\text{inter-zonal}}$: Vector represents the inter-zonal power flows with the dimension of L_R by 1

L: Number of branches in the full network

L_R : Number of branches in the reduced network

Since the reduced equivalent is generated based on the assigned zones and the power flow on the equivalent transmission lines (the inter-zonal power flows), the inter-zonal power flows can be written based on the PTDF definition:

$$(\mathbf{P}_{flow}^{\text{inter-zonal}})_R = \mathbf{\Phi}_R (\mathbf{P}_{inj})_R \tag{5.3}$$

where

$(\mathbf{P}_{flow}^{\text{inter-zonal}})_R$: Inter-zonal power flow vector in the reduced system with the dimension of L_R-by-1;

$\mathbf{\Phi}_{R:}$ PTDF matrix of the reduced system with the dimension of L_R-by-N_R;

$(\boldsymbol{P}_{inj})_{R:}$ Bus net injection vector of the reduced system with the dimension of N_R-by-1;

$N_{R:}$ Number of non-slack buses in the reduced network.

As we discussed in section 4.2.1, for the full system, the dc PTDF is calculated as $diag(1/\boldsymbol{x})\mathbf{C}[\boldsymbol{C}^T diag(1/\boldsymbol{x})\boldsymbol{C}]^{-}$. Therefore, this property also holds for the reduced system. Therefore, (5.3) can be further written as:

$$\begin{aligned}\left(\mathbf{P}_{flow}^{inter-zonal}\right)_R &= \mathbf{\Phi}_R\left(\mathbf{P}_{inj}\right)_R \\ &= diag(1/\mathbf{x}_R)\mathbf{C}_R\left[\mathbf{C}_R^T diag(1/\mathbf{x}_R)\mathbf{C}_R^T\right]^{-1}\left(\mathbf{P}_{inj}\right)_R\end{aligned} \tag{5.4}$$

where

$\boldsymbol{x}_{R:}$ branch reactance vector of the reduced system with the dimension of L_R-by-1;

$\boldsymbol{C}_{R:}$ node-branch incidence matrix of the reduced system with the dimension of L_R-by-$N_{R.}$

In the reduced system, the injection at each bus is the sum of the injections at the corresponding buses within each zone in the full system [33]:

$$(\boldsymbol{P}_{inj})_R = \mathbf{\Pi}_g \boldsymbol{P}_{inj} \tag{5.5}$$

where

$\prod_g$: The sum the bus injections with the dimension of N_R-by-N matrix;

In order to quantify the contribution of each injection to the inter-zonal power flows, each inter-zonal power flow is the summation of all these contributions from different bus injections.

First, the matrix $\mathbf{\Gamma}$ is constructed based on the following guidelines:

- It contains only 0's and 1's.
- Element $\Gamma(i,j)$ at row i column j is 1 if, in the original system, bus i belongs to zone j.
- Element $\Gamma(i,j)$ at row i column j is 0 if, in the original system, bus i does not belong to zone j.

Then, the contribution of each injection to the inter-zonal power flows is written as [33]:

$$\mathbf{\Psi} = \mathbf{\Pi}_{flow}\mathbf{\Phi} diag(\mathbf{P}_{inj})\mathbf{\Gamma} \tag{5.6}$$

where

$$diag(P_{inj}) = \begin{bmatrix} P_{inj}^{(1)} & 0 & \cdots & 0 \\ 0 & P_{inj}^{(2)} & & \\ \vdots & & \ddots & \\ 0 & & & P_{inj}^{(N)} \end{bmatrix}$$

For the full system, summing up each row of Ψ yields the corresponding inter-zonal power flow:

$$P_{flow}^{inter-zonal} = \begin{bmatrix} \sum_{j=1}^{N_R} \Psi^{(1,j)} \\ \sum_{j=1}^{N_R} \Psi^{(2,j)} \\ \vdots \\ \sum_{j=1}^{N_R} \Psi^{(L_R,j)} \end{bmatrix} \tag{5.7}$$

Based on (5.7), the contribution of each injection to the inter-zonal power flows for the reduced system are:

$$\Psi = \Phi_R diag\left[(P_{inj})_R\right] \tag{5.8}$$

Combining (5.6), (5.7) and (5.8) yields

$$\Psi = \Phi_R diag(\Pi_g P_{inj}) = \Pi_{flow} \Phi diag(P_{inj}) \Gamma \tag{5.9}$$

Therefore, the reduced PTDF matrix Φ_R is:

$$\Phi_R = \Pi_{flow} \Phi diag(P_{inj}) \Gamma \left\{diag(\Pi_g P_{inj})\right\}^{-1} \tag{5.10}$$

Then, applying the reactance evaluation process discussed in section 0, the optimal set of reactances for this reduced equivalent can be obtained by using (4.34), (4.35) and (4.36).

$$1/\mathbf{x}_R = [(\mathbf{\Lambda}^*)^T \mathbf{\Lambda}^*]^{-1}(\mathbf{\Lambda}^*)^T \begin{bmatrix} P_{i->j} \,/\, \delta_{ij}^* \\ \mathbf{0} \end{bmatrix} \tag{5.11}$$

For (5.11), two bus voltage angles from within zone *i* and zone *j* are chosen and denote them by δ_i and δ_j. So, the difference between these two representative bus voltage angles is $\delta_{ij} = \delta_i - \delta_j$. Also, the original ac inter-zonal power flow over equivalent branch *i*-*j* is $P_{i->j.}$

5.3 Numerical example

This part continues the numerical examples demonstrated in section 4.5.

5.3.1 7-bus system

- Normally loaded case

In this part, the 7-bus system is aggregated into a 4-bus system by using k-means++ method based on the equivalent dc PTDFs. The bus clustering is shown in Fig. 5.1.

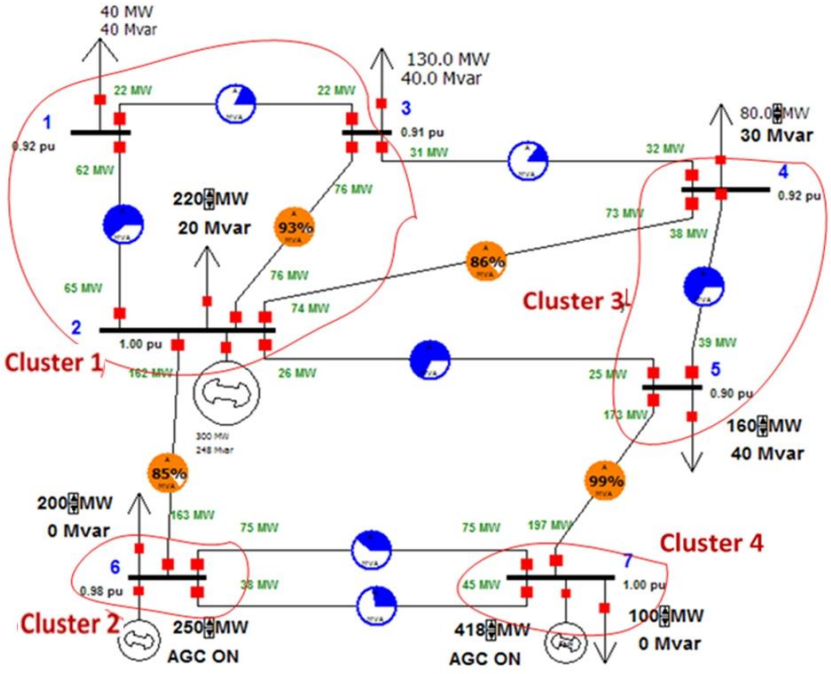

Fig. 5.1 7->4 bus reduced equivalent

Based on the bus-aggregation technique described in 5.2, the equivalent reactances and the dc PF flow for the 4-bus optimal-reactance dc reduced equivalent and the classical dc reduced equivalent, both with single loss multipliers, are calculated. There are two loading situations discussed in this section: normally loaded case and heavily loaded case.

The results are summarized in Table 5.1.

Table 5.1 7->4 bus reduced equivalents for optimal dc and classical dc model(normally loaded)

Branch		Optimal-reactance dc reduced equivalent		Classical dc reduced equivalent		ac
From_bus	To_bus	Equivalent reactance (p.u.)	Power flow (MW)	Equivalent reactance (p.u.)	Power flow (MW)	Power flow(MW)
1	2	0.3755	-153.58	0.3791	-156.71	-153.84
1	3	0.1607	58.18	0.1559	66.71	58.55
2	4	0.7215	-107.38	0.5316	-106.71	-105.53
3	4	0.7846	-184.16	0.7302	-173.29	-182.38

The power flow errors in percentage of each branch for both models are compared in Fig. 5.2. The maximum power flow error in percentage of the optimal-reactance dc reduced equivalent is about 2%, while the maximum power flow error of the classical dc is about 15%. The power-flow comparison results are summarized in Table 5.2.

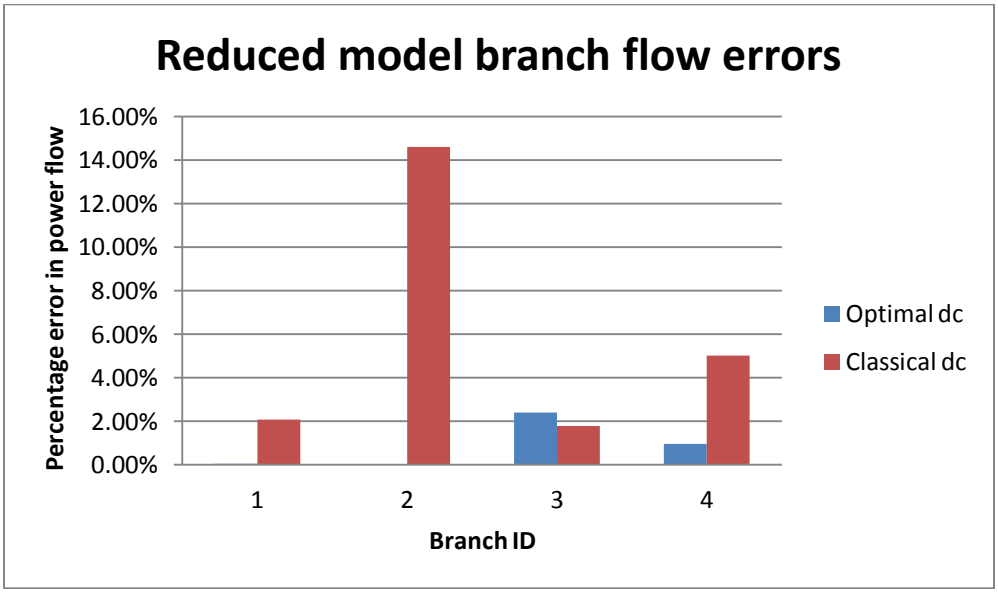

Fig. 5.2 Reduced model branch flow errors in percentage

Table 5.2 7->4 bus reduced model comparison of power flow errors aggregated results

	Optimal dc model	Classical dc model
Maximum error (MW)	2.53	9.14
Average error(MW)	1.08	5.67
Maximum error (%)	2.41%	14.61%
Average error(%)	0.85%	5.87%

- Heavily loaded case

Since the k-means ++ method used for bus clustering is based on the equivalent dc PTDFs obtained in section 4.3, the bus aggregation strategy for this heavily loaded case is different from the one under the normally loaded case.

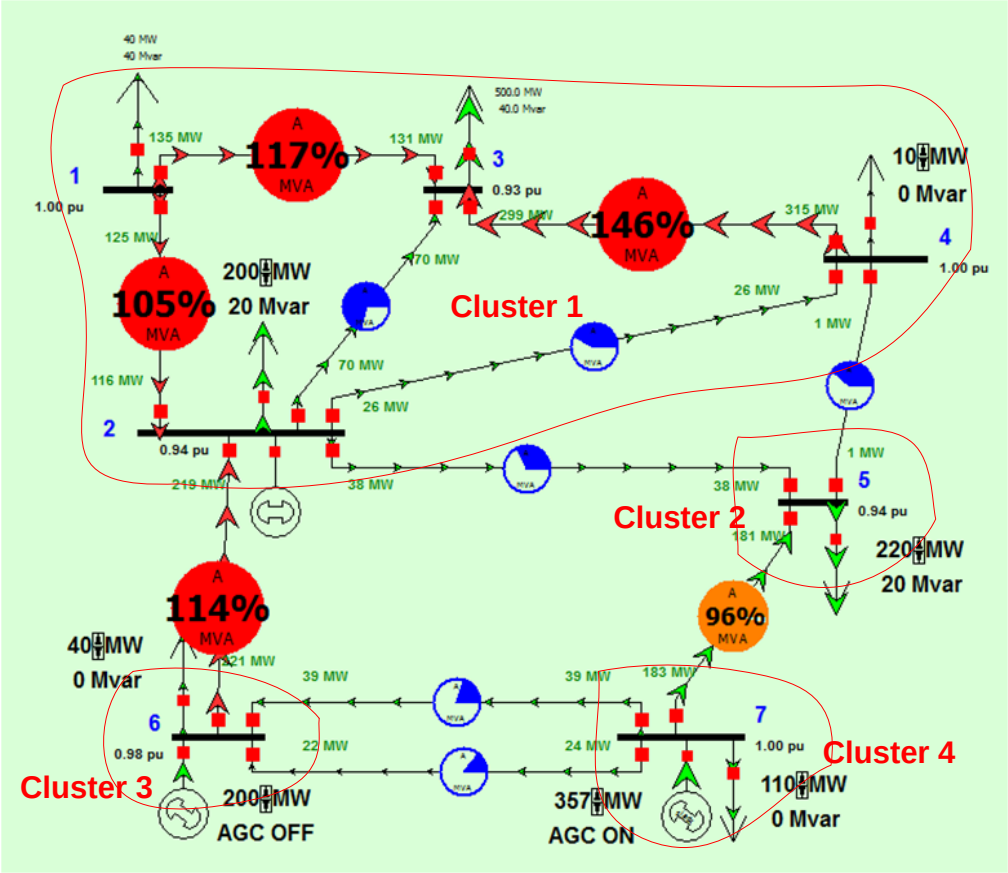

Fig. 5.3 7->4 bus reduced equivalent

By applying the bus-aggregation technique described in 5.2, the reduced equivalent for the optimal-reactance dc model and the dc model, both with single multiplier are calculated. The results are summarized in Table 5.4.

Table 5.3 7->4 bus reduced equivalents for optimal dc and dc model with single multiplier (heavily loaded)

Branch		Optimal dc reduced equivalent with single multiplier		reduced dc equivalent with single multiplier		ac
From_bus	To_bus	Equivalent reactance (p.u.)	Power flow (MW)	Equivalent reactance (p.u.)	Power flow (MW)	Power flow(MW)
1	2	0.1350	38.47	0.0903	58.09	38.87
1	3	0.1307	-219.43	0.0706	-208.09	-218.58
2	4	0.2823	-182.78	0.1636	-161.91	-181.17
3	4	0.2870	-61.79	0.1364	-48.09	-61.27

For this heavily loaded case, the power flow errors in percentage of each branch for both models are shown in Table 5.4. The maximum power flow error in percentage of optimal dc reduced equivalent is about 1%, while the maximum power flow error of the dc model with single multiplier is almost 50%.

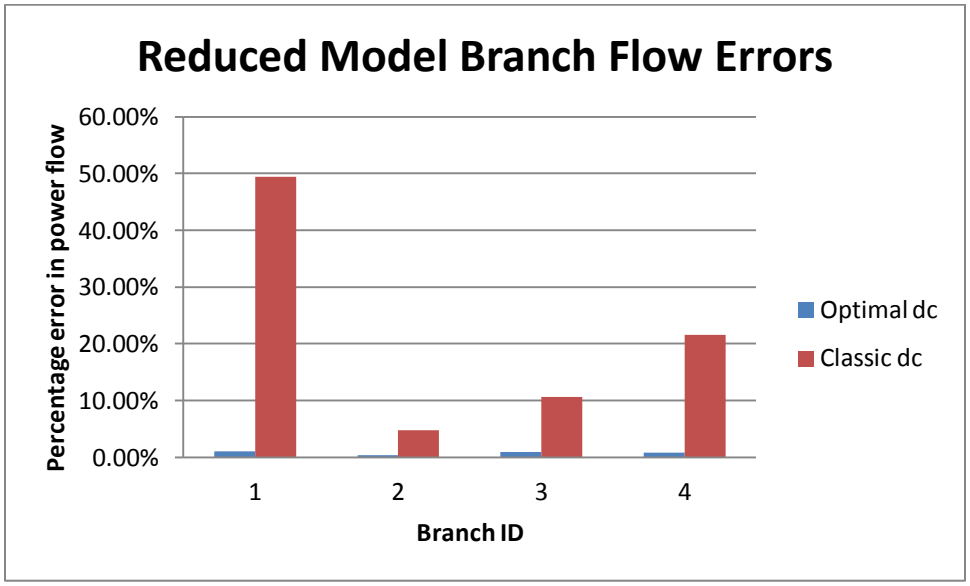

Fig. 5.4 Reduced model branch flow errors in percentage

The detailed power-flow comparison results are summarized in Table 5.7.

Table 5.4 7->4 bus reduced model comparison of power flow errors aggregated results

	Optimal dc model	Classical dc model
Maximum error (MW)	1.61	19.25
Average error(MW)	0.84	15.53
Maximum error (%)	1.03%	49.45%
Average error (%)	0.79%	21.6%

5.3.2 118-bus system under normally loaded situation

In this case, the 118-bus system is aggregated into a 20-bus system based on the k-means++ method using the equivalent dc PTDFs. The bus clustering is shown in Appendix B and the topology of the reduced equivalent is shown in Fig. 5.5.

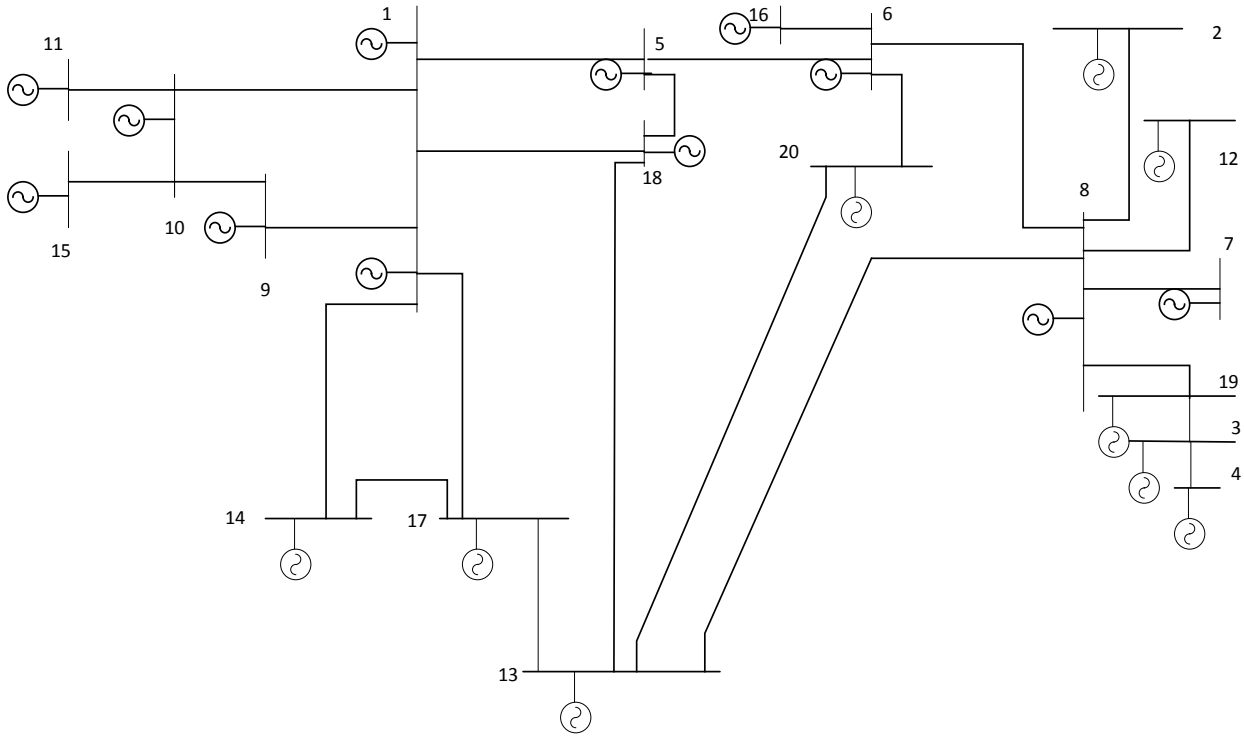

Fig. 5.5 118->20 reduced equivalent

Then, the reduced equivalent for the optimal-reactance dc model and the classical dc model, both with single multipliers, are calculated and the dc power flow results compared with the ac results. The results are summarized in Table 5.5.

Table 5.5 118->20 bus reduced model comparison of power flow errors aggregated results

	Optimal dc model with single multiplier	Classical dc model with single multiplier
Maximum error (MW)	11.20	45.23
Average error(MW)	4.16	11.21
Maximum error (%)	42.55%	226.15%
Average error (%)	9.58%	23.32%

As shown in Fig. 5.6, the power flow error in percentage of optimal dc reduced equivalent is much lower than the power flow error of the dc model with single multiplier.

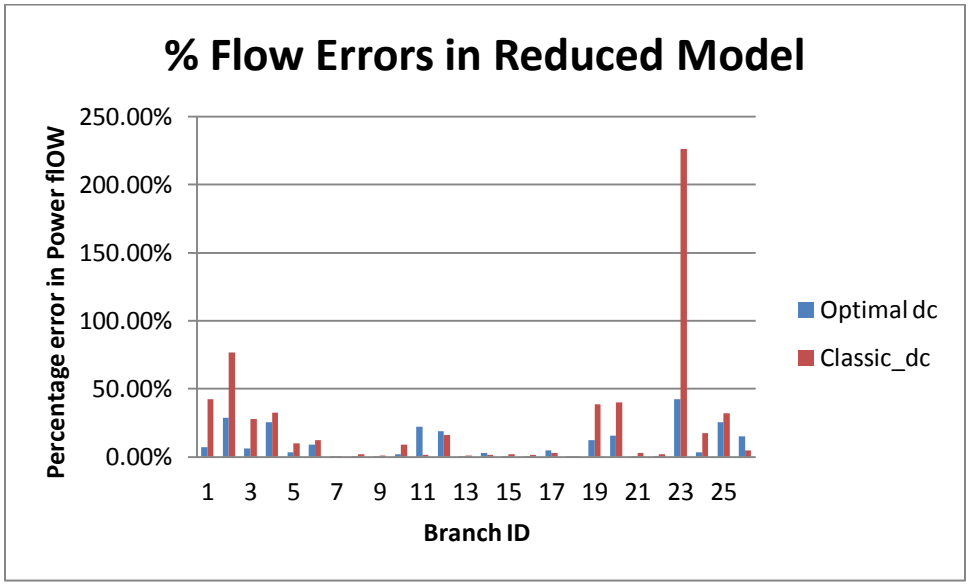

Fig. 5.6 Reduced model branch flow errors in percentage for 118-bus system

5.4 Speeding up the reactance evaluation

As we discussed in section 5.2, (4.36) and (5.11) were used in generating the network equivalent reactance for the full system and the reduced system. Since the size of the Λ^* matrix is ($N \bullet L$ + constraint number) by L, solving (4.36) and (5.11) are not only computationally expensive but also requires an amount of memory that can only be found as of this writing in a supercomputer. For example, for an ERCOR reduced equivalent model with 2000 buses and 5000 branches, the dimension of Λ^* is about 10^7 by $5 \cdot 10^3$. In order to apply the bus-aggregation

technique to a large-scale system like EI, three improved strategies were proposed for improving the execution time, and memory requirements for calculating the equivalent line reactances.

5.4.1 Sparsity techniques

Note that Λ^* is a very large sparse matrix with the dimension of $(L \bullet N + 1)$ by L. Also, there are many intermediate matrices constructed in the solution process that are extremely sparse. Hence, sparsity techniques can be applied to advantage throughout the entire computation process, speeding up the calculation process as well as reducing the storage requirements.

5.4.2 Redundancy elimination

By looking into the structure of Λ^*, there is a significant number of duplicate rows in the Λ^* matrix. By adding a weighting matrix into the optimization formulation, these duplicate rows can be removed without reducing the rank of the matrix and without reducing the accuracy of the calculated reactances. Generally, the number and location of duplicate rows depend on the topology of the network. Recognizing that there is a one-to-one correspondence between each block of the Λ^* matrix and a unique bus number in the reduced network, it became possible to use the effective topology pattern in each block to identify the duplicate rows within each block. The duplicate rows correspond to those buses whose node valency is equal to 2. By reducing the duplicate rows of the Λ^* matrix, the computational burden for evaluating branch reactances can be greatly reduced. For example, for the 6073-bus ERCOT system, the number of buses with a valency of 2 is about 2292. Therefore, about 13 million rows of the Λ^* matrix (30%) can be eliminated. This method will produce larger gains for the 62,000-bus EI system. The number of buses with a valency of 2 is about 22,000. As a result, about 1.2 billion rows of the Λ^* matrix (27%) can be eliminated from the full Λ^* matrix for the EI model. Eliminating the duplicate rows and adjusting the weights appropriately has little effect of the accuracy. While this approach

yields reactance values that are almost identical to that when no rows are eliminate, the computational requirements are still large. This begs an approach that combines accuracy with less computational complexity.

5.4.3 Threshold

Even though the duplicate rows are eliminated by adjusting the weighting matrix values appropriately, the number of rows of Λ^* is still quite large. It was found that engineering-based criteria could be used to eliminate a large number of rows of Λ^* without suffering a significant degradation in branch-reactance accuracy. The criteria involved using a threshold on equation coefficients. An explanation of this criterion and its applications follows.

Just as each sub-matrix of Λ^* can be associated with a different bus of the reduced network, each equation within each sub-matrix can be associated with a different branch within the reduced network. From state estimation theory, and with the particular structure of Λ^*, equations within Λ^* with the smallest coefficients have the least effect on the ultimate estimation of the branch reactances. Equations with the smallest coefficients are those associated with branches most distant from the bus associated with the sub-matrix of interest. With this insight, an engineering-based criterion for eliminating equations with small coefficients was examined, which is using a minimum threshold criterion on equation coefficients on the Λ^* matrix for equation retention.

In summary, using threshold values to eliminate a fraction of the redundant equations in the over-determined dc-network parameter estimation problem:

1) Has negligible effect on line flow accuracy;
2) Yields significant speed advantages;
3) Gives gains that grow exponentially with size of reduced equivalent.

5.4.4 Numerical example

In this section, numerical experiments were conducted using the 6073-bus system ERCOT system. The objective of this numerical experiment is to compare the time consumption and the accuracy of the network equivalent with and without applying the improved strategies. For these experiments, the execution times recorded were for an Intel 3.16 GHz, Core 2 Duo processor with 4 GB DDR RAM and 6MB L2 Cache.

1) Execution time comparison

In this section, different network equivalents with different sizes are generated based on the bus-aggregation technique. The execution time for reactance evaluations by using the full Λ^* with those using the reduced Λ^* matrix with equations eliminated is compared for each reactance evaluation process. In this case, the threshold is set to be 0.004 for the reactance evaluation process. Table 5.6 summarizes the comparison results.

Obviously, the larger the network equivalent is, the more execution time required for calculation the equivalent reactances. Without any improvement strategies, the reactance evaluation process for a 500-bus reduced equivalent takes about 4 hours; whereas, it only takes 50s to finish the reactance evaluation process with the improvement strategies. Considering the execution time ranges from 1.85 s to 13466.21 s, the execution time in Table 5.6 is best plotted using a logarithmic scales as shown in

Fig. 5.7. Also, the speeding–up factor describing the gain in terms of the size of the network equivalent is calculated as:

$$\text{speeding - up factor} = \frac{\text{excution time without improments}}{\text{excution time with improments}}$$

The speed-up factor for each case is plotted in Fig. 5.8.

Table 5.6 Execution time comparisons with/without improvement strategies

Equivalent line evaluation comp. / Size	Execution Time				Gain	
	Without improvements (Sec)		With improvements (Threshold=0.004) (Sec)		Speeding-up factor	
	(sec*)	Log_{10}	(sec)	Log_{10}	/	Log_{10}
100-bus	1.85	0.267	1.48	0.170	1.25	0.097
200-bus	8.41	0.925	5.3	0.724	1.586	0.201
300-bus	28.71	1.458	13.83	1.141	2.0759	0.317
400-bus	3224.49	3.508	24.73	1.393	130.38	2.115
500-bus	13466.21	4.129	50.11	1.700	268.73	2.429

As shown in

Fig. 5.7 and Fig. 5.8, it is clearly shown that the larger the reduced network, the more gain the improvement strategies provides. The difference is pretty obvious when the size of the network equivalent reaches 400 buses.

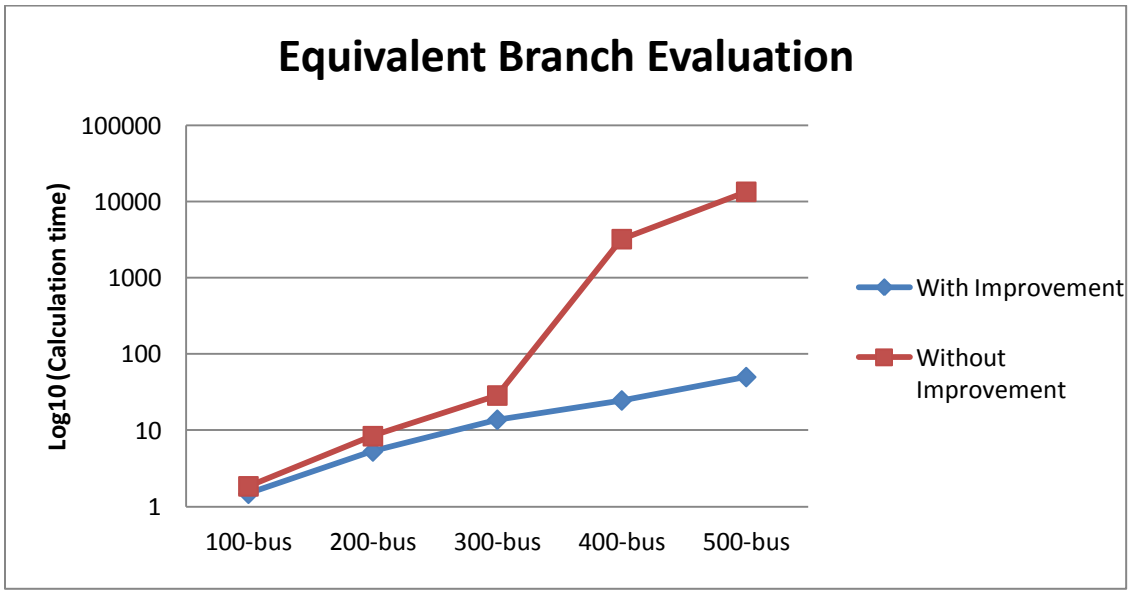

Fig. 5.7 Execution time of equivalent branch evaluation based log algorithm

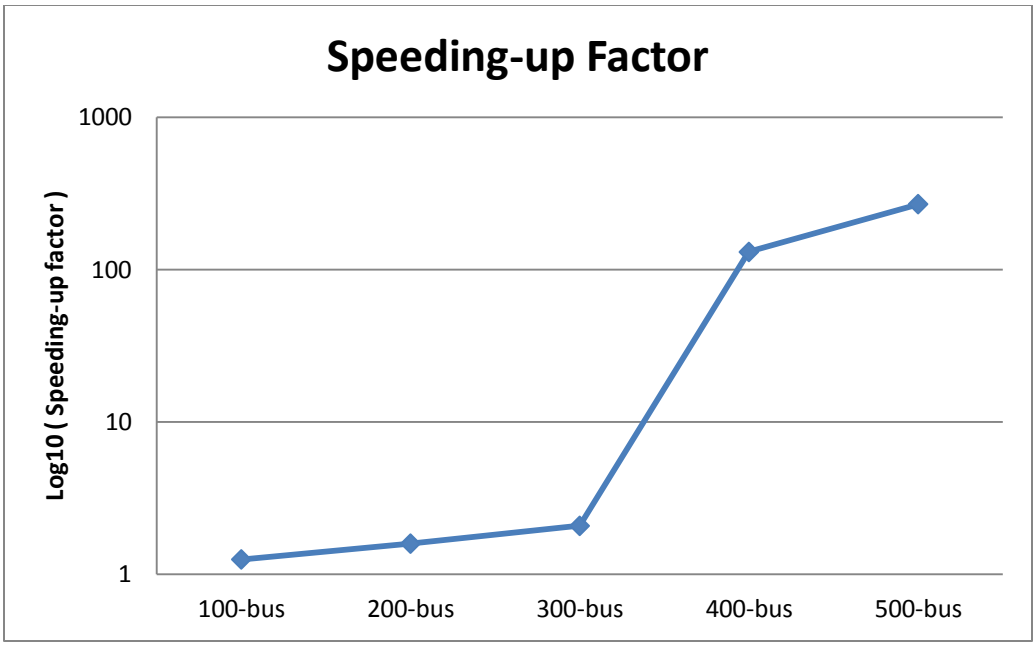

Fig. 5.8 Speed-up factors for equivalent branch evaluation of different equivalent

2) Accuracy comparison

The objective of this study is to find a minimum threshold that could meet the accuracy requirements and reduce the calculation burden dramatically.

In this section, the bus aggregation technique was applied to the full 6073-bus ERCOT system to produce a topology corresponding to a 100-bus system with 482 branches. For the experiments described in this section, redundancy elimination and threshold elimination are also studied together. Three comparisons of the equivalent reactances calculated by using the full Λ^* with those using the reduced Λ^* matrix are conducted: Dimension reductions based on different thresholds is conducted and acceptability determined using accuracy of the equivalent reactances and accuracy of the power flow results. In the following cases, the same constraints are applied for each experiment and fourteen thresholds are used in the equivalent branch evaluation process after the application of bus-aggregation technique for different network equivalents.

- Dimension reduction

As it is shown in Fig. 5.9, the threshold varies between 0.001 to 0.05. As expected, the percentage of the retained rows in the Λ^* matrix is decreases monotonically as the increase of the threshold value. Even though the threshold is set to be 0.001, 70% of the rows in the Λ^* matrix has been eliminated, which reduced the number of calculations significantly. When the threshold reaches about 0.05, only 9% percent of the rows in the Λ^* matrix remains.

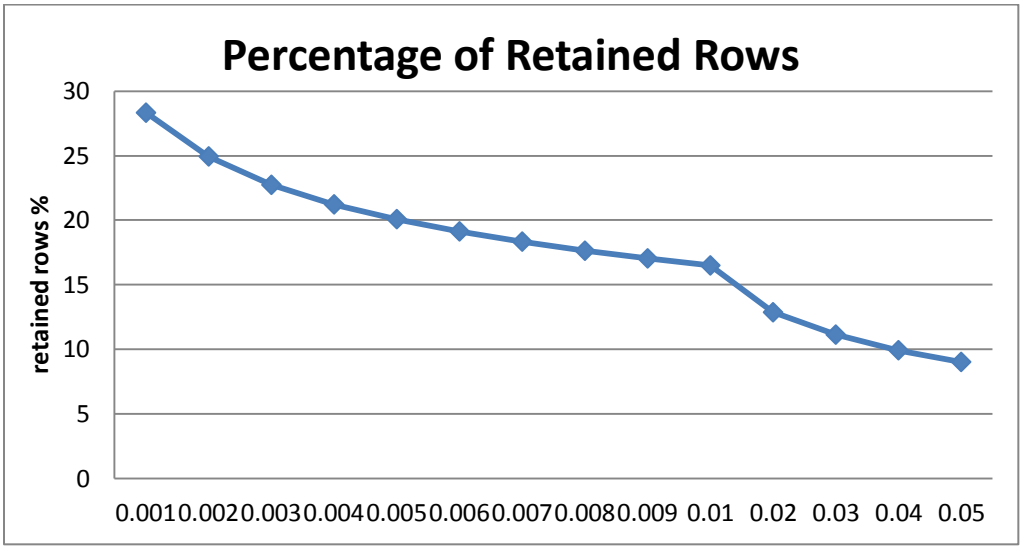

Fig. 5.9 Dimension reduction of Λ^* for different thresholds

- Susceptance value comparison

In this section, the reactances calculated based on the reduced Λ^* matrix are compared to the reactances based on the full Λ^* matrix. As expected, with the increase of the threshold, the errors of reactace grow gradually. After the threshold hits 0.01, the errors introduced by the row elimination appears to dramatically increase as shown in Fig. 5.10; however at that point the increments between thresholds is ten times the previous increments.

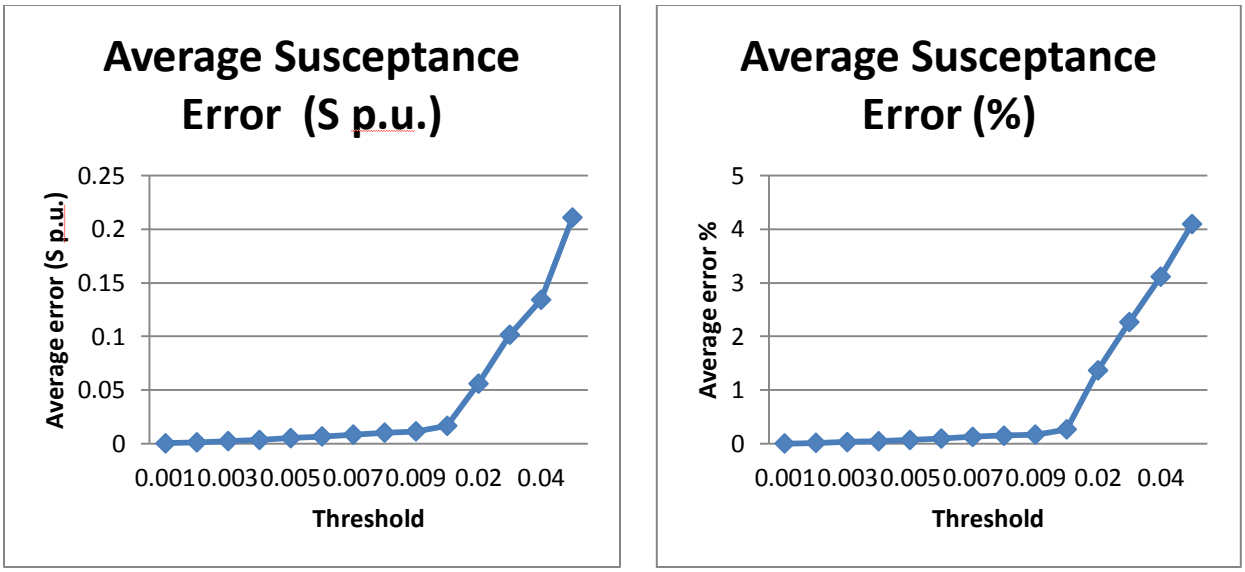

Fig. 5.10 Susceptance comparisons for different thresholds

The reactance-magnitude-error-duration curve corresponding to the aforementioned thresholds is shown in Fig. 5.11, which is used to demonstrate the percent of time that a specific reactance-magnitude error is exceeded. Since the power flow error in percentage for the larger threshold (larger than 0.01) is much larger than ones from the smaller threshold, only the results from the threshold that is less than 0.01 are shown. As shown in Fig. 5.11, the errors that exceed 1% are pretty low.

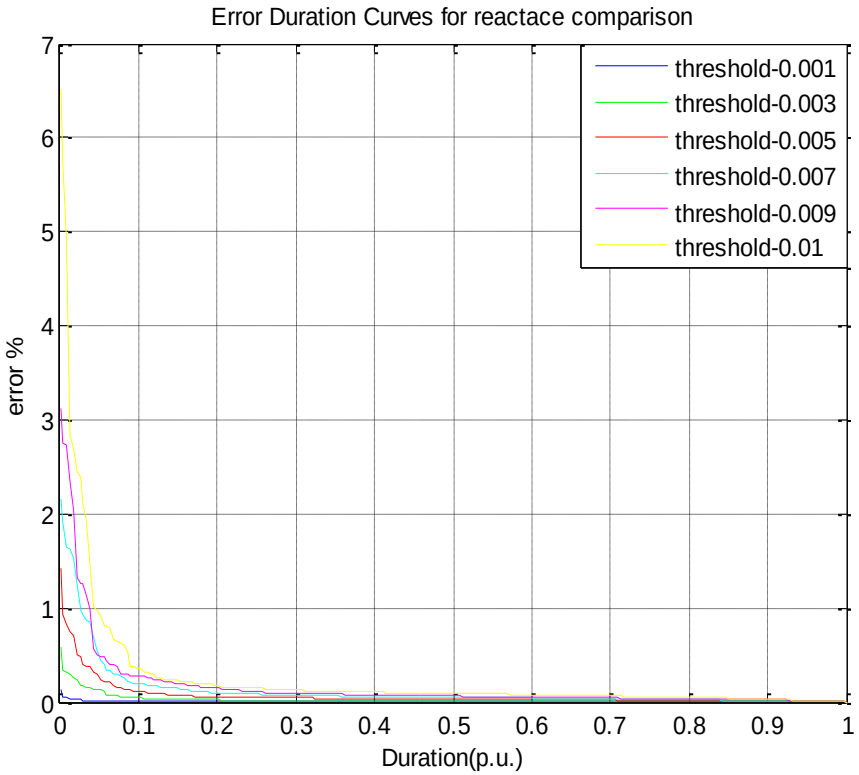

Fig. 5.11 Reactance error duration curve

- Power flow comparison

In this part, the branch power flows calculated based on the reduced Λ^* matrix are compared with the power flows obtained using the reactances calculated from the full Λ^* matrix.

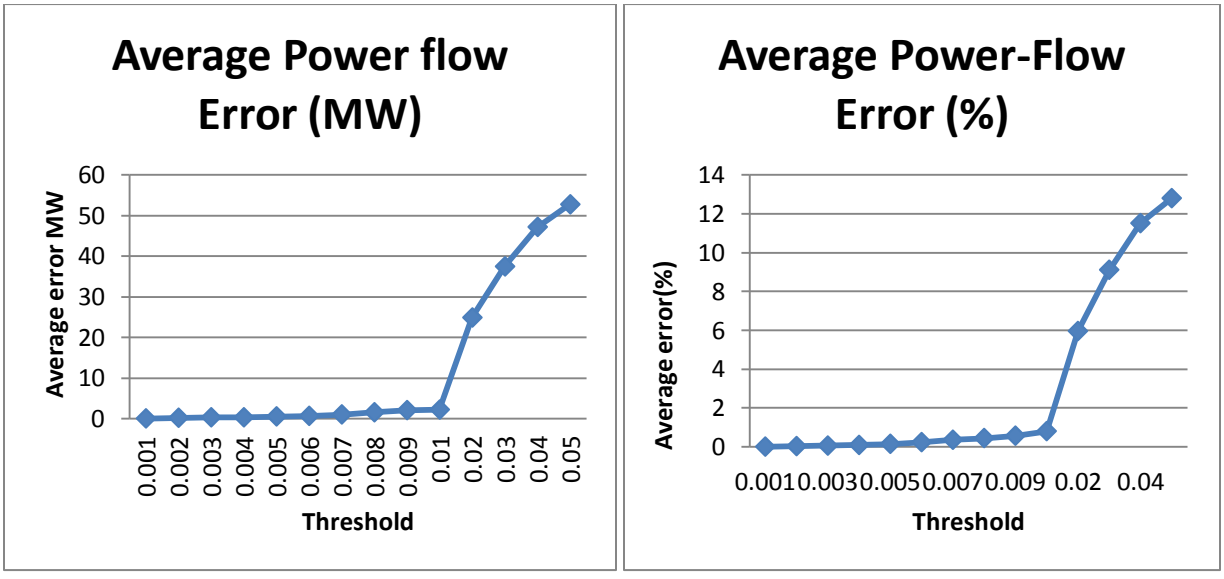

Fig. 5.12 Average errors of power flow

The reactance comparison error-duration curve is shown in Fig. 5.13. This plots shows, in percent, the number of branch flow that exceed a given error. The maximum error in percentage for power flow is about 22%.

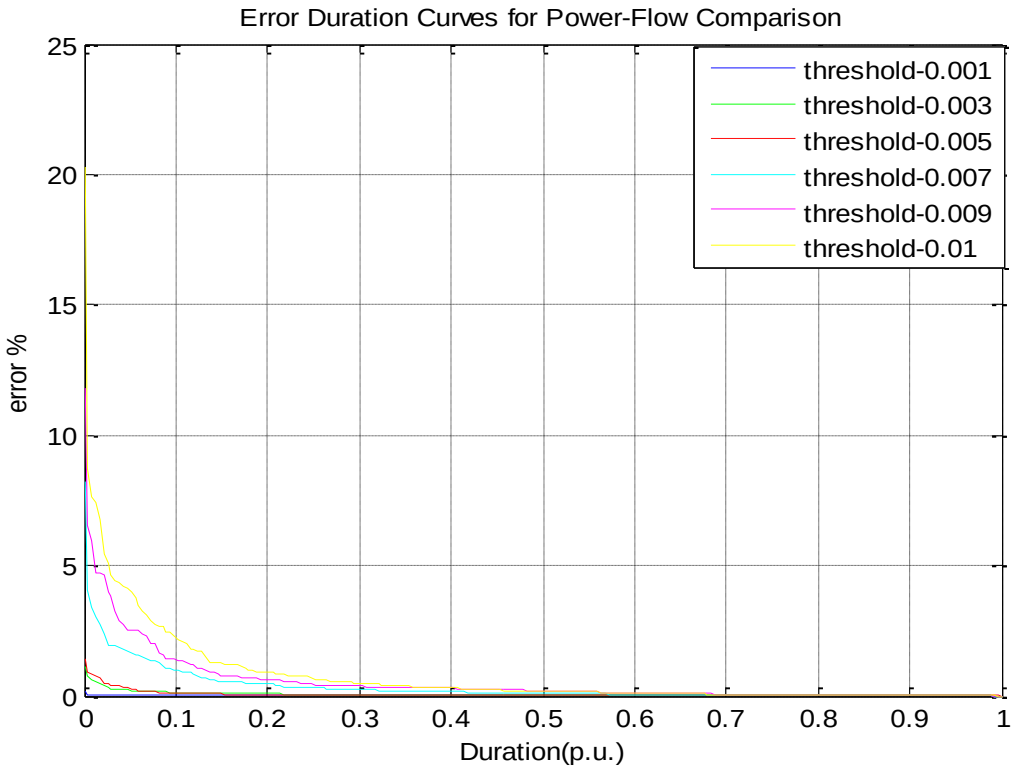

Fig. 5.13 Power-flow error duration curve

All the simulation results are summarized in Table 5.7.

Table 5.7 Suceptance and power-flow comparisons for different thresholds

Case No.		1	2	3	4	5	6	7	8	9	10	11	12	13	14
Thresholds		0.001	0.002	0.003	0.004	0.005	0.006	0.007	0.008	0.009	0.01	0.02	0.03	0.04	0.05
No. of retained rows		13660	12026	10965	10235	9683	9226	8844	8503	8217	7954	6204	5370	4786	4349
No. of retained rows (%)		28.33%	24.94%	22.74%	21.22%	20.08%	19.13%	18.34%	17.63%	17.04%	16.49%	12.86%	11.14%	9.92%	9.02%
Reactance comparison	Max_error (s.p.u.)	0.01	0.08	0.15	0.19	0.32	0.39	0.46	0.50	0.56	0.83	2.01	3.72	4.38	5.89
	Max_error (%)	0.13	0.50	0.57	0.92	1.41	1.79	2.17	2.54	3.11	6.51	34.96	62.98	74.33	78.13
	Avg_error (s.p.u.)	<1e-3	<1e-2	<1e-2	<1e-2	0.01	0.01	0.01	0.01	0.01	0.02	0.06	0.10	0.13	0.21
	Avg_error (%)	<1e-2	0.02	0.03	0.04	0.07	0.10	0.13	0.15	0.17	0.27	1.37	2.27	3.12	4.10
Branch power flow comparison	Max_error (MW)	0.41 (0.01%)	6.18 (0.04%)	8.70 (0.06%)	5.54 (0.17%)	8.81 (0.27%)	15.63 (0.48)	23.21 (0.71%)	26.91 (0.83%)	38.73 (0.29%)	56.98 (0.56%)	685.44 (5.17%)	980.84 (7.4%)	1232.62 (9.3%)	1419.72 (10.72%)
	Max_error (%)	0.15	0.61	1.15	2.01	3.20	5.58	8.24	9.52	11.80	20.26	104.12	165.09	198.76	212.50
	Avg_error (MW)	0.02	0.18	0.29	0.30	0.52	0.65	1.00	1.53	2.06	2.20	24.88	37.46	47.19	52.75
	Avg_error (%)	0.0073	0.03	0.06	0.09	0.15	0.24	0.36	0.45	0.57	0.81	5.96	9.11	11.52	12.80

5.5 Conclusion

The main objective of the bus-aggregation technique is to obtain a set of optimal transmission reactances for the reduced equivalent model such that its inter-zonal power flows matches the inter-zonal power flows of the original system.

The algorithm for calculating the reduced equivalent is derived step by step. The buses are aggregated on a zonal basis by k-means++ method. Each zone is represented by a single bus. Within each zone, all the generators and loads are aggregated and retained at the equivalent bus. Also, all the intra-zonal transmission lines are ignored while the inter-zonal transmission lines are aggregated and represented by a single equivalent transmission line in the reduced equivalent. Zones are connected by equivalent lines if and only if there is at least one transmission lines branch directly connecting these two zones. After the topology of the reduced equivalent is determined, the reactance evaluation algorithm is applied to determine the equivalent transmission line reactances that best fit the PTDF matrix of the reduced equivalent network.

In this chapter, the bus aggregation method is applied to the optimal-reactance dc model proposed in CHAPTER 4 . The numerical examples are continued with two systems: the 7-bus system under the normally and heavily loaded case and the modified IEEE118-bus system under the normally loaded case. In the reduced equivalent comparison, the optimal dc model performs much better than the dc model with the single multiplier. However, the MW errors of the optimal 20-bus reduced dc model are larger than acceptable. There are two likely causes: First, since the k-means ++ bus clustering method is a critical step to achieve the accuracy of the reduced model, the different selection of the k-means++ starting vector (seed) may result in very different bus

clusters, some of which will be better than others. Second, and more likely is that one cannot represent this 118-bus system accurately with a 20 bus model.

In order to apply the bus-aggregation technique to the large-scale system like the EI or ERCOT, three improved strategies were proposed for improving the execution time, and memory requirements for calculating the equivalent line reactances.

First, sparsity techniques were applied though the entire computation process.

Second, a significant number of duplicate rows in the Λ^* matrix were eliminated by adding a weighting matrix into the optimization formulation. These duplicate rows were removed without reducing the rank of the matrix and without reducing the accuracy of the calculated reactances.

Third, an engineering-based criteria was used to eliminate a large number of rows of Λ^* without suffering a significant degradation in branch-reactance accuracy. The criterion involved using a threshold on equation coefficients.

From the numerical examples conducted on the ERCOT system, it is clearly shown that using speed-up improvement strategies has negligible effect on line flow accuracy if appropriate thresholds are used. Further, even very low thresholds yield significant speed advantages and gives gains that grow exponentially with size of reduced equivalent. The larger the reduced network required, the larger the gain provided by the improvement strategies.

CHAPTER 6 . CONCLUSION AND FUTURE WORK

6.1 Conclusion

In this thesis, several dc power-flow models are analyzed theoretically and evaluated numerically; a novel dc PF model is developed, implemented and tested; the possibility of applying these dc models in the various applications has been explored and demonstrated. The major conclusions are drawn as follows:

The state-independent dc power-flow model (Classical dc PF model) assumes a lossless network, one-per-unit voltage values, and small voltage angle differences. The impact of these approximations and how errors accumulate during the deriving process has been analyzed and evaluated numerically.

The state-dependent dc PF models (hot-start dc PF model with net loss dispersal, hot-start dc PF model with halved localized loss compensation, hot-start alpha-matching dc PF model and cold-start dc PF model with net loss dispersal) are constructed based on an initial ac solution. Based on an ac base-case solution, different loss compensation methods are applied to find reasonable MW losses compensation strategies. For the global loss compensation method, by scaling up all the loads in the system, the dispersed dc models compensates for the MW losses globally. For the localized loss compensation method, by modeling 50% of the branch loss as equivalent injections at both sides of the branch, a localized-loss dc model can be constructed. For base-point matching, by specifying the branch admittance h and solving the matching values α_i, α_j, the α-matching dc model can be constructed and match the base-case perfectly. These four dc PF models were discussed in detail and their performance evaluated numerically. Accuracy tests using these three dc models are conducted on two power systems: a modified IEEE 118-bus system, and the 62,000-bus Eastern Interconnection (EI) system. Errors introduced by these dc

power-flow models in the power-flow results and LMP calculations are quantified and compared. Also, contingency analysis is performed to evaluate the change in accuracy of these models for operating conditions that deviate from the base case. For power-flow result comparison, the alpha-matching dc PF model performs the best. However, in the OPF result comparison, the alpha-matching model does not reveal the congestion pattern for the IEEE118 system predicted by the ac OPF solution.

A novel hot-start optimal dc power-flow model based on ac power transfer distribution factor (PTDF) was proposed. As shown in the numerical examples, this optimal dc model not only matches the ac PF solution well, but also preserves the congestion pattern obtain from the OPF results of the original ac model.

The bus-aggregation technique was applied to obtain a set of optimal branch reactances for the reduced equivalent model such that its inter-zonal dc power flows match the inter-zonal ac power flows of the original system. The buses were aggregated on a zonal basis using the k-means++ method. Each zone was represented by a single bus. Within each zone, all the generators and loads were aggregated and retained at the equivalent bus. Also, all the intra-zonal transmission lines were ignored while the inter-zonal transmission lines were aggregated and represented by a single equivalent transmission line in the reduced equivalent. Zones were connected by equivalent lines if and only if there was at least one branch connecting these two zones. After the topology of the reduced equivalent was determined, the reactance evaluation algorithm was applied to determine the equivalent transmission line reactances that best fit the PTDF matrix of the reduced equivalent network.

The three improved strategies were proposed for applying the bus-aggregation technique to the large-scale system like EI or ERCOT to improve the execution time, and memory

requirements when calculating the equivalent line reactances. As shown in numerical example, the speed-up improvement strategies have negligible effect on line flow accuracy if appropriate thresholds are used. Further, even very low thresholds yield significant speed advantages and gives gains that grow exponentially with size of reduced equivalent. The larger the reduced network required, the larger the gain provided by the improvement strategies.

6.2 Future work

To further improve the adaptability of the proposed dc model, the following work is suggested for the future:

- For the **Ψ** matrix used in the linear least squares process to evaluate the equivalent dc PTDFs, it is shown that the calculation towards this matrix is computationally expensive but also requires a large amount of memory. Other than the application of sparsity techniques, the dimension of the **Ψ** matrix can be further reduced by including less ac PTDFs into the evaluation process and adding additional constraints to take into account the consistency of the PTDFs. This strategy must take into account on the network topology in addition to branch reactance magnitudes. The selection of the constraints and the reduction of the ac PTDFs are very critical to the accuracy of the equivalent dc PTDFs.

- For the bus aggregation technique, there are no line limits on the inter-zonal equivalent branches. If this approach is to be used to generate networks for OPF studies, methods that impose reasonable line limit on those equivalent transmission lines need to be developed.

- Since bus clustering is a critical step in achieving accuracy with a bus aggregation approach, bus clustering by using different PTDFs calculated based on different dc PF models can be compared.

- A comparison of the performance for all these dc models after using the bus aggregation technique.

REFERENCES

[1] T. Shrum, "Greenhouse gas emission: policy and economics", [Online]. Available: http://www.vlib.us/kansasenergy/GHG_Review_FINAL.pdf.

[2] Intergovernmental Panel on Climate Change (IPCC), "Climate change 2007: Synthesis report", [Online]. Available: http://www.ipcc.ch/pdf/assessment-report/ar4/syr/ar4_syr.pdf.

[3] U.S Energy Information Administration, "Emissions of greenhouse gases in the United States 2008," Dec. 2009, Available:http://www.eia.doe.gov/oiaf/1605/ggrpt/pdf/0573(2008).pdf.

[4] H. Hondo, "'Life cycle GHG emission analysis of power generation systems: Japanese case," [Online]. Available: http://campus.udayton.edu/~physics/rjb/PHY399Winter2007/Hondo%20-%20GHG%20LCA%20for%20power%20generation.pdf.

[5] R. Bharvirkar, D. Burtraw, and A. Krupnick, , "Nox emissions trading and episodic air quality violations in Maryland", Final report prepared for the power plant research program, State of Maryland (May), 2003.

[6] T. Gayer, "Market-based approaches to environmental regulation", [Online]. Available: http://faculty.arec.umd.edu/jhorowitz/MIC013-book.pdf.

[7] A. Midttun and A. L. Koefoed, "Effectiveness and negotiability of environmental regulation," [Online]. Available: http://bookstore.teriin.org/docs/journals/IJRG-01-Paper5.pdf.

[8] J. Bradbury, "Electricity markets increasingly favor alternatives to coal", [Online]. Available: http://pdf.wri.org/factsheets/factsheet_us_electricity_markets_favor_alternatives_to_coal.pdf.

[9] National Renewable Energy Laboratory (NERL),"Bulk electric power systems", [Online]. Available: http://www.nrel.gov/docs/fy12osti/52409-4.pdf

[10] M. Gavrilas, O. Ivanov, and G. Gavrilas. "REI equivalent design for electric power systems with genetic algorithms." WSEAS Transactions on Circuits and Systems 7.10 (2008): 911-921.

[11] B. Botts, L.L.P, "Energy industry facing increased environmental regulations in 2011", [Online]. Available: http://www.bakerbotts.com/energy-industry-facing-increased-environmental-regulations-in-2011-02-25-2011/.

[12] A. Papaesmmanouil and G. Andersson, "On the reduction of large power system models for power market simulations," [Online]. Available: http://www.eeh.ee.ethz.ch/uploads/tx_ethpublications/PSCC2011_Antonios.pdf.

[13] M.P. Selvan, K.S. Swarup, Large scale power system computations with object-oriented design, IEEE PES General Meeting., Vol.1, 2004,pp.330-334.

[14] J. B. Ward, "Equivalent circuits for power flow studies," AIEE Trans. Power Appl. Syst., vol. 68, pp. 373–382, 1949.

[15] W. Snyder, "Load-flow equivalent circuits–an overview," IEEE PES Winter Meeting, New York, Jan. 1972.

[16] F.F. Wu and A. Monticelli, "Critical review of external network modelling for online security analysis," Electrical Power & Energy Systems, vol.5, no. 4, 1983.

[17] S. Deckmann, A. Pizzolante, A. Monticelli, B. Stott, and O. Alsac, "Studies on power system load flow equivalencing," IEEE Trans. Power App. Syst., vol. PAS-99, no. 6, pp. 2301–2310, Nov./Dec. 1980.

[18] A. M. V. Amerongen and H. P. V. Meeteren, "A generalized Ward equivalent for security analysis," SM, 455-5, p.1519, June. 1982

[19] H. Duran and N. Arvanitidis, "Simplification for area security analysis: A New look at equivalencing," IEEE Trans. Power App. Syst., vol. PAS-91, pp. 670-679, 1972.

[20] A. Monticelli, S. Deckmann, A. Garcia and B. Stott, "Real-time external equivalents for static security analysis," IEEE Trans. Power App. Syst., vol. PAS-98, No. 2, pp. 498-508, Mar./Apr. 1979.

[21] J. Machowski, A. Cichy, F. Gubina and P .Omahen, "External subsystem equivalent mode for steady-state and dynamic security assessment," IEEE Trans. Power Sys., vol. 3, No. 4, Nov. 1988

[22] L. A. Zhukov, "Construction of power system electromechanical equivalents," Izv. Akad. Nauk SSSR, Energy. and Transp., No. 2, 1965.

[23] E. H. Allen, J. H. Lang, and M. D. Ilic, "A Combined Equivalenced-Electric, Economic, and Market Representation of the Northeastern Power Coordinating Council U.S. Electric Power Systems," IEEE Trans. Power Syst., vol. 23, no. 3, pp. 896-907, Aug. 2008.

[24] Shi, D., Shawhan, D. L., Li, N., Tylavsky, D. J., Taber, J. T., Zimmerman, R. D., and Schulze, W. D. "Optimal generation investment planning: Pt. 1: network equivalents", North American Power Symposium (NAPS), Sep. 2012, Urbana-Champion, USA

[25] P. Dimo, "Nodal analysis of power systems", Abacus Press, Kent, England, 1975.

[26] W. F. Tinney and W. L. Powell, “The REI approach to power network equivalents,” IEEE PICA Conference Proceedings, Minneapolis, pp. 384-390, July 1983.

[27] E. C. Housos, G. Irisarri, R. M. Porter and A. M. Sasson, “Steady state network equivalents for power system planning applications,” IEEE Trans. Power App. Syst., vol. PAS-99, no. 6, Nov./Dec. 1980.

[28] J. F. Dopazo, G. Irisarri and A. M. Sasson, “Real-time external system equivalent for on-line contigency analysis,” IEEE Trans. Power App. Syst., vol. PAS-98, no. 6, Nov./Dec. 1979.

[29] M. Gavrilas, , O. Ivanov, and G. Gavrilas. "REI equivalent design for electric power systems with genetic algorithms." WSEAS Transactions on Circuits and Systems 7, no. 10 (2008): 911-921.

[30] H. K. Singh and S. C. Srivastava, “A reduced network representation suitable for fast nodal price calculations in electricity markets,” IEEE Power Engineering Society General Meeting, vol. 2, pp. 2070-2077, June 2005.

[31] X. Cheng and T. J. Overbye, "PTDF-based power system equivalents," IEEE Trans. Power Syst., vol. 20, no. 4, pp. 1868-1876, Nov. 2005.

[32] H. Oh, “A new network reduction methodology for power System Planning Studies,” IEEE Trans. Power Syst., vol. 25, no. 2, pp. 677-684, May 2010.

[33] D. Shi and D. J. Tylavsky, "An improved bus aggregation technique for generating network equivalents," IEEE PES General Meeting, July 2012, San Diego, USA.

[34] H. Oh, "Aggregation of buses for a network reduction," Power Systems IEEE Transactions, vol.27, no.2, pp.705-712, May 2012.

[35] C. Duthaler, M. Emery, G. Andersson, and M. Kurdizem, “Analysis of the use of PRDF in the UCTE transmission grid,” in Proc. 16th PSCC, Glasgow, U.K., Jul. 2008.

[36] K. Purchala, L. Meeus, D. Van Dommelen, and R. Belmans, “Usefulness of dc power flow for active power flow analysis,” in Proc. IEEE PES General Meeting, Jun. 2005

[37] P.Yan and A. Sekar, “Study of linear models in steady state load flow analysis of power systems,” in Proc. IEEE PES Winter Meeting, 2002.

[38] T.J. Overbye, X.Cheng, and Y. Sun, “A comparison of the ac and dc power flow models for LMP calculations,” in Proc. 37th Hawaii Int. Conf. System Sciences, 2004.

[39] D. Van Hertem, J. Verboomen, R. Belams, and W. L. Kling, “Useful-ness of DC power flow for active power flow analysis with flow controlling devices, ” in Proc. 8th Int. Conf. AC and DC Power Transmission, Mar. 2006.

[40] F. Li and R. Bo, “DCOPF-based LMP simulation: Algorithm, comparison with ACOPF, and sensitivity,” IEEE Transactions on Power Systems, vol. 22, no. 4, pp. 1475 –1485, Nov. 2007.

[41] M.Liu and G. Grouss, “Effectiveness of the distribution factor approximations used in congestion modeling,” in Proc. 14th PSCC, Seville, Spain, Jun. 2002.

[42] B. Stott, J. Jardim, and O. Alsac, “DC power flow revisited,” IEEE Transactions on Power Systems, vol. 24, no. 3, pp. 1290–1300, Aug. 2009.

[43] D. Kirschen, G. Strbac, and I. Ebrary, “Fundamentals of power system economics,” New York: John Wiley & Sons 2004, pp. 141-200.

[44] A. Wood and B. Wollenberg, “Power system generation, operation and control,” New York: Wiley, 1996.

[45] J. Glover, M. Sarma, and T. Overbye, Power System Analysis and Design: 4th Edition. Thomson Engineering, 2011, pp. 281-333.

[46] J. Grainger and W.S. Jr., Power system analysis. McGraw-Hill Science/Engineering/Math, 1994

[47] B.F. Wollenberg and W.O. Stadlin, ”A real-time optimizer for security dispatch,” IEEE Trans. Power App. Syst., vol. PAS-93, pp. 1640-1649, 1974.

[48] H. Pinto, F. Magnago, S. Brignone, O. Alsac, and B. Stott,”Security constrained unit commitment: Network modeling and solution issues,” in IEEE PSCE Conf., Oct.29-Nov.1, 2006, pp. 1759-1766.

[49] R. Kaye and F. Wu, “Analysis of linearized decoupled power flow approximations for steady-state security assessment,” IEEE Transactions on Circuits and Systems, vol. 31, no. 7, pp. 623–636, 1984.

[50] A. Gopal, D. Niebur, and S. Venkatasubramanian, "DC power flow based contingency analysis using graphics processing units," 2007 IEEE Lausanne Power Tech, vol., no., pp. 731-736, 1-5 July 2007.

APPENDIX A

ONE LINE DIAGRAM FOR IEEE 118-BUS SYSTEM

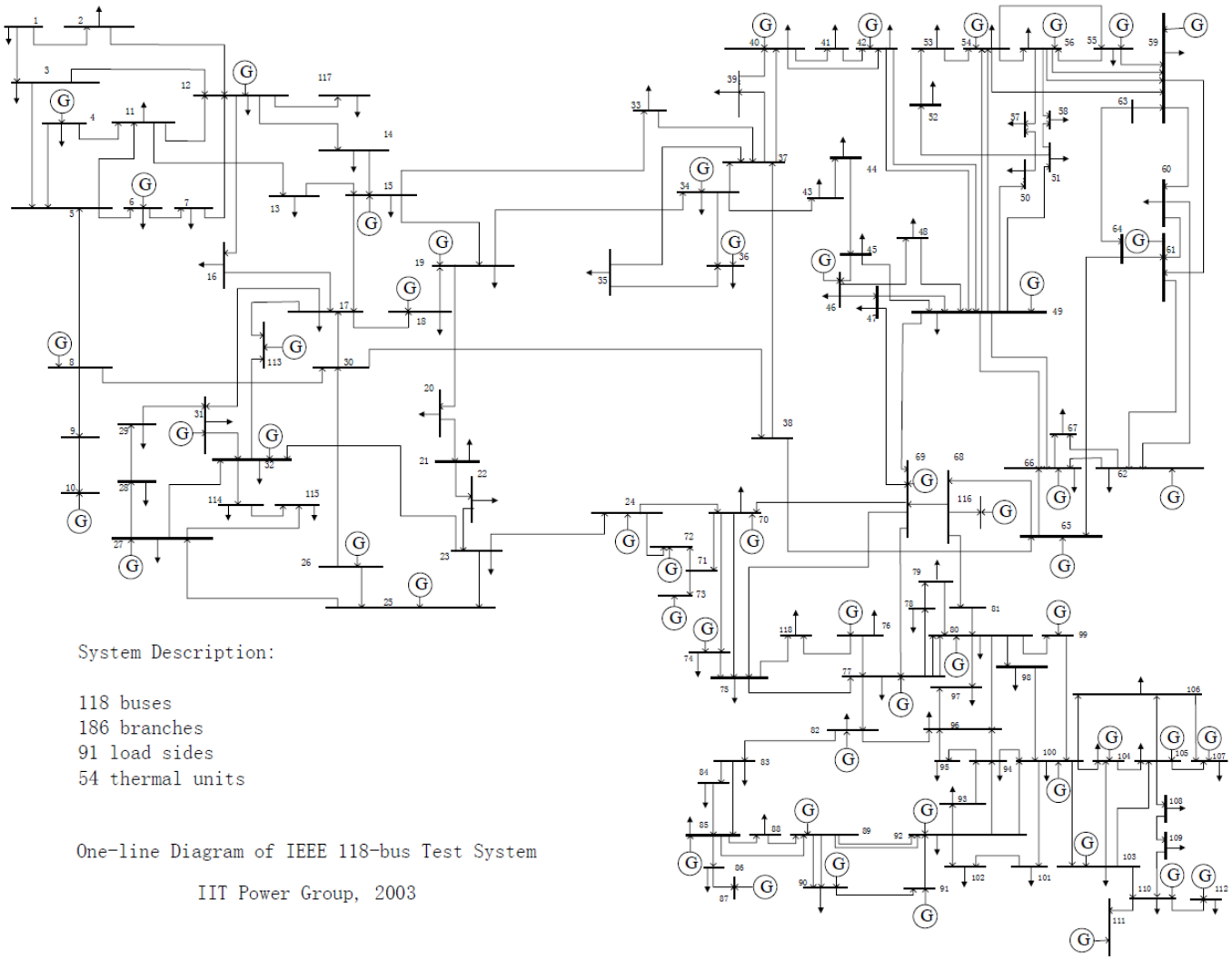

System Description:

118 buses
186 branches
91 load sides
54 thermal units

One-line Diagram of IEEE 118-bus Test System

IIT Power Group, 2003

APPENDIX B

BUS CLUSTERING FOR 118->20 BUS REDUCED EQUIVALENT

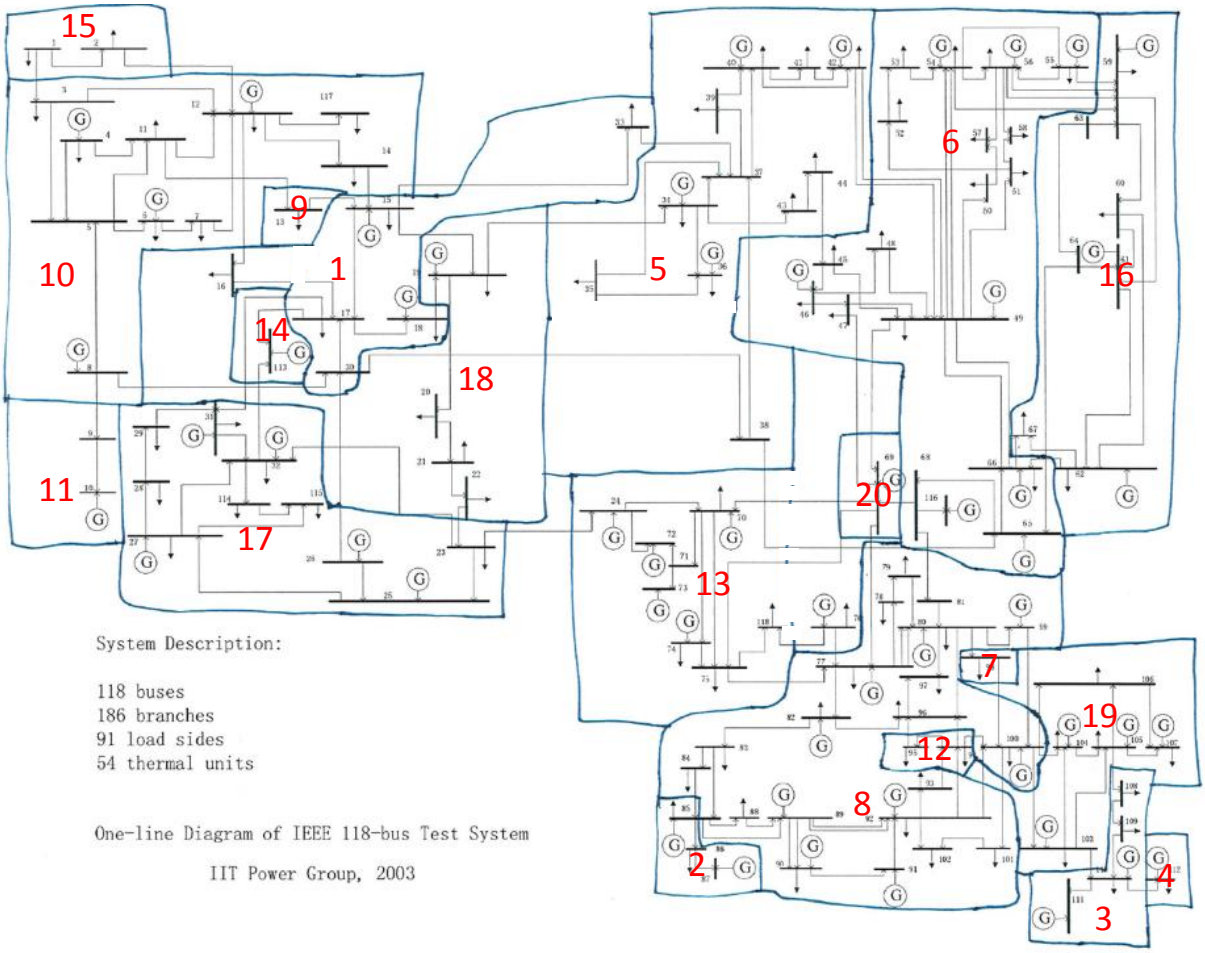

System Description:

118 buses
186 branches
91 load sides
54 thermal units

One-line Diagram of IEEE 118-bus Test System

IIT Power Group, 2003